

UNIVERSITY OF CALIFORNIA

Los Angeles

Multi-wavelength Optical Code-Division-Multiple-Access
Communication Systems

A dissertation submitted in partial satisfaction of the
requirement for the degree of Doctor of Philosophy
in Electrical Engineering

by

Cedric Fung Lam

1999

The dissertation of Cedric Fung Lam is approved.

Ming-C. Wu

Izhak Rubin

Mario Gerla

Eli Yablonovitch, Committee Chair

University of California, Los Angeles

1999

With Love and Affection for

My Parents

TABLE OF CONTENTS

TABLE OF CONTENTS	v
LIST OF FIGURES	viii
ACKNOWLEDGMENTS	xiv
VITA	xvi
PUBLICATIONS AND PRESENTATIONS	xvii
ABSTRACT OF THE DISSERTATION	xix
CHAPTER 1 INTRODUCTION	1
1.1 MOTIVATION	1
1.2 BASIC COMMUNICATION CONCEPTS AND THE SPREAD SPECTRUM TECHNIQUES	3
1.3 DISSERTATION ORGANIZATION.....	8
CHAPTER 2 RESEARCH AND DEVELOPMENT IN OPTICAL CDMA SYSTEMS	10
2.1 INTRODUCTION.....	10
2.2 TIME DOMAIN ENCODING USING OPTICAL DELAY LINE LOOPS	10
2.3 COHERENT SPECTRAL PHASE ENCODING OF ULTRA-SHORT OPTICAL PULSES	14
2.4 NON-COHERENT SPECTRAL INTENSITY ENCODING.....	16
2.5 CONCLUSION: IMPORTANT DESIGN ISSUES IN OPTICAL CDMA.....	18
CHAPTER 3 NON-COHERENT SPECTRAL INTENSITY ENCODED BIPOLAR OPTICAL CDMA SYSTEMS	20
3.1 PRINCIPLE.....	20

3.2	EXPERIMENTAL DEMONSTRATION USING WDM COMPONENTS AND HADAMARD CODES	22
3.3	EXPERIMENTAL DEMONSTRATION USING A CASCADED MACH-ZEHNDER ENCODER ..	28
3.4	PERFORMANCE EVALUATION.....	38
3.5	DISCUSSION AND CONCLUSION.....	47
CHAPTER 4 MULTI-WAVELENGTH SPECTRAL PHASE ENCODED OPTICAL CDMA NETWORK		52
4.1	TRANSMITTER	53
4.2	RECEIVER.....	57
4.3	CARRIER/SIDE BANDS SEPARATION AND COMBINING	59
4.4	ENCODER DESIGN.....	60
4.5	PERFORMANCE EVALUATION.....	69
4.6	DISCUSSIONS	76
4.7	CONCLUSION	76
CHAPTER 5 DEMULTIPLEXING TDM, WDM AND CDM SIGNALS		78
5.1	INTRODUCTION.....	78
5.2	DEMULTIPLEXING TDM SIGNALS	79
5.3	DEMULTIPLEXING WDM SIGNALS.....	80
5.4	DEMULTIPLEXING CDM CHANNELS	86
5.5	CONCLUSION	90
CHAPTER 6 CONCLUSION		92
APPENDIX A HADAMARD CODES.....		98
APPENDIX B PROCEDURE FOR CALIBRATING THE CASCADED MACH- ZEHNDER ENCODER		102

APPENDIX C	NUMBER OF MODES IN MULTI-MODE FIBERS.....	105
APPENDIX D	THROUGHPUT CALCULATION FOR NON-COHERENT COMPLEMENTARY SPECTRALLY ENCODED CDMA	106
APPENDIX E	A RECTANGULAR SHAPED WAVELENGTH FILTER FOR WDM DEMULTIPLEXING	108
I.	PHOTONIC CRYSTAL FILTER DESIGN.....	109
A.	<i>Simple 1-D Photonic Crystal</i>	<i>109</i>
B.	<i>Photonic Crystals with Effective Bragg Mirrors as Reflectors.....</i>	<i>110</i>
C.	<i>Apodization of Bragg Mirrors.....</i>	<i>114</i>
D.	<i>Physical Implementation of Rectangular Shaped Frequency Filters</i>	<i>115</i>
II.	WAVELENGTH SWITCHING USING LOGARITHMIC FILTER CHAINS	117
BIBLIOGRAPHY		121

LIST OF FIGURES

Figure 1.1	Time-frequency space usage in (a) TDMA, (b) WDMA, (c) CDMA.	2
Figure 1.2	Principle of Amplitude Modulation (AM)	3
Figure 1.3	Block diagram of coherent homodyne communication system.....	4
Figure 1.4	Block diagrams of direct sequence spread spectrum (DS-SS) communication system, (a) transmitter and (b) receiver.....	5
Figure 2.1	Time domain optical CDMA encoding of high peak intensity ultra-short pulses using delay line loops: (a) encoder, (b) encoder output and (c) decoder.	11
Figure 2.2	Time domain encoding using cascaded ladder encoder.....	13
Figure 2.3	Coherent spectral phase encoded optical CDMA system using ultra-short pulses.	14
Figure 2.4	Frequency and time domain waveforms of coherent spectral phase encoded system: (a) narrow pulse spectrum, (b) pseudo-random (PN) sequence in frequency domain, assuming 0 and π phase encoding which corresponds to +1 and -1 multiplication in amplitude here, (c) pulse spreading due to phase encoding and (d) pulse despreading for matched and unwanted channels.....	15
Figure 2.5	Non-coherent spectral intensity encoded optical CDMA system.....	17
Figure 3.1	System structure of bipolar spectrally encoded optical CDMA. A balanced broadband source is spectrally encoded and received by a balanced receiver. The complementary spectra produced by the spectral filter, $ T ^2$ and $\overline{ T ^2}$, represent the complementary intensity transfer functions of the spectral filter outputs.....	21

Figure 3.2	Balanced differential opto-electronic CDMA transmitter and receiver. The outputs from the two input sources produce complementary spectra. Modulation is performed by alternating between the two input sources electrically. For matched encoding functions, either a +1 or a -1 is registered at the balanced receiver output depending on whether the transmitter sends a direct spectrum or its complementary spectrum. Unmatched channels are rejected as zero output.	23
Figure 3.3	Experimental set-up used to emulate the balanced transmitter. A multi-wavelength laser diode array output is switched between the two input ports of the encoder using an electro-optic 2×2 switch which is driven by the input data obtained from a $2^{15}-1$ pseudo-random pattern generator.	25
Figure 3.4	Eye diagrams obtained for the (1010) encoding when the receiver is set to decode: (a) the matched code (1010); (b) the unmatched code (1100) and (c) the unmatched code (1001). Error free transmission is obtained for the matched code. Unmatched codes are rejected.	26
Figure 3.5	The BER plot against the received power at 155Mbps speed for the matched transmitter and receiver pair, which uses the code (1010).	27
Figure 3.6	The schematic diagram of a multistage Mach-Zehnder encoder. Complementary outputs are produced at each output by switching on and off the balanced sources alternately. The phase shifters produce the different spectral outputs.	29
Figure 3.7	The simulated spectral output from a seven-stage Mach-Zehnder encoder. The free spectral range is 640GHz in the computation. The complicated spectral output represents a secret code. The two lower diagrams are the expanded sections of the diagram above them as indicated by the grey lines.	33

Figure 3.8	Layout of the experimental 7-stage Mach-Zehnder encoder. The black dots are connectors to thin film heaters and thermo-electric temperature stabilizers.....	34
Figure 3.9	A pigtailed 7-stage Mach-Zehnder encoder diagram.....	35
Figure 3.10	The experiment setup to demonstrate the non-coherent spectrally encoded bipolar CDMA system.....	36
Figure 3.11	Picture of the optical breadboard setup for the experiment of non-coherent spectral intensity encoded optical CDMA system using cascaded Mach-Zehnder encoder.....	37
Figure 3.12	An eye-diagram taken at 100Mbps speed using a $2^{15}-1$ pseudo-random bit sequence. The measured BER is 10^{-9}	38
Figure 3.13	Bit Error Rate (BER) vs. number of active users for (a) single-mode system and (b) multi-mode system.	45
Figure 3.14	Throughput vs. number of subscribers for (a) single-mode and (b) multi-mode systems.	46
Figure 3.15	Noise to signal ratio versus number of active users for spectral intensity encoded CDMA system and spectrally sliced WDM systems. K is the total number of spectral slices, which corresponds to the total number of allowable users in the system.	50
Figure 4.1	Multi-wavelength optical CDMA network.	52
Figure 4.2	Transmitter of multi-wavelength optical CDMA system.....	54
Figure 4.3	Multi-wavelength optical CDMA receiver.....	57
Figure 4.4	A Mach-Zehnder interferometer (MZI) together with Fabry-Perot (FP) filter as carrier add/drop filter.....	60
Figure 4.5	A ring resonator as carrier add/drop filter.	60
Figure 4.6	The feedback Mach-Zehnder phase encoder.	61

Figure 4.7	By properly setting l_f , the feed forward path length difference, and θ , the MZI functions as a 2×2 switch in either through or cross state for the mode-locked wavelength components.	62
Figure 4.7a	Series connected FBMZI's to produce families of orthogonal spectral phase codes.	63
Figure 4.8	Distribution of the phase differences between the 0 and π states for different feedback lengths. There is no common factor between q and N . $N=32$	64
Figure 4.9	Distribution of the encoded phase differences between the 0 and π states for different feedback lengths. q and N are not co-prime and the common factor between them is 4. $N=32$	66
Figure 4.10	Four codes formed by cascading two different FBMZI stages.	66
Figure 4.11	Proposed waveguide circuits for cascaded FBMZI to save real estates.	69
Figure 4.12	Bit Error Rate (BER) vs. Number of Active Users for (a) ASK and (b) PSK.	73
Figure 4.13	Throughput vs. Number of Subscribers for (a) ASK and (b) PSK.	75
Figure 5.1	A multi-channel TDM signal frame.	79
Figure 5.2	Demultiplex TDM channels using $\log_2 N$ cascaded delay lines.	80
Figure 5.3	WDM demultiplexers using (a) cascaded micro-cavity filters, (b) ruled grating with Stimax configuration and (c) integrated waveguide gratings.	82
Figure 5.4	Channel selection (add/drop) using the WDM demultiplexers shown in Fig. 5.3 has complexity N	83

Figure 5.5	WDM channels are demultiplexed with a logarithmic number of switches (a) input multi-wavelength signal, (b) transmission function of each stage, (c) schematic diagram of the demultiplexer.	84
Figure 5.6	A multi-wavelength signal add/drop multiplexer using a Mach-Zehnder interferometer and rectangular shaped wavelength filters (see Appendix E).	87
Figure 5.7	Generating multi-wavelength complementary intensity encoded Hadamard codes using multi-wavelength add/drop demultiplexers.	88
Figure 5.8	Generating multi-wavelength phase encoded Hadamard codes.	90
Figure E.1	A simple photonic crystal consists of alternate layers of dielectric materials. To produce equal width pass band and stop band, this system requires a refractive index contrast of 5.83.	109
Figure E.2	The top view of a periodic rectangular shaped frequency filter consisting of effective Bragg Mirrors separated apart by distances y determined by the required free spectral range. The difference between the refractive indices n_1 and n_2 is 8.5%.	110
Figure E.3	The simulated transmission and reflection of the effective Bragg mirror used in the Fig. E.2. 11 periods of quarter-wave stacks are used in the simulation and the result obtained corresponds to a 40nm wide region around the 1.55 μ m center wavelength.	112
Figure E.4	The simulated transmission and reflection of the filter in Fig. E.2 over a 40nm wide region around the 1.55 μ m center wavelength. 19 effective Bragg mirrors are separated by distances, which will produce four periods in the simulated frequency range. The fringes in the pass bands are due to the reflections at the two end mirrors.	113
Figure E.5	The simulated transmission and reflection of a Gaussian apodized filter. The pass band ripples are suppressed by the apodization.	115

Figure E.6	The perspective view of an apodized periodic rectangular shaped frequency filter in a ridged waveguide structure. The Bragg reflectors with apodized reflectivity are formed by etching grooves in the ridged waveguide. This figure shows the number of layers in each Bragg reflector as prescribed by Equation (E.4) and as used in the numerical simulation.	116
Figure E.7	Wavelength selection using 2×2 optical switches and cascaded complementary periodic rectangular shaped spectral filter pairs.	117
Figure E.8	Simulated result for two filters (thick and thin lines) which are slightly different in periodicity. Over a 40nm wide region around the 1.55μm center wavelength, eight periods are included. The two filters look “complementary” to each other.	118
Figure E.9	Obtaining the direct and complementary spectral outputs from the transmitted and reflected filter outputs using an optical circulator.	119
Figure E.10	Obtaining the direct and complementary spectral outputs from a Mach-Zehnder Interferometer (MZI). Identical filters are incorporated in two arms of equal length. The direct and complementary outputs propagate in opposite directions.	119

ACKNOWLEDGMENTS

First, I would like to express my heartfelt gratitude to my advisor Professor Eli Yablonovitch for his academic advice and direction, constant encouragement, and financial support during my graduate school years at UCLA. I would also like to thank Professor Ming Wu for providing the lab space and necessary measurement equipment for the experiments, Professor Greg Pottie for valuable discussions especially during the initial stage of this research, Drs. Dennis Tong and Rutger Vrijen for experimental assistance.

I am indebted to many people during my four and half years at UCLA as a graduate student. First and most importantly, I am extremely grateful for my parents, who have sacrificed themselves to give my brother and me the best education. Their unreserved love and support for these many years is what makes this Ph.D. degree possible. For this, I believe they deserve this degree more than anyone else does. I am also very grateful for my brother Stanley Lam and his girlfriend Kanas Shum, who have taken the responsibility of taking care of our parents while I was studying and writing this dissertation away from home.

Many friends in Hong Kong have given me lots of care and support in these years, despite the geographical separation. I would like to thank Mr. Sam Tai who mailed me numerous books and music from Hong Kong to help me alleviate my homesickness. My gratitude extends to Mr. Patrick Wun, Mr. Chi-Kan Yuen, Miss Choi-Fun Chung, and

Miss Desiree Lam, whose unflinching support from Hong Kong and companionship through mails and e-mails have helped me gone through various hardships in these years.

I must thank Miss Jennifer Fan for her unselfish emotional backup, attentive care and unflinching understanding. Many people from our unofficial UCLA 'HKers' Association have made my life at UCLA full of joys. Without them, my graduate school would have been just lonely nights and mere academic work. I cannot exhaust all the members of this unofficial yet tightly bonded Association. But I would like to specially thank Dr. Dennis Tong, Miss Asta Ho, Mr. Eric Lam, Dr. Kanson Lau, Mr. David Chan, and Miss Angela Cheung.

Many American friends have also given me tremendous help during the past four and half years. In particular, I would like to share my pride with Mr. Jason Gillick, Mr. Steven Chin, Mr. Christopher Ward and Mr. Shane Dultz.

Besides, I would like to thank my god-brother Dr. Wei Chang and his family, who have given me a home in California. Last but not least, I have to specially thank the Sir Edward Youde Memorial Fund of the Hong Kong Government. Without it I would not be able to pursue my studies at UCLA.

VITA

November 21, 1970 Born, Kunming, China

1992 Research Assistant
Electrical and Electronic Engineering Department
The University of Hong Kong, Hong Kong

1993 B.Eng. (First Class Honors)
Electrical and Electronic Engineering
The University of Hong Kong, Hong Kong

1993 – 94 Teaching Assistant
Electrical and Electronic Engineering Department
The University of Hong Kong, Hong Kong

1994 – 97 Sir Edward Youde Fellow

1995 Teaching Associate
Electrical Engineering Department
University of California, Los Angeles

1995 - 1999 Research Assistant
Electrical Engineering Department
University of California, Los Angeles

1995 - 1999 System Administrator
Optoelectronics Lab
University of California, Los Angeles

1996 M.Sc. Electrical Engineering
University of California, Los Angeles

1996 - 1998 Teaching Fellow
Electrical Engineering Department
University of California, Los Angeles

PUBLICATIONS AND PRESENTATIONS

1. C.F. Lam and E. Yablonovitch, "Multi-wavelength Optical Code Division Multiplexing", To appear in *Future Trends in Microelectronics: Off the Beaten Path*, John Wiley, 1999.
2. C.F. Lam, R. Vrijen, D.T.K. Tong, M.C. Wu and E. Yablonovitch, "Multi-wavelength Optical Code Division Multiplexing", (Invited paper), *Critical Reviews of Optical Science and Technology on Wavelength Division Multiplexing*, SPIE Photonics West '99, Jan 1999, San Jose, California.
3. C.F. Lam, R. Vrijen, D.T.K. Tong, M.C. Wu and E. Yablonovitch, "Experimental Demonstration of Spectrally Encoded Optical CDMA System Using Mach-Zehnder Encoder Chains", paper CThU4, *IEEE/OSA CLEO'98*, May 1998, San Francisco.
4. C.F. Lam, D.T.K. Tong, M.C. Wu and E. Yablonovitch, "Experimental Demonstration of Bipolar Optical CDMA System Using a Balanced Transmitter and Complementary Spectral Encoding", *IEEE Photonics Technology Letters*, Vol. 10, No. 10, pp1504-1506, Oct. 1998.
5. C.F. Lam, R.B. Vrijen, P. Chang-chien, D. Sievenpiper and E. Yablonovitch, "A Tunable Wavelength Demultiplexer Using Logarithmic Filter Chains", *IEEE/OSA Journal of Lightwave Technology*, Vol. 16, No. 9, 1998, pp1657-1662.
6. C.F. Lam, R.B. Vrijen, P. Chang-chien, D. Sievenpiper and E. Yablonovitch, "A Tunable Wavelength Demultiplexer Using Cascaded Photonic-Crystal Filters", *OSA Optics & Photonics News*, Jan. 1998, Vol. 9, No. 1, pp49.
7. C.F. Lam and E. Yablonovitch, "Shot-noise-induced Crosstalk in Spectrally Encoded Optical CDMA Systems", Paper FM2 in *OSA Annual Meeting*, October 12-17, 1997, Long Beach, CA.

8. C.F. Lam and E. Yablonovitch, "A Fast Wavelength Hopped CDMA System for Secure Optical Communications", *Proc. SPIE Conference on Computer and Network Security*, Nov. 1997, Dallas, Texas.
9. C.F. Lam, R. Vrijen, D.T.K. Tong, M.C. Wu and E. Yablonovitch, "Spectrally Encoded CDMA System Using Mach-Zehnder Encoder Chains", *Proc. SPIE Conference on Computer and Network Security*, Nov. 1997, Dallas, Texas.
10. C.F. Lam and E. Yablonovitch, "A Configurable Wavelength Demultiplexer Using Periodic Filter Chains", *1997 Digest of the LEOS Summer Topical Meetings*, Montreal, Canada, IEEE.
11. C.F. Lam and E. Yablonovitch, "Terabit Switching and Security Enhancement in a WDM/TDM Hybrid System", *1997 Digest of the LEOS Summer Topical Meetings*, Montreal, Canada, IEEE.
12. C.F. Lam and E. Yablonovitch, "Multi-Wavelength, Optical Code-Division-Multiplexing Based on Passive, Linear, Unitary, Filters", *Proc. 1995 International Symposium on Signals, Systems and Electronics (ISSSE' 95)*, San Francisco, IEEE, pp299-302.
13. D.F. Sievenpiper, C.F. Lam, E. Yablonovitch, "Two-Dimensional Photonic- Crystal Vertical-Cavity Array for Nonlinear Optical Image Processing", *Applied Optics*, Vol. 37, No. 11, pp2074-2078, 10 Apr. 1998.

ABSTRACT OF THE DISSERTATION

Multi-wavelength Optical Code-Division-Multiple-Access

Communication Systems

by

Cedric Fung Lam

Doctor of Philosophy in Electrical Engineering

University of California, Los Angeles, 1999

Professor Eli Yablonovitch, Chair

There has been tremendous interest in applying spread spectrum and code division multiple access (CDMA) techniques to fiber optic communication systems. In this dissertation, we review the previous work on optical CDMA systems, and we propose and then demonstrate new optical CDMA system designs. The explosive growth in bandwidth demand during the recent years have compelled engineers to achieve one bit per hertz or more bandwidth utilization in optical fibers. We point out that in order to achieve efficient bandwidth utilization, full orthogonality is required in optical CDMA system. At the same time, one would like to avoid having an optical local oscillator, which significantly increases the system complexity. We have studied two spectrally encoded optical CDMA systems, both of which give us full orthogonality. A balanced optical detector, which ‘computes’ the difference between two photodetectors signals, is

used to obtain negative outputs from positive-only optical intensity signals, thus achieving full orthogonality in both systems.

The first system, complementary spectral intensity encoding, is a fully non-coherent. A novel balanced transmitter has been invented for this system. Unfortunately, the performance of this system is limited by beat noise interference, sometimes called speckle noise. In the second system, spectral phase encoding, a multi-wavelength mode-locked laser source is employed. Spectral phase encoding is applied to various frequency components. By sending the unmodulated carrier along the optical fiber to the receiver, we can achieve the effect of coherent demodulation without using an optical local oscillator. While this system can avoid speckle noise, it is eventually limited by cumulative shot noise. We will show in this dissertation, that cumulative shot noise is unavoidable in all optical CDMA systems. Therefore the ultimate achievable performance of optical CDMA systems under shot noise limitation will be analyzed in this work.

Lastly, we compare time division multiplexing (TDM), wavelength division multiplexing (WDM) and CDM systems, and show that logarithmic demultiplexing complexity can be achieved in all three systems. A corresponding WDM filter having a rectangular-shaped wavelength transfer function, for logarithmic demultiplexing, is also described in Appendix E.

Chapter 1 Introduction

1.1 *Motivation*

Code division multiple access (CDMA) systems using the technique of spread spectrum communication have been used in radio communication systems in an effort to improve radio spectral usage efficiency. The Qualcomm company in San Diego has commercialized the technology in the last few years. Recently, there has been a lot of interest in applying the concepts of CDMA to optical fiber communication systems.

We have seen very rapid development of the Internet and the information superhighway, all over the world. The growth rate in the bandwidth demand is at a speed faster than Moore's law, which is used to describe the improvement rate of Silicon integrated circuits. According to studies in ref [1], the annual growth rate of trans-Atlantic communication capacity in the 1990 was 75%. Today's telecommunication networks have widely adopted optical fiber as the backbone transmission medium. It has the advantage of low loss, low noise and very high bandwidth. The optical fiber in itself has at least 10 Tera-hertz bandwidth. However, the projected bandwidth available in future mainstream Silicon circuit is only 10 Giga-hertz. There are three orders of magnitude difference in the bandwidth available in optical fibers and silicon circuits. In order to make full use of the available bandwidth in optical fibers and satisfy the bandwidth demand in future information networks, it is a necessary to multiplex low rate data streams onto optical fiber to increase the total throughput.

A multiple access scheme is required for multiplexing and demultiplexing traffic on a shared physical medium [2]. The three major multiple access schemes are described pictorially in Fig. 1.1. Digital communication allows the possibility of time division multiple access (TDMA). In a TDMA system, each channel occupies a time slot, which interleaves with the time slots of other channels. In a wavelength division multiple access (WDMA) system, each channel occupies a narrow bandwidth around a center wavelength or frequency. The modulation format and speed at each wavelength can be independent of those of other channels. A channel in a CDMA system occupies the same frequency-time space as all the other CDMA channels. Each CDMA channel is distinguished from other CDMA channels by a unique CDMA spreading code.

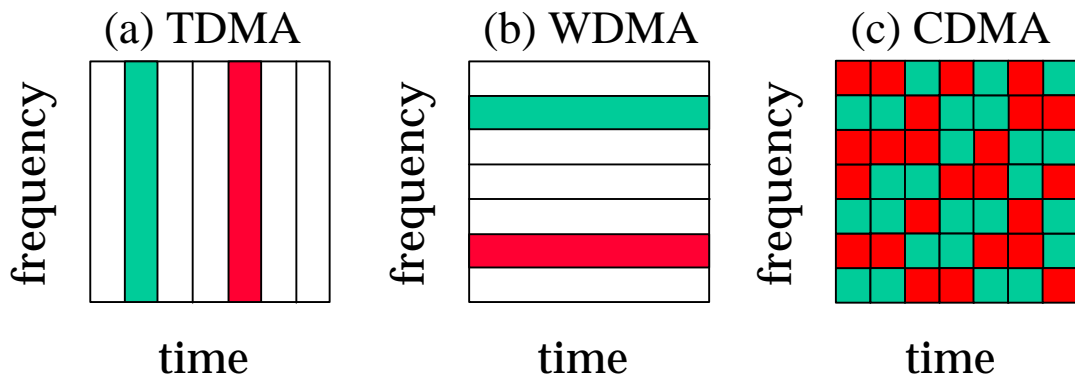


Figure 1.1 Time-frequency space usage in (a) TDMA, (b) WDMA, (c) CDMA.

Both TDMA and WDMA systems have been widely studied in both industry and academia. Although CDMA has been heavily studied in radio communications, and has proven itself as a viable technology, it is a relatively new technology in the fiber optic domain. Since optical fiber is a very different medium compared to radio links, one would expect optical CDMA systems to have similarity, as well as differences from its

radio version. This project aims at finding the most suitable form of CDMA systems which can be applied to optical fiber links, as an alternative way to the multiplexing of optical signals. The potential benefit and difficulties of fiber optic CDMA systems will also be studied in this project.

1.2 Basic Communication Concepts and the Spread Spectrum Techniques

In this section, we review some of the basic concepts in communications. These concepts will eventually lead to our final optical CDMA system design.

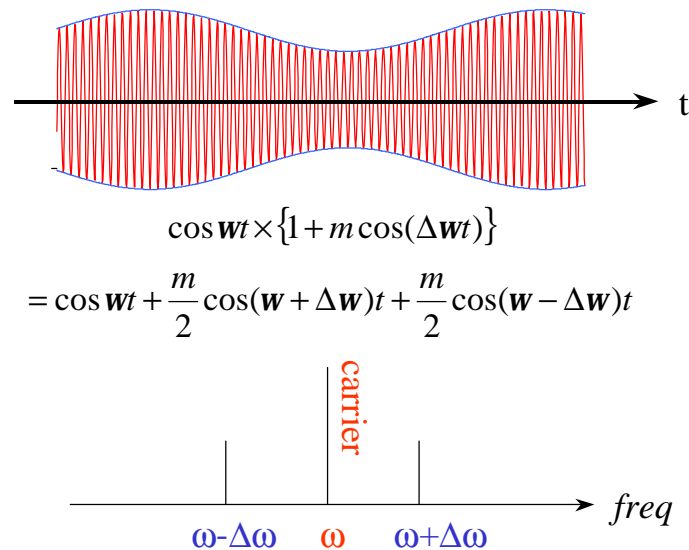


Figure 1.2 Principle of Amplitude Modulation (AM)

The simplest and crudest telecommunication system uses amplitude modulation (AM). In an AM system, the transmitted signal is used to modulate the amplitude of a carrier (Fig. 1.2). This modulation produces side bands, which carry the information.

The transmitted waveform consists of both the pure carrier tone and the side bands due to modulation. An AM receiver is simply an envelope detector, which is physically a square law (intensity) detector, followed by a low pass filter. The squaring operation mixes the side bands with the pure carrier to give the demodulated signal. The transmitted pure carrier is like an externally supplied local oscillator. It travels through the same optical path as the side bands and is always in synchronous with the transmitter. Because of this externally supplied local oscillator, there is no local oscillator required at the receiver, which significantly reduces the complexity of the receiver.

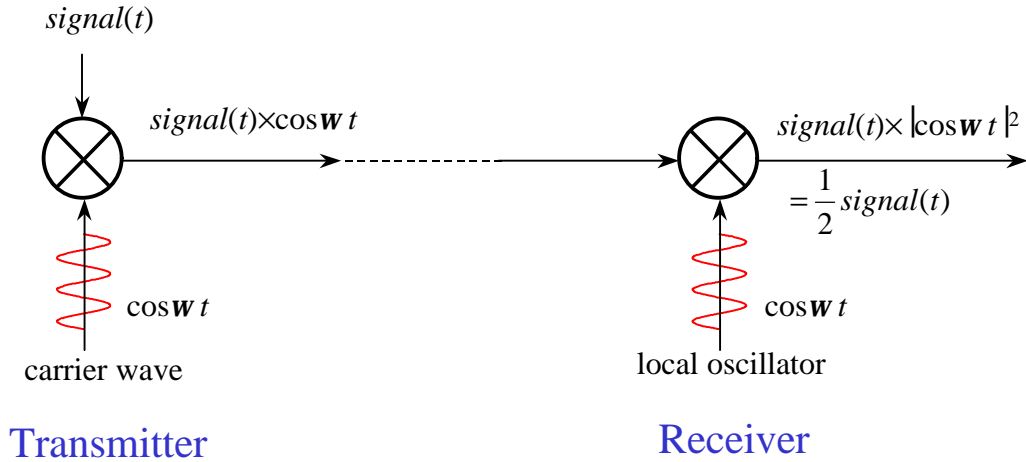


Figure 1.3 Block diagram of coherent homodyne communication system.

Figure 1.3 shows an alternative approach to transmitting information using coherent homodyne communication systems. The signal is mixed with the carrier at the transmitter to generate the side bands that are transmitted to the receiver. At the receiver, in order to recover the information from the side bands, a local oscillator, which regenerates the carrier wave is required. Demodulation is achieved by mixing the local oscillator with the received signal. In order to correctly demodulate the signal, it is

necessary to synchronize the local oscillator with the transmitter carrier using phase locking. In an AM system, on the other hand, the local oscillator is supplied by the transmitter and no phase locking is required.

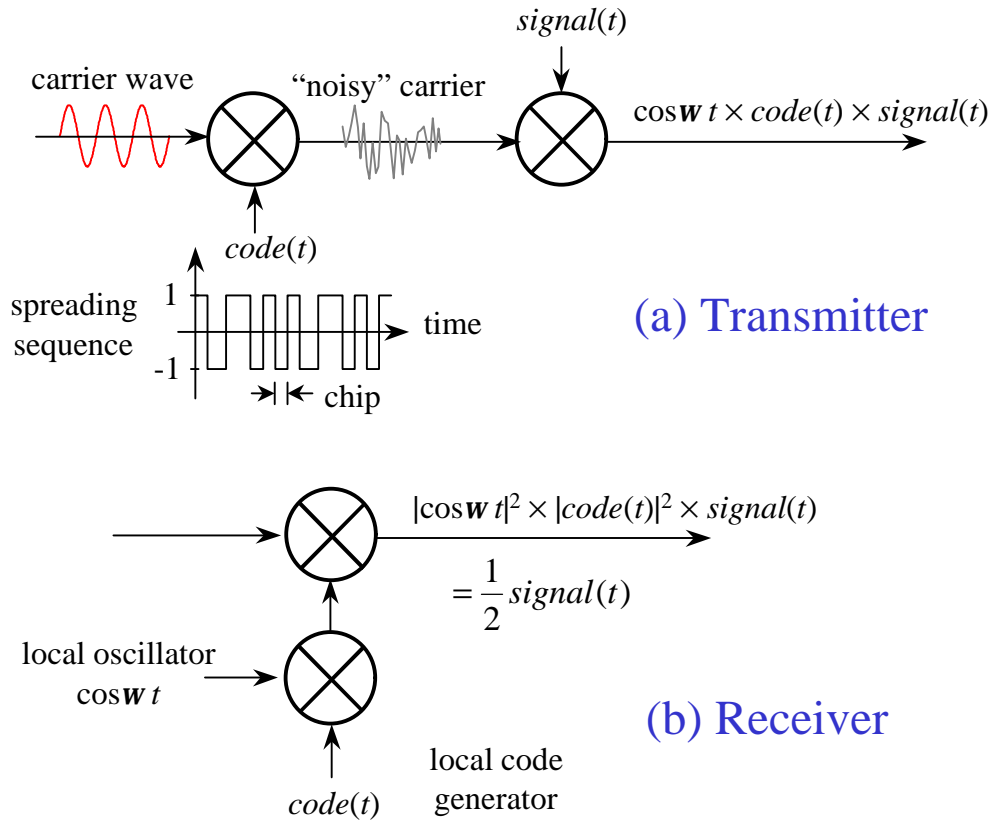


Figure 1.4 Block diagrams of direct sequence spread spectrum (DS-SS) communication system, (a) transmitter and (b) receiver.

Usually, the carrier wave is a pure sinusoidal tone. However, instead of using a pure sinusoid as the carrier wave, one can also "encode" the carrier wave with a secret code to generate a noisy-looking carrier. Shown in Fig. 1.4(a) is the block diagram of a direct sequence spread spectrum (DS-SS) communication system [3,4]. The carrier is first mixed with a pseudo-random spreading sequence. This mixing operation generates a

noisy-looking "carrier" which occupies a bandwidth defined by the bandwidth of the spreading sequence. The encoded carrier is then modulated by the information to obtain the transmitted signal. Usually, the pseudo-random spreading sequence is a high frequency long period sequence, which occupies a much larger bandwidth than the signal bandwidth. Its spectral density can be well approximated as being white Gaussian. It is not difficult to see from the block diagram that the resultant power spectral density due to both the encoding operation and signal modulation is the convolution of the signal spectrum with the code spectrum, centered at the sinusoidal carrier frequency. Thus the signal power is spread over the approximate bandwidth occupied by the spreading code.

The same noisy-looking carrier needs to be used at the receiver to recover the transmitted data. This is obtained using a local oscillator at the receiver [Fig. 1.4(b)] with the exact same code as used at the transmitter for the spreading operation. The reconstructed secret carrier is mixed with the received signal to recover (demodulate) the transmitted data.

On the face of it, spread spectrum communication is very wasteful of bandwidth. However, one can use codes, which are orthogonal to each other, as different channels. In this way, many encoded orthogonal channels can coexist in the same frequency band. The receiver uses the appropriate code to extract the desired channel. This is called *code division multiple access (CDMA)*. Code division multiplexing preserves the total channel capacity when spread spectrum is used [3-6].

There are certain advantages of using spread spectrum or CDMA for communications. First, there is an inherent security enhancement associated with the

spreading and despreading operation. Without knowing the correct CDMA code used for signal spreading at the transmitter, the receiver would not be able to retrieve the signal [3-4, 7-9]. Moreover, since a wide spectrum is used, it is more difficult for a jammer to wipe out the whole spectrum than a narrow band signal [3-4,10]. Therefore, spread spectrum systems are jamming resistant. By spreading the signal over a very wide bandwidth, the average signal spectral density can be below the noise spectral density so that the signal is covert. It is also more difficult for multi-path interference to destroy a whole broad-bandwidth signal than a narrow band signal, because it is impossible to have destructive inference at all the frequency components simultaneously. Thus spread spectrum systems are multi-path resistant [3-6]. The multi-path effect is equivalent to what optics people know as the “speckle” in the spatial intensity distribution of a laser output.

If the code space is made very big, then each user in a CDMA system can pick a code at random without worrying much that it will interfere with other users. This tremendously simplifies network management.

In the DS-SS system shown in Fig. 1.4, the frequency of the sinusoidal carrier is broadened by the spreading code. The spreading code fluctuates in frequency faster than the time required to define the instantaneous frequency. In optical spectroscopy, this defines the condition for homogeneous spectral broadening. Thus DS-SS is analogous to homogeneous broadening in spectroscopy. The first proposed spread spectrum system was actually a frequency hopped spread spectrum (FH-SS) system, in which the carrier frequency changes from time to time according to a pseudo-random hopping sequence.

That is analogous to inhomogeneous broadening in spectroscopy. The FH-SS system was originally patented by the Hollywood actress Hedy Lamarr in 1941 [11]. In her initial disclosure, Lamarr wrote:

"... it is veritabily impossible for an enemy vessel to 'jam' or in any way to interfere with the radio-direction of such a previously synchronized torpedo because, simply, no ship may have enough stations aboard or nearby to 'jam' every air-wavelength possible or to otherwise succeed except by barest accident to deflect the course of oncoming radio controlled torpedo $\frac{3}{4}$ unless, of course, it happened to have the exact synchronization pattern between sender-ship and torpedo."

The invention was then classified and in later years used by the US secret service. Recently, the technology has been commercialized for wireless telephony to improve radio spectrum efficiency, and is now used in all the major US cities.

1.3 Dissertation Organization

In this chapter, we have stated the objective of this project and given a general introduction to the spread spectrum communication technique and CDMA systems. A general review of the previous research on fiber optic CDMA systems, their merits and problems will be given in Chapter 2. The key issues in designing optical CDMA systems will also be stated. A non-coherent, orthogonal and bipolar optical CDMA system using complementary spectral encoding will be presented in Chapter 3. Chapter 3 includes the description of two experimental demonstrations. One demonstration uses wavelength division multiplexing (WDM) components and multi-wavelength sources to realize completely programmable Hadamard codes. Another demonstration uses a novel

cascaded Mach-Zehnder encoder. Performance analysis of non-coherent complementary spectrally encoded optical CDMA will be given at the end of Chapter 3. In Chapter 4, we describe a new multi-wavelength optical CDMA system using phase encoding of a mode-locked laser source which is able to avoid the speckle noise limitation existing in the non-coherent complementary spectrally encoded scheme. We will discuss general demultiplexing complexity (the number of active switches required to demultiplex a single channel out of N multiplexed signals) in TDMA, WDMA and CDMA in Chapter 5. Chapter 6 concludes the dissertation. A novel WDM demultiplexer using rectangular shaped wavelength filters is proposed and computationally simulated in Appendix E. This filter has been used in Chapter 5 for analyzing the demultiplexing complexity of WDMA systems.

Chapter 2 Research and Development in Optical CDMA Systems

2.1 Introduction

Over the last one to two decades, there has been a lot of interest and research in optical CDMA systems. More than 250 papers have been written in this area since 1985 [12]. A vast number of different schemes using time domain or frequency domain encoding approaches have been proposed. Coherent or non-coherent manipulations of optical signals have been used in different proposals and various codes have been devised for optical CDMA systems. In this chapter, we try to give a general review of the previous work.

2.2 Time Domain Encoding Using Optical Delay Line Loops

The first optical CDMA proposals were found in Hui [13] and Prucnal [14-15]. It was intended as a multiple access protocol in a local area network (LAN).

Intensity modulation and direct detection (IM-DD) has been established as the most suitable signal modulation and detection scheme in optical communication systems. Although coherent detection schemes are also possible, it is very costly to have a local oscillator at the optical frequency. In contrast, most radio communication systems make use of coherent schemes, which detect the electrical field. While the optical signal intensity is a positive-only quantity, the electrical field is a bipolar quantity, which can be both positive and negative. In order to preserve the simplicity of IM-DD, optical CDMA systems are designed very differently from their radio versions. The use of the positive-

only intensity detection makes it tricky to achieve full orthogonality in optical CDMA systems.

The earliest optical CDMA proposals made use of optical delay line networks (Fig. 2.1) to encode a high-peak ultra-fast optical pulse into a low intensity pulse train which is multiplexed with the encoded pulse trains from other transmitters at a star coupler. A similar delay line encoder network is used at the receiver to reconstruct the high-peak narrow pulse using conjugate delay lines. The decoding operation is an intensity correlation process. Incorrectly positioned pulses in the pulse train will form a background interference signal. In an intensity correlated system which involves positive only signals, the cross-channel background interference owing to the lack of full orthogonality is quite severe.

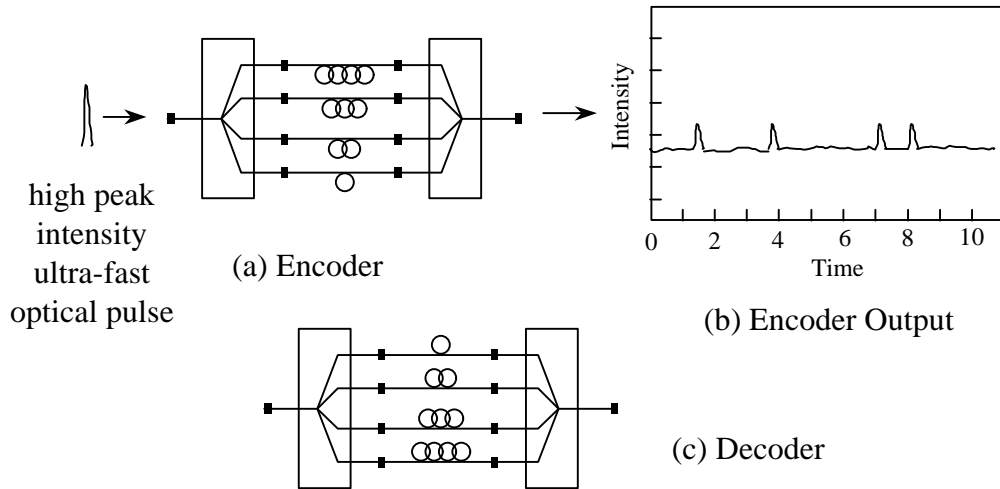


Figure 2.1 Time domain optical CDMA encoding of high peak intensity ultra-short pulses using delay line loops: (a) encoder, (b) encoder output and (c) decoder.

The research in these non-coherent optical CDMA schemes led to the invention of a few major code groups such as optical orthogonal codes (OOC) [16-18], prime

sequence codes [19-20], etc. In order to reduce crosstalk, these codes are all designed to have very long code lengths and small code weights so that there is very little temporal overlap between pulses from different users at the intensity correlator output. The code length is approximately the square of the number of codes that can be reasonably supported.

Because of the long code length and small code weight used, optical CDMA systems using delay line loops are very spectrally inefficient. A sub-picosecond pulsed optical source having a pulse width much smaller than the bit duration is required. Even with very carefully designed codes, co-channel user interference due to non-orthogonality gives a severe performance penalty. The bit error rate (BER) is usually quite high and the number of allowable coactive users is very limited [16-22].

Due to the extremely fast growth in bandwidth demand in the recent years, it is now necessary to make full use of the entire bandwidth capacity available in optical fibers. Engineers are striving to achieve a bandwidth efficiency of one bit per hertz, or even better, in optical communication systems. However, at the time that optical CDMA systems using delay line networks were proposed, it was thought that the tera-bit communication capacity in optical fibers would never be fully utilized. Even multi-gigabit networks were highly respected at that time. Although optics has been used for carrying signals, all the switching and multiplexing operations were performed in the electronic domain. Optoelectronic (OE) and electro-optic (EO) conversions occur at the terminal equipment. The OE-EO conversion was regarded as the bottleneck to "high-speed" multiplexing. Therefore, optical CDMA systems were proposed to make use of

the “redundant” bandwidth in optical fibers to alleviate the electronic processing overhead at the network interface.

Since optical CDMA systems effectively provide a means for asynchronous multiplexing of optical signals, it removes some of the electronic multiplexing overhead and improves the network throughput. Forward error correction (FEC) is not easy in today's high-speed optical communication networks. However, in those days, the channel speed was relatively low and error correction was common in other layer protocols, because the unreliable underlying copper wire medium was assumed much noisier than an optical fiber. Using error correction could compensate for the relatively high BER due to co-channel interference.

Apart from being bandwidth inefficient and having relatively poor BER due to interference, the delay line encoder is also very energy inefficient. Unless each different time delay in the encoded chip sequence is represented by a different wavelength, the power combining process at both the encoder and decoder is very lossy. It is known that a splitting loss of $10\log N$ dB is incurred when N branches are combined. In other words, longer codes suffer from heavier encoding and decoding losses.

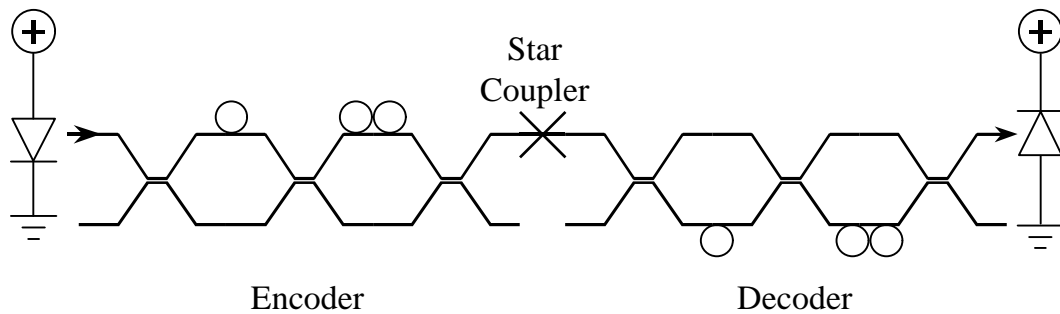


Figure 2.2 Time domain encoding using cascaded ladder encoder.

In order to reduce the splitting loss due to encoding and decoding, a system using the cascaded ladder encoder (Fig. 2.2) has been proposed [23-25]. The cascaded ladder encoder has the form of a Mach-Zehnder interferometer (MZI). Light pulses entering the ladder encoder is split into two halves by a beam splitter. Each half travels through a different path length defined by the delay loop incorporated into the MZI. If the delay loop is long enough, the two separated pulses will not interfere as they would in a normal MZI and they escape from the output of the MZI as a series of lower intensity pulses. Several stages of the ladder encoders with different encoding delay loops can be cascaded to generate longer codes. The power loss due to encoding and decoding is now down to 6dB. However, because of the particular structure used, the number of different codes that can be generated is very limited.

2.3 Coherent Spectral Phase Encoding of Ultra-short Optical Pulses

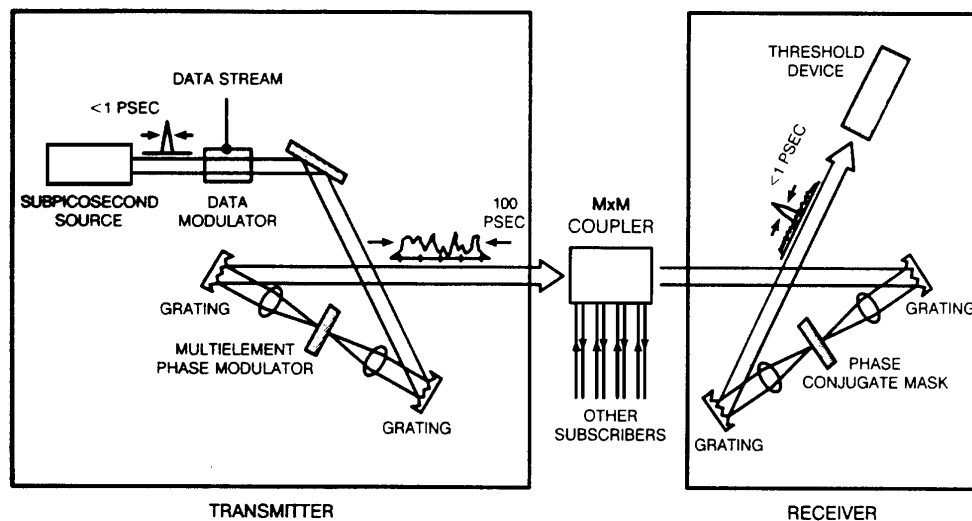


Figure 2.3 Coherent spectral phase encoded optical CDMA system using ultra-short pulses.

Coherent spectral phase encoding was first proposed by Weiner et. al. [26-27]. An ultra-short optical pulse that contains a broad spectrum is spectrally encoded. The spectrum of the ultra-short pulse is first spatially dispersed using a diffraction grating (Fig. 2.3). A spectral phase encoding grid is employed to apply different phase shifts at various spatially resolved spectral components. As a result of the phase encoding, the original sharp ultra-short pulse [Fig. 2.4(c)] in the time domain is transformed into a low intensity signal with longer duration. The broadened pulse duration is approximately inversely proportional to the spectral resolution of the phase encoder.

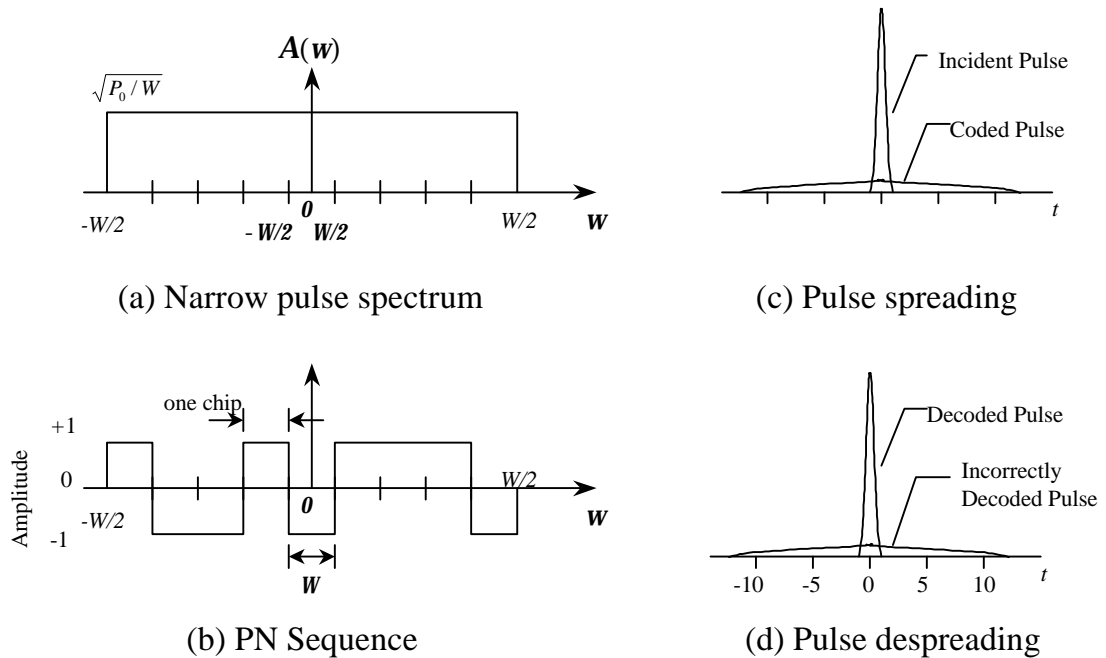


Figure 2.4 Frequency and time domain waveforms of coherent spectral phase encoded system: (a) narrow pulse spectrum, (b) pseudo-random (PN) sequence in frequency domain, assuming 0 and π phase encoding which corresponds to $+1$ and -1 multiplication in amplitude here, (c) pulse spreading due to phase encoding and (d) pulse despreading for matched and unwanted channels.

To decode the signal, a conjugate phase shifter matched to the one used at the transmitter is employed. For matched transmitter output, the phase encoding will be removed at the receiver and the high-peak intensity sharp pulse will be reconstructed. The signals from unmatched transmitters will be further scrambled [Fig. 2.4(d)] at the receiver and they form a background interference. The reconstructed sharp pulse is distinguished from the background signal by an optical threshold device, or by non-linear optics.

Salehi and Weiner [26] investigated codes consisting of arbitrary 0 and π phase shifts which can be considered as +1 and -1 multiplication in amplitude in the frequency domain [Fig. 2.4(a)&(b)]. The encoding and decoding concepts have also been demonstrated experimentally [27].

Similar to the time domain encoded system described previously, the background interference generated by co-channel users degrades the network performance. Moreover, the phase encoding operation is very sensitive to dispersion in optical fibers. To obtain good results, dispersion compensation or dispersion shifted fiber needs to be used. The non-linear optical threshold detection scheme is also very cumbersome to implement.

2.4 Non-coherent Spectral Intensity Encoding

Zacarrin and Kavehrad first described this approach [28-33]. It is similar to the coherent phase encoded system in the sense that the frequency components from a broadband optical source are resolved first. Each code channel then uses a spectral amplitude encoder to selectively block or transmit certain frequency

components (Fig. 2.5). A balanced receiver with two photodetectors is used as part of the receiver. The receiver filters the incoming signal with the same spectral amplitude filter (called the direct filter) used at the transmitter as well as its complementary filter. The outputs from the complementary filters are detected by the two photodetectors connected in a balanced fashion. For an unmatched transmitter, half of the transmitted spectral components will match the direct filter and the other half will match the complementary filter. Since the output of the balanced receiver represents the difference between the two photodetector outputs, unmatched channels will be cancelled, while the matched channel is demodulated.

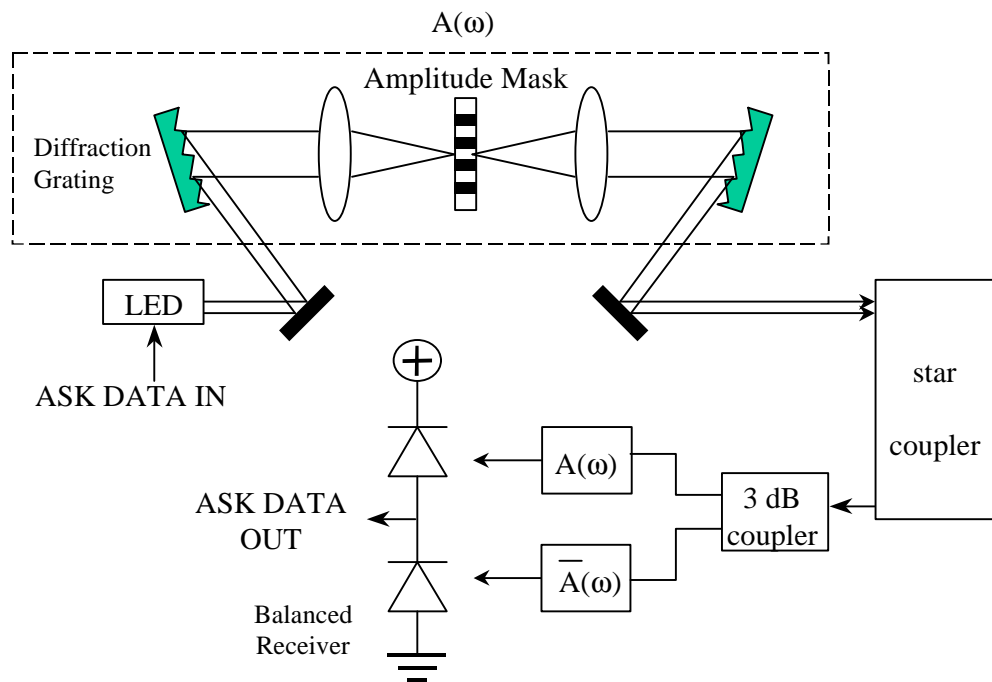


Figure 2.5 Non-coherent spectral intensity encoded optical CDMA system.

Since there is a subtraction between two photodetectors, it is possible to design codes so that full orthogonality can be achieved with the non-coherent spectral intensity

encoding approach. In principle, orthogonality eliminates the crosstalk from other users. Bipolar signaling can also be obtained by sending complementary spectrally encoded signals [32-33]. There is a 3-dB power advantage for bipolar signaled systems. However, the performance of this type of systems is spoiled by the intensity fluctuations arising from the beating between optical waves at the same wavelength, but coming from different users, which we call speckle noise. The details of non-coherent spectral intensity encoded system will be discussed in the next chapter.

2.5 Conclusion: Important Design Issues in Optical CDMA

As pointed out before, in order to achieve efficient spectral usage and to obtain the good performance that the telecommunications community is striving for, it is important to have systems that have full orthogonality so that co-channel crosstalk can be minimized. To achieve full orthogonality, while preserving the simplicity of intensity detection, and to avoid cumbersome coherent detection, is not straightforward. This forms the main challenge in this research.

All optical CDMA networks are generally broadcast and select systems. In a broadcast and select network, the receiver receives the signals from all the transmitters. Ideally, all the unmatched channel signals are cancelled due to orthogonal encoding. Nevertheless, a receiver detects the optical energy from the unmatched transmitters. In spite of signal orthogonality, shot noise does not subtract but is always additive, increasing with the total detected signal intensity. Therefore, detecting the signals from all users gives rise to cumulative shot noise, which amounts to cross-talk and interference.

Another important issue is the speckle noise that we will discuss in the next chapter. In a CDMA system, all the users simultaneously occupy the same frequency-band. They all transmit using the same wavelengths. When light waves of the same wavelengths from different users fall onto the photodetectors simultaneously, they will interfere with each other and give rise to large fluctuations in signal intensity. This is called speckle noise and can be even more severe than cumulative shot noise, as we will see.

Code orthogonality, shot noise and speckle noise, are the three important fundamental issues in the design of optical CDMA systems and they form the foci of this dissertation.

Chapter 3 Non-coherent Spectral Intensity Encoded Bipolar Optical CDMA Systems

In this chapter, we describe our non-coherent spectral intensity encoded optical CDMA system. While being non-coherent and employing intensity detection, this system is nonetheless able to achieve full orthogonality and bipolar signaling. Two demonstrations will be described in this chapter. (1) The first employs commercially existing wavelength division multiplexing (WDM) components and Hadamard Codes and (2) the second employs a novel cascaded Mach-Zehnder encoder. Unfortunately, the performance of these types of systems is limited by speckle noise, and we will give the performance analysis in this chapter.

3.1 Principle

The block diagram of a non-coherent spectral intensity encoded bipolar CDMA system is shown in Fig. 3.1. As mentioned before, one of the important goals here is to obtain full orthogonality. The optical signal intensity that we are dealing with here is a positive quantity. However, to achieve full orthogonality, both positive and negative quantities are required. The way to obtain negative quantities with the positive optical intensity signal is use an analog subtraction operation. A balanced receiver does the analog subtraction. The output from the balanced receiver is the difference of the signals detected by the two photodetectors, which is sometimes positive and sometimes negative.

The 0 and 1 binary digits are represented by two complementary encoded spectra. So if a 0 bit is transmitted, a directly encoded spectrum is transmitted and if a 1 bit is

transmitted, its complementary spectrum is transmitted. The filter in front of the balanced receiver sends all the frequency components in the direct spectrum (of the matched transmitter) to the upper photodetector and those in the complementary spectrum to the lower photodetector. Therefore, the complementary encoded spectra are interpreted as positive and negative (bipolar) outputs. Unmatched channels are encoded such that half of its spectral components are matched to either of the two complementary spectra of the transmitter filter, no matter whether a 0 or 1 is transmitted. Therefore, the balanced receiver cancels the unmatched channel signals, and full orthogonality is achieved.

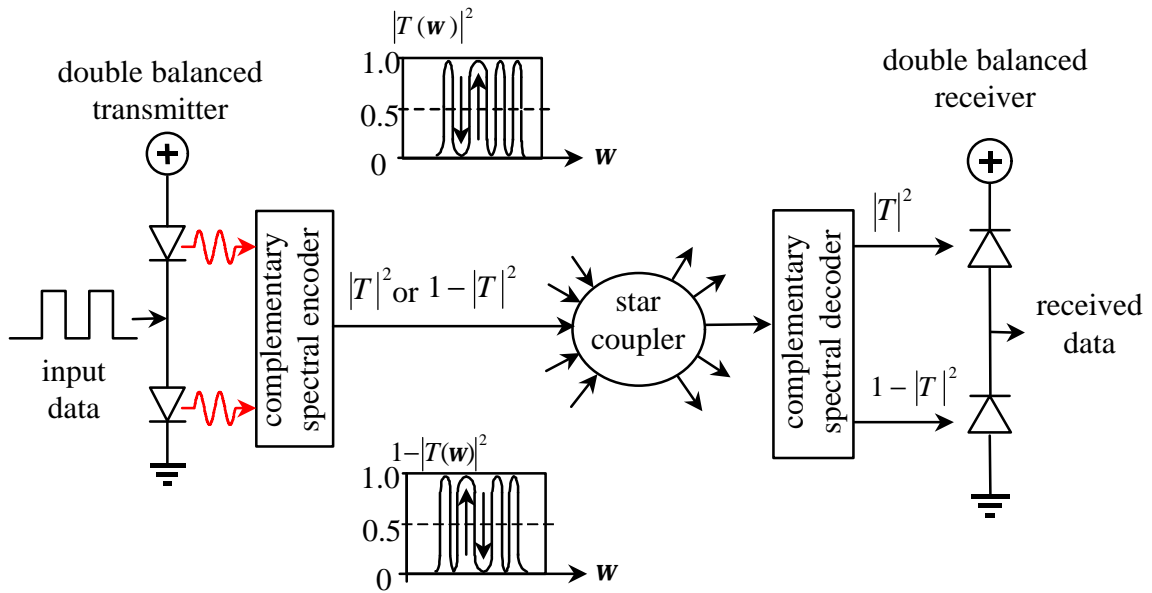


Figure 3.1 System structure of bipolar spectrally encoded optical CDMA. A balanced broadband source is spectrally encoded and received by a balanced receiver. The complementary spectra produced by the spectral filter, $|T|^2$ and $1 - |T|^2$, represent the complementary intensity transfer functions of the spectral filter outputs.

A novel electrically driven balanced transmitter is used to generate complementary spectra. It consists of a pair of broadband light sources connected in a balanced fashion. The input data differentially modulate the intensity of the two balanced light sources. Examples of broadband sources are super luminescent light emitting diodes (SLDs), erbium doped fiber amplifiers (EDFA) biased into super-luminescent mode, mode-locked lasers, and multi-wavelength laser diode arrays. The spectra of the broadband sources pass through a spectral encoder, which selectively transmits or blocks certain spectral components. In the next sections, we will describe two experimental demonstrations.

3.2 Experimental Demonstration Using WDM Components and Hadamard Codes

The transmitter and receiver structures are shown in Fig. 3.2. In the transmitter, two wavelength division demultiplexers are used to disperse the outputs from the balanced transmitter. An array of 2×2 optical switches are employed to select each wavelength component from either one of the two broadband optical sources to the transmitter output.

When a switch b_i in the array is in the BAR state, wavelength I_i from the upper optical source of the balanced transmitter is transmitted, while I_i from the lower optical source is transmitted when the switch b_i is in the CROSS state. The states of the switches, $\{b_1, b_2, \dots, b_n\}$, thus define the encoded spectrum at the output WDM multiplexer. Data modulation is achieved by direct modulation of the balanced optical

sources, generating the direct and complementary encoded output spectra defined by $\{b_1, b_2, \dots, b_n\}$ for the 0 and 1 bits. The encoded spectra from various transmitters are broadcast to the receivers through a star coupler.

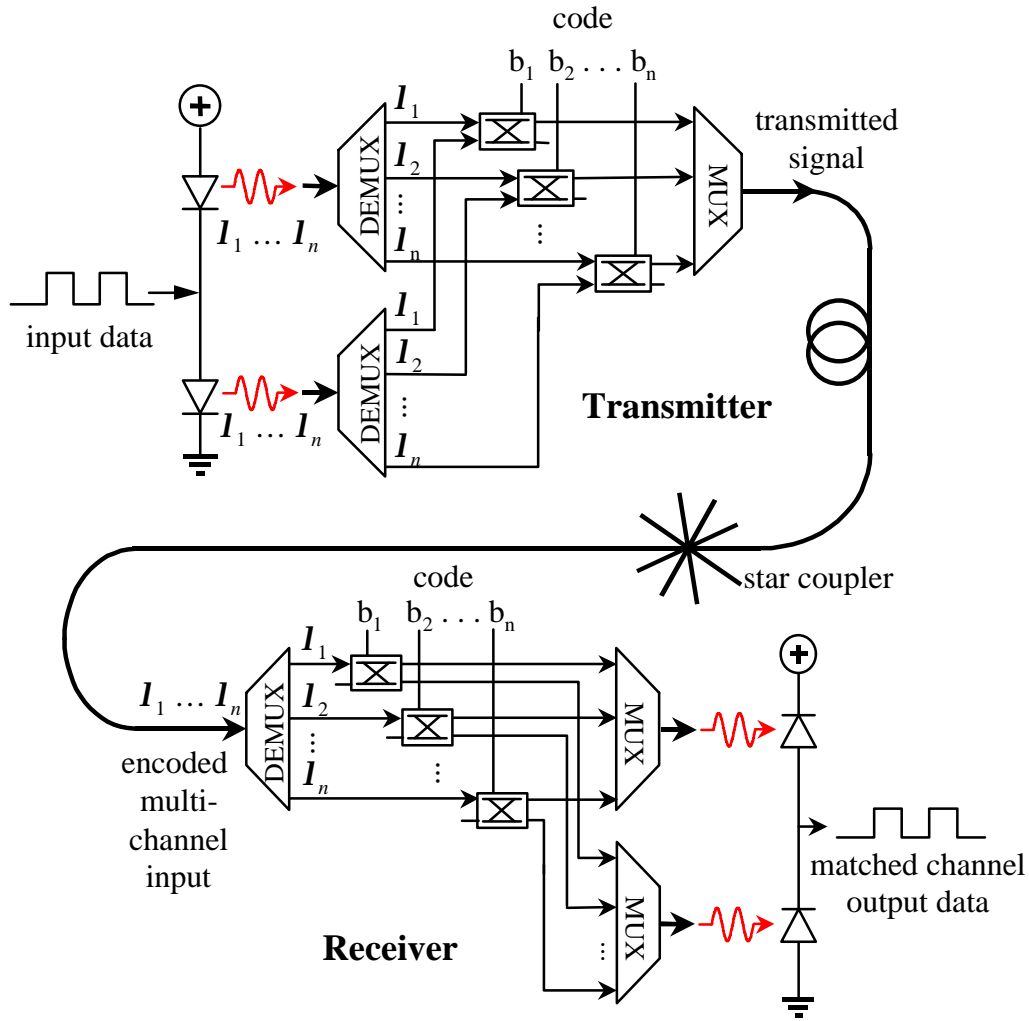


Figure 3.2 Balanced differential opto-electronic CDMA transmitter and receiver. The outputs from the two input sources produce complementary spectra. Modulation is performed by alternating between the two input sources electrically. For matched encoding functions, either a +1 or a -1 is registered at the balanced receiver output depending on whether the transmitter sends a direct spectrum or its complementary spectrum. Unmatched channels are rejected as zero output.

Figure 3.2 also illustrates the details of the decoder. The decoder has a similar structure as the encoder, but provides the reciprocal optical path. The same encoding switch array is used for the decoding purpose. The received multi-wavelength signal is first decomposed in the wavelength domain using a WDM demultiplexer. The 2×2 switch array combines the spectral components corresponding to a direct encoded spectrum of the matched transmitter at the upper photodetector, and those corresponding to its complementary encoded spectrum at the lower photodetector. Therefore, in a matched channel, the direct and complementary encoded spectra produce a +1 and -1, respectively, at the output of the balanced detector. However, a signal from an unmatched transmitter results in the received spectrum equally split between the two complementary spectral outputs of the decoder, generating zero output at the balanced detector.

An experimental prototype was constructed to demonstrate this idea. In this demonstration, a four-wavelength laser diode array is employed as the broadband optical source. The four wavelengths are $\lambda_1 = 1542\text{nm}$, $\lambda_2 = 1547\text{nm}$, $\lambda_3 = 1552\text{nm}$, and $\lambda_4 = 1557\text{nm}$, corresponding to the passband peaks of the four-wavelength WDM multiplexers used in the setup. In order to emulate the balanced transmitter, a 2×2 electro-optic switch is employed to route the laser diode array output between the two input ports of the encoder (Fig. 3.3). The 2×2 optical switch is driven by a $2^{15}-1$ pseudo-random pattern at 155 Mbps which serves as the input data. Hadamard codes [35], which are obtained by selecting as codes the rows of a Hadamard matrix, are used in this experiment. Details about Hadamard Codes can be found in Appendix A. The 4×4

Hadamard matrix used in this experiment has the rows (1111), (1010), (1100) and (1001). Each bit in a code vector corresponds to a wavelength component. Each row of the Hadamard matrix corresponds to an encoded spectrum. For example, the (1010) row represents the situation of setting the 2×2 switches corresponding to λ_1 and λ_3 to the BAR state, and others to the CROSS state. The (1111) row corresponds to on-off keying of all the wavelengths and is not used since it is a trivial code. The decoded signal is received by a commercial balanced photodetector, followed by an amplifier and a low pass filter to remove the out of band high frequency noise.

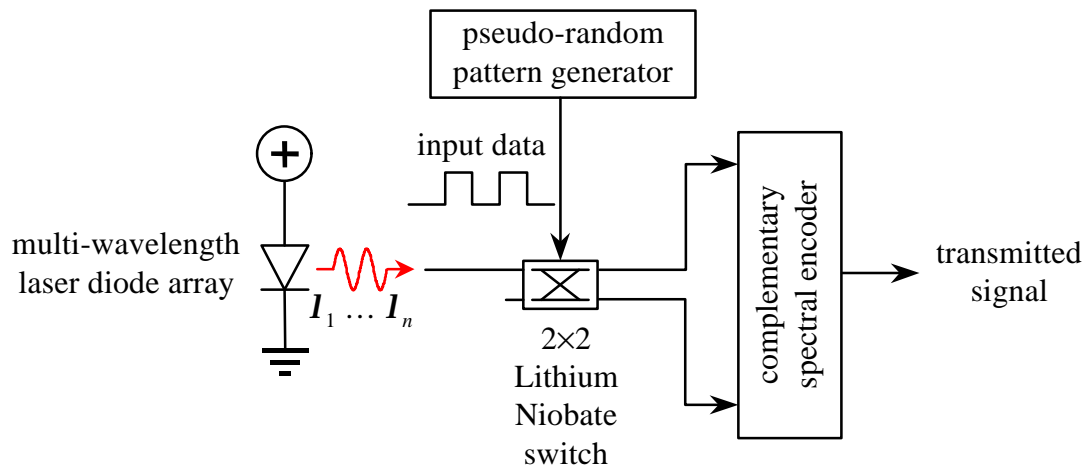
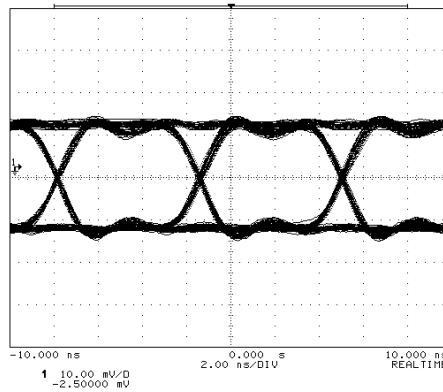


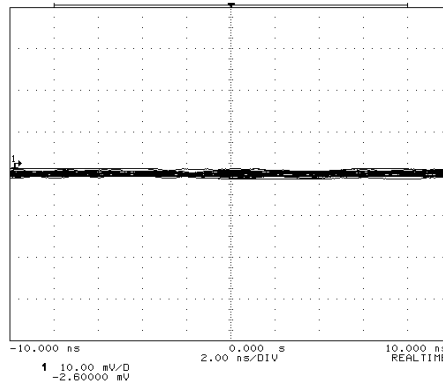
Figure 3.3 Experimental set-up used to emulate the balanced transmitter. A multi-wavelength laser diode array output is switched between the two input ports of the encoder using an electro-optic 2×2 switch which is driven by the input data obtained from a $2^{15}-1$ pseudo-random pattern generator.

Figure 3.4(a) shows the eye diagram of an error free transmission at 155 Mbps with the encoder and decoder both set to (1010). The rejection of the unmatched spectrum at (1100) and (1001) by the decoder are also shown in Fig. 3.4(b) and 3.4(c),

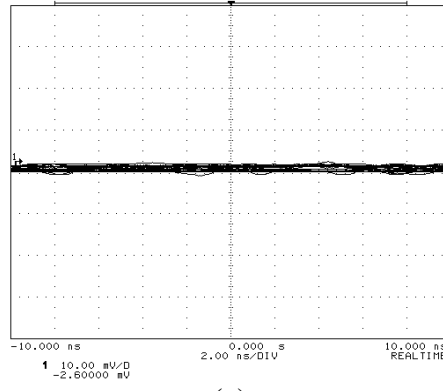
respectively. For both unmatched spectra, the output from the balanced detector is almost zero and a rejection ratio of better than 20dB is achieved.



(a)



(b)



(c)

Figure 3.4 Eye diagrams obtained for the (1010) encoding when the receiver is set to decode: (a) the matched code (1010); (b) the unmatched code (1100) and (c) the unmatched code (1001). Error free transmission is obtained for the matched code. Unmatched codes are rejected.

The bit-error-rate (BER) for the matched spectrum of (1010) is plotted against the received optical power in Fig. 3.5. A BER of 10^{-9} is obtained for a received optical power of -22.25 dBm. The measured BER is mainly limited by the noise of the detector pre-amplifier, which has a noise equivalent power of $40\text{pW}/\sqrt{\text{Hz}}$.

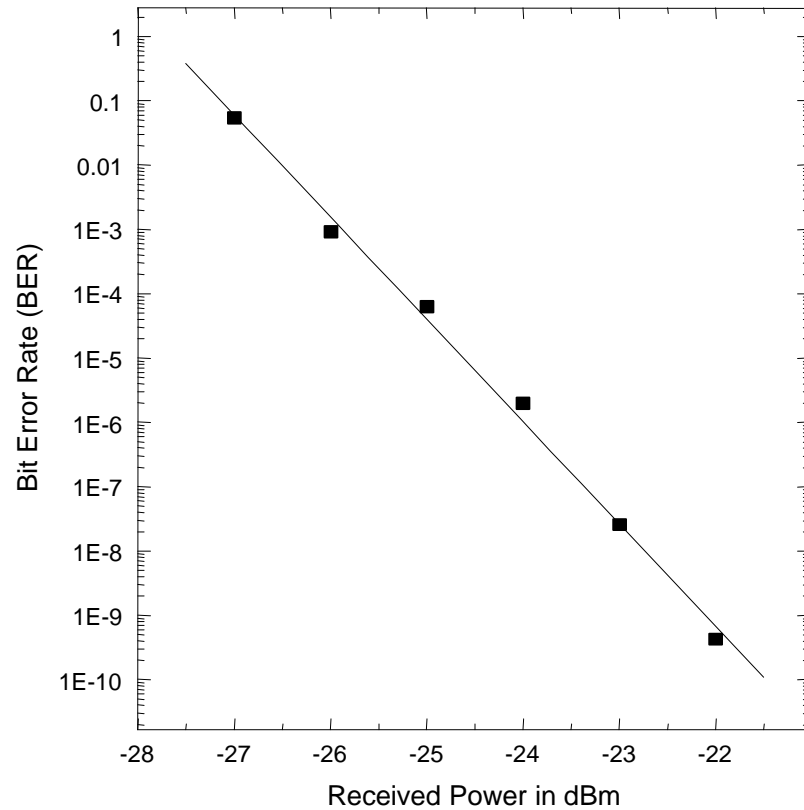


Figure 3.5 The BER plot against the received power at 155Mbps speed for the matched transmitter and receiver pair, which uses the code (1010).

Fast code hopping in nanoseconds can be realized by using electro-optic switches in the encoder and decoder for high security applications and for optical packet switching. The uniformity of the extinction ratios within the switch array is a potential concern for channel crosstalk. Under the scheme of balanced detection, non-uniform extinction ratios of the cross-bar switches may introduce a finite output for unmatched

channels as crosstalk. However, as the number of wavelengths increases, this crosstalk is reduced due to statistical averaging. The number of wavelengths also determines the size of code family, system capacity and security. Current state-of-the-art monolithic multi-wavelength distributed feedback laser arrays provide 40 wavelengths [36]. Alternatively, mode-locked lasers, which have been demonstrated with 206 wavelengths [37] could also be used. Free space diffraction gratings and arrayed waveguide WDM multiplexer-demultiplexers (MUX-DEMUX) with more than 100 wavelengths are available [38].

With a moderate number of wavelengths, the security of the system can be improved by permuting the wavelengths first before an orthogonal encoding is imposed. Also, since each transmitter transmits energy for both the 0 and 1 bits, attempted demodulation by simple amplitude detection fails. In the presence of multiple users transmitting asynchronously on the same channel, it is even more difficult to extract the information unless the correct code is used. Moreover, since each wavelength can be independently controlled, the producible code book can be very general and is only limited by physical properties such as the available source bandwidth and the WDM MUX-DEMUX resolution, etc.

3.3 Experimental Demonstration Using a Cascaded Mach-Zehnder Encoder

The encoder and decoder structures shown in the previous section using cross-bar switches appears quite complicated. In order to reduce the complexity of the encoder and decoder, we propose a novel cascaded Mach-Zehnder encoder in this section.

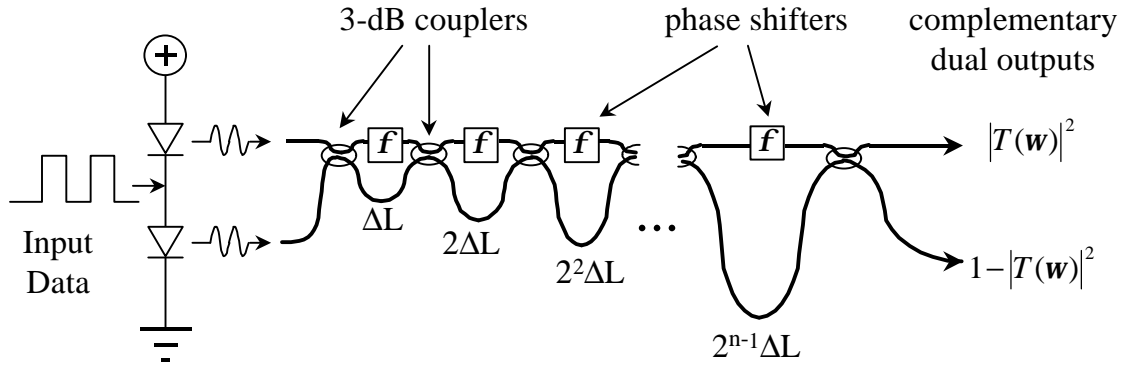


Figure 3.6 The schematic diagram of a multistage Mach-Zehnder encoder. Complementary outputs are produced at each output by switching on and off the balanced sources alternately. The phase shifters produce the different spectral outputs.

A natural way to generate complementary spectra is to use a Mach-Zehnder interferometer (MZI) [34]. Figure 3.6 shows the schematic diagram of a cascaded Mach-Zehnder (MZ) encoder that has been used in our experiment. When a broadband input is applied to one of the MZI input ports, complementary spectral output are generated at the two output ports due to the phase delays in the unbalanced arms. The MZ encoder is designed in such a way that the path length difference of each stage doubles that of the previous stage. A phase shifter is incorporated in each stage to tune the encoded output. The frequency domain intensity transfer function of a single stage MZI is just a simple sinusoid versus frequency. If the path length difference in the two arms is doubled, the free spectral range (FSR) of the MZI will be halved. In addition, if a $\pi/2$ phase shift is applied to one arm, then the original sine transfer function will change to cosine. Therefore, by cascading MZIs with different FSR and change the phase encoding at each stage from 0 to $\pi/2$, a very complicated encoding spectrum can be realized.

Furthermore, when the input source to a MZ encoder is switched from one input port to the other, the original complementary spectral outputs will swap their positions at the two output ports. Hence, by differentially modulating the input sources at the balanced transmitter, complementary spectral outputs are generated at the MZI output ports. This forms the basis of our Mach-Zehnder based complementary spectral encoder for bipolar optical CDMA.

Mathematically, we can represent the complementary spectral intensity transfer function of the Mach-Zehnder encoder of user k as:

$$T_k(\boldsymbol{\omega}) = \frac{1}{2} + f_k(\boldsymbol{\omega}) \quad (3.1)$$

$$\text{and } \overline{T_k(\boldsymbol{\omega})} = \frac{1}{2} - f_k(\boldsymbol{\omega}) \quad (3.2)$$

where $-1/2 \leq f_k(\boldsymbol{\omega}) \leq 1/2$. Here, we have chosen $1/2$ as the reference level for the transfer function without loss of generality.

If the broadband source has a power spectral density $A(\boldsymbol{\omega})$ in the frequency range from $\boldsymbol{\omega}_1$ to $\boldsymbol{\omega}_2$, the encoded signals of the k th user when a 0 bit and a 1 bit are transmitted are:

$$X_k(\boldsymbol{\omega}) = X_k^0(\boldsymbol{\omega}) = A(\boldsymbol{\omega}) \cdot T_k(\boldsymbol{\omega}) \quad (3.3)$$

$$\text{and } X_k(\boldsymbol{\omega}) = X_k^1(\boldsymbol{\omega}) = A(\boldsymbol{\omega}) \cdot \overline{T_k(\boldsymbol{\omega})} \quad (3.4)$$

The balanced detector output of the j th receiver due to the k th transmitter is:

$$Y_{jk} = \int_{\boldsymbol{\omega}_1}^{\boldsymbol{\omega}_2} \Re X_k(\boldsymbol{\omega}) [T_j(\boldsymbol{\omega}) - \overline{T_j(\boldsymbol{\omega})}] d\boldsymbol{\omega} \quad (3.5)$$

where \Re is the responsivity of the balanced photodetectors.

Assuming $A(\mathbf{w}) = 1$ and the responsivity \Re is constant in the frequency range of interest $\mathbf{w}_1 \leq \mathbf{w} \leq \mathbf{w}_2$, the output is:

$$Y_{jk} = \begin{cases} \Re \int_{\mathbf{w}_1}^{\mathbf{w}_2} f_j(\mathbf{w}) + 2f_k(\mathbf{w})f_j(\mathbf{w})d\mathbf{w} & 0 \text{ bit} \\ \Re \int_{\mathbf{w}_1}^{\mathbf{w}_2} f_j(\mathbf{w}) - 2f_k(\mathbf{w})f_j(\mathbf{w})d\mathbf{w} & 1 \text{ bit} \end{cases} \quad (3.6)$$

For big enough encoded spectral range $\mathbf{w}_2 - \mathbf{w}_1$, i.e. $\mathbf{w}_2 - \mathbf{w}_1 \gg 1/\tau_{\min}$ where τ_{\min} is the time delay introduced by the encoder stage with the least propagation path imbalance, $\int_{\mathbf{w}_1}^{\mathbf{w}_2} f_k(\mathbf{w})d\mathbf{w} \approx 0$. Therefore, orthogonal codes are obtained when $f_k(\mathbf{w})$ and $f_j(\mathbf{w})$ are orthogonal:

$$\int_{\mathbf{w}_1}^{\mathbf{w}_2} f_k(\mathbf{w})f_j(\mathbf{w})d\mathbf{w} = 0 \quad i \neq j \quad (3.7)$$

In this case, the input power spectrum due to an unmatched channel is split equally at the two optical output ports of the receiver.

For the matched transmitter and receiver pairs, the detected signal is:

$$Y_k = Y_{kk} = \begin{cases} +2\Re \int_{\mathbf{w}_1}^{\mathbf{w}_2} f_k^2(\mathbf{w})d\mathbf{w} & 0 \text{ bit} \\ -2\Re \int_{\mathbf{w}_1}^{\mathbf{w}_2} f_k^2(\mathbf{w})d\mathbf{w} & 1 \text{ bit} \end{cases} \quad (3.8)$$

which is bipolar.

The frequency transfer function of a multistage Mach-Zehnder interferometer can be easily obtained as follows. Each 3-dB beam splitter can be represented using a 2×2 transfer matrix [34]:

$$S = \frac{1}{\sqrt{2}} \begin{pmatrix} 1 & j \\ j & 1 \end{pmatrix} \quad (3.9)$$

A delay line of length L and a phase shifter with phase shift q can be modeled as:

$$D(L, \mathbf{w}) = \begin{pmatrix} e^{-j\frac{wL}{2c}} & 0 \\ 0 & e^{j\frac{wL}{2c}} \end{pmatrix} \quad (3.10)$$

and $\Phi(q) = \begin{pmatrix} e^{-j\frac{q}{2}} & 0 \\ 0 & e^{-j\frac{q}{2}} \end{pmatrix}$ (3.11)

where $j = \sqrt{-1}$ and c is the speed of light. The total transfer function of an n stage Mach-Zehnder interferometer is thus given by:

$$\begin{aligned} H(\mathbf{w}) &= S\Phi(\mathbf{q}_n)D(L_n, \mathbf{w})S\Phi(\mathbf{q}_{n-1})D(L_{n-1}, \mathbf{w})\Lambda S\Phi(\mathbf{q}_1)D(L_1, \mathbf{w})S \\ &= \begin{pmatrix} h_{11}(\mathbf{w}) & h_{12}(\mathbf{w}) \\ h_{21}(\mathbf{w}) & h_{22}(\mathbf{w}) \end{pmatrix} \end{aligned} \quad (3.12)$$

The complementary power spectral transfer functions $T(\mathbf{w})$ and $\overline{T(\mathbf{w})}$ can be found from:

$$\begin{pmatrix} T(\mathbf{w}) \\ \overline{T(\mathbf{w})} \end{pmatrix} = \begin{pmatrix} |h_{11}(\mathbf{w})|^2 \\ |h_{12}(\mathbf{w})|^2 \end{pmatrix} \quad (3.13)$$

The analytical expression of Equation (3.13) is not analytically tractable but it can be calculated numerically using the computer. Figure 3.7 shows the computed frequency transfer function of the seven stage MZI shown in Fig. 3.6. The longest delay stage corresponds to a free spectral range of 10GHz. All the phase shifters are set to zero. The plots represent a spectral encoding function, which is very complicated and therefore has good qualities to be used for secure data transmissions.

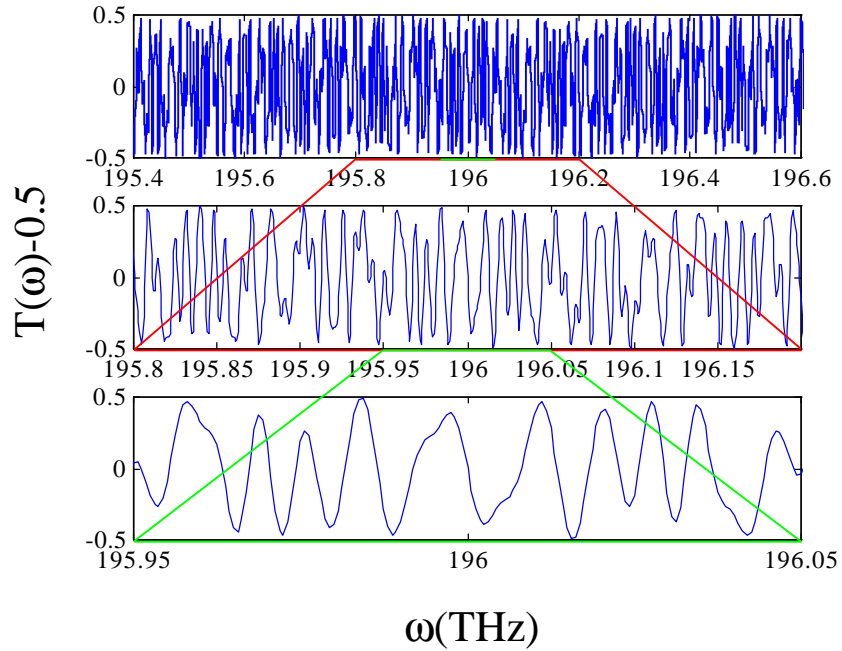


Figure 3.7 The simulated spectral output from a seven-stage Mach-Zehnder encoder. The free spectral range is 640GHz in the computation. The complicated spectral output represents a secret code. The two lower diagrams are the expanded sections of the diagram above them as indicated by the grey lines.

To demonstrate the principle of the balanced transmitter and cascaded Mach-Zehnder encoder, a pair of multi-stage Mach-Zehnder encoders were fabricated on single-mode rectangular Silica waveguide. The optical path differences in the Mach-Zehnder interferometers are chosen such that the longest stage Mach-Zehnder has a free spectral range of 10GHz. As shown in Fig. 3.6, the path difference in each Mach-Zehnder interferometer stage is twice that of the previous stage. The total free spectral range of the encoder is 640GHz for the fabricated waveguide. Thin film heaters are incorporated in the MZI stages to introduce variable phase shift at various stages by the thermo-optic effect. Each thin film heater has a resistance of about 50Ω and is able to generate a 2π

phase shift with 4W input heating power. A thermo-electric cooler removed the waste heat. The phase shifts and the MZI arm imbalance are transformed into spectral intensity modulation in the MZI outputs. Fig. 3.8 shows the layout of the fabricated encoder on a 64mm × 44.5mm silicon wafer. The thin film heaters are omitted in Fig. 3.8. The waveguide device is packaged and pigtailed as shown in Fig. 3.9 so that it can be easily used in experiments. Appendix B contains the procedure to calibrate the MZ encoders so that they can be “matched” in the experiment.

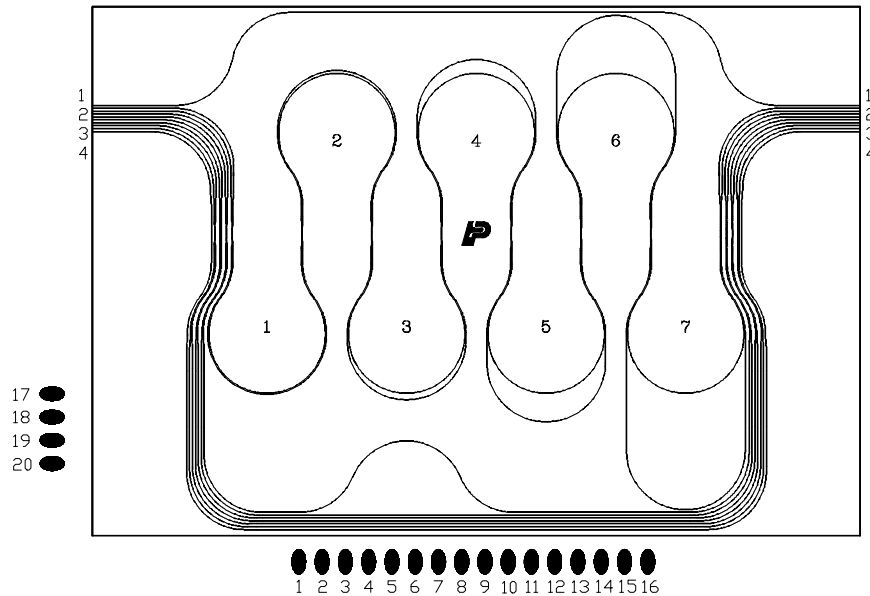


Figure 3.8 Layout of the experimental 7-stage Mach-Zehnder encoder. The black dots are connectors to thin film heaters and thermo-electric temperature stabilizers.

A continuous broadband source, as opposed to the discrete multi-wavelength source used in the previous section, was employed in this experiment. Instead of using differentially modulated LED’s as shown in the block diagram in Fig. 3.1, to demonstrate

the concept, we used a homemade EDFA pumped in to the super-luminescent mode as our light source (Fig. 3.10). Since the output of an EDFA is already within the single mode fiber, it obviates the need to couple super-luminescent LED's to single mode optical fibers. The EDFA output has a 3-dB bandwidth of about 10nm around the 1530nm center wavelength. To emulate a balanced transmitter, the output of the EDFA is switched between the two input ports of the transmitter Mach-Zehnder (MZ) encoder using a commercial electro-optic 2x2 optical switch (UTP, 2x-150-010-B-1-2), which is driven by the input data stream obtained from a pseudo-random pattern generator. The super-luminescent EDFA, 2x2 electro-optic switch and the multistage MZ encoder comprise the transmitter.

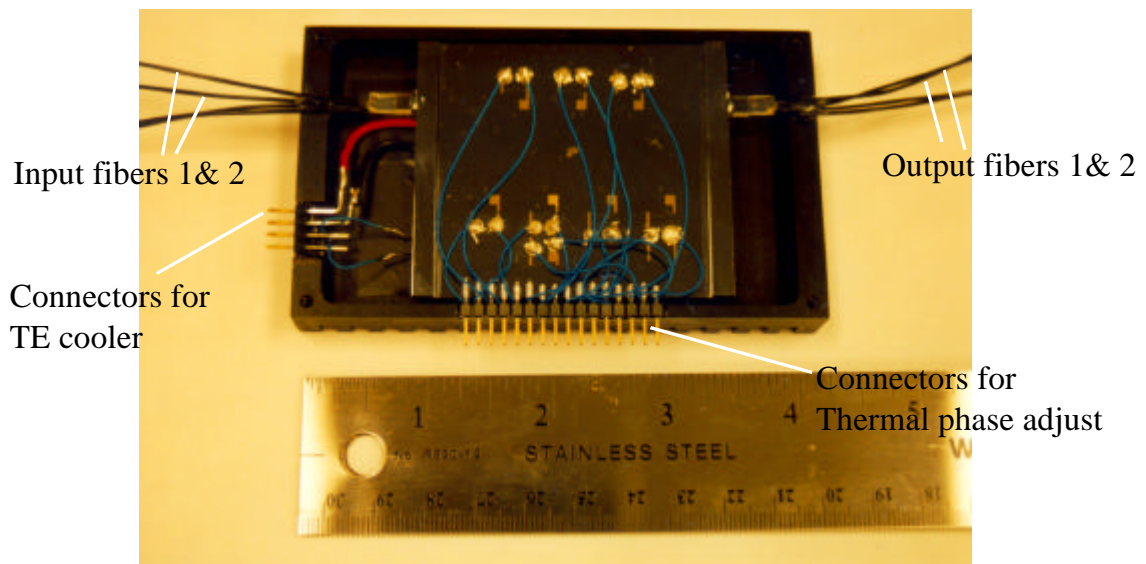


Figure 3.9 A pigtailed 7-stage Mach-Zehnder encoder diagram.

The system set-up is shown in Fig. 3.10. The encoded signal is amplified by a second EDFA to compensate for the insertion loss of the components in the optical path. The amplified signal is received by the receiver, which uses the same multistage MZI as

the decoder. The outputs of the MZI decoder are connected to a balanced receiver. Electrical currents are applied to the thin film heaters in the MZ encoder and decoder. The system is driven by an HP708434 bit error rate test-set (BERT) which generates a $2^{15}-1$ pseudo-random bit pattern and measures the BER at the receiver. Figure 3.11 shows the optical breadboard for the experiment.

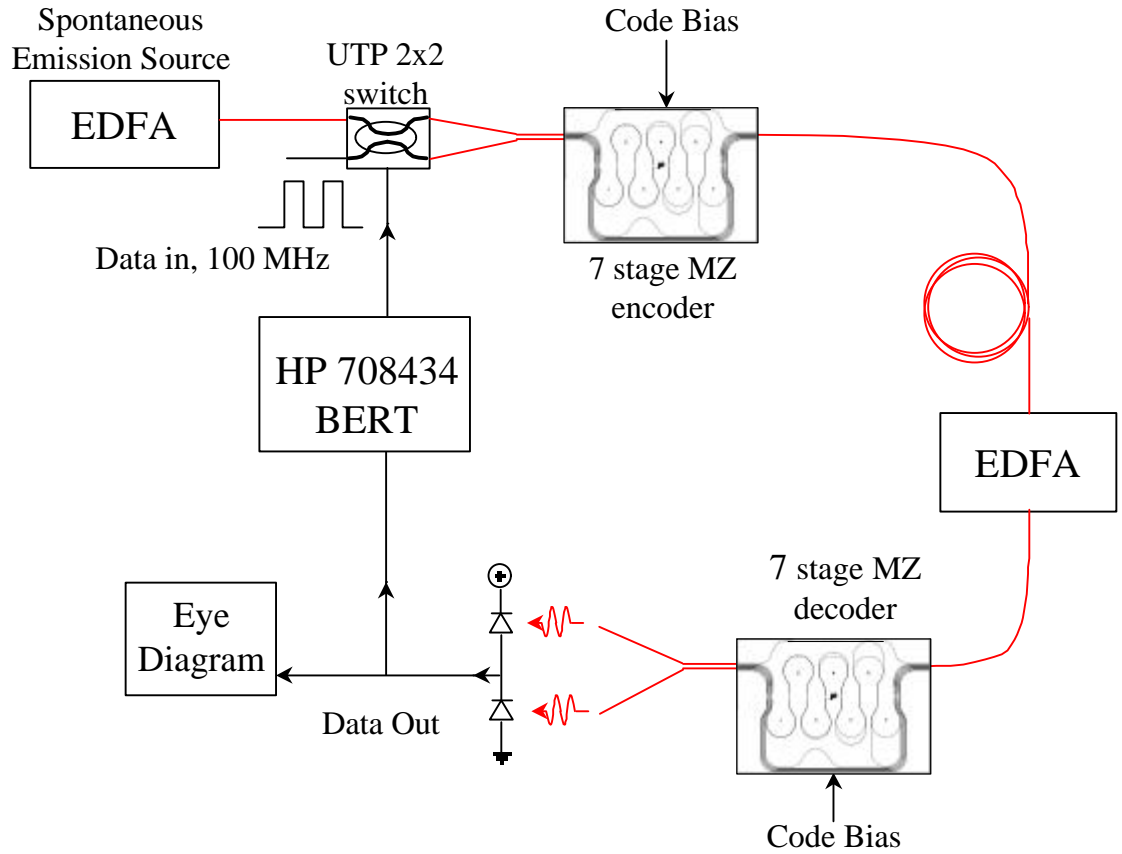


Figure 3.10 The experiment setup to demonstrate the non-coherent spectrally encoded bipolar CDMA system.

When the transmitter code setting matches the receiver code by tuning the phase shifters in the encoder and decoder, the transmitted signal is recovered at the receiver. When the transmitter and receiver code settings are made different by introducing

$\pi/2$ phase shifts at any stage, the decoder outputs are balanced and the receiver gives zero output. This confirms the rejection of unmatched codes. Fig. 3.12 shows the eye diagram at the receiver output for a pair of matched codes in a test run with a $2^{15}-1$ pseudo-random bit sequence. The eye is closed when the codes are unmatched at the transmitter and the receiver. The fluctuations in the high and low levels of the eye diagram are due to spontaneous emission noise in the output of the EDFA. Spontaneous emission noise is analogous to “speckle” noise except that it arises from multiple Er atoms rather than multiple users. The eye diagram corresponds to a BER of 10^{-9} at a data rate of 100MHz.

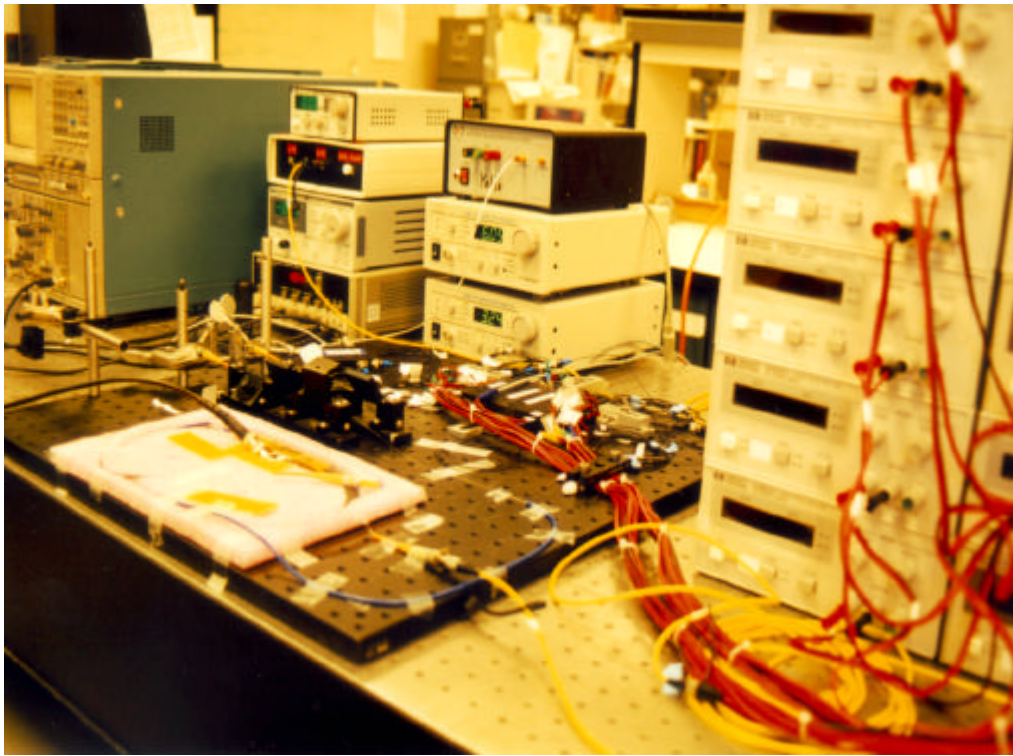


Figure 3.11 Picture of the optical breadboard setup for the experiment of non-coherent spectral intensity encoded optical CDMA system using cascaded Mach-Zehnder encoder.

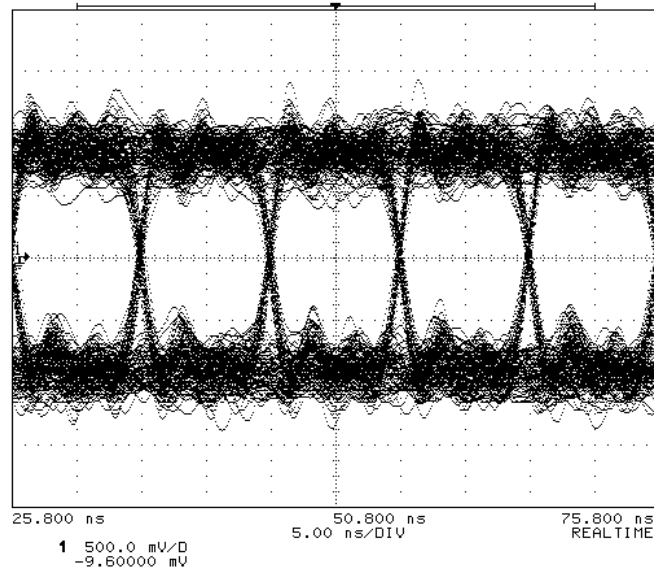


Figure 3.12 An eye-diagram taken at 100Mbps speed using a $2^{15}-1$ pseudo-random bit sequence. The measured BER is 10^{-9} .

3.4 Performance Evaluation

In this section, we discuss the noise and interference mechanisms in non-coherent spectrally encoded bipolar optical CDMA systems and assess the fundamental performance limitation of these types of systems.

We assume that each receiver receives equal power P_{rec} from each transmitter. In the best case, all the codes are orthogonal to each other and we assume this is the case. Ideally, when the transmitter code and the receiver code are matched to each other, all the received power goes to either the upper or the lower photodetector of the receiver¹

¹ This happens when the $f_k(\mathbf{w}) = \pm 1/2$ in Equations (3.1) and (3.2).

depending on whether a 0 or a 1 bit is sent by the transmitter. Otherwise, the balanced receiver will receive equal power $P_{rec}/2$ by both of its photodetectors. Perfectly orthogonal codes that satisfy the above conditions have been proposed and studied by other authors [29, 32-33]. Therefore, the photocurrent generated at the balanced receiver output is:

$$I_{sig} = \begin{cases} +\Re P_{rec} & \text{for a 0 bit} \\ -\Re P_{rec} & \text{for a 1 bit} \end{cases} \quad (3.14)$$

As in all other communication systems, the receiver is subject to thermal noise given by [34]:

$$\langle I_{th}^2 \rangle = \frac{4kT}{R_L} B_d = 8p k T B_d^2 C \quad (3.15)$$

where k is the Boltzman constant, T the temperature and R_L the receiver load resistance. We have also used $B_d = 1/T_b = 1/2pR_L C$ in equation (3.15) where T_b is the bit period and C is the load capacitance. For state-of-the-art technology, C is ≈ 0.02 pF. At a receiver bit rate of 1Gbps, the thermal noise is $\sqrt{\langle I_{th}^2 \rangle} = 4.57 \times 10^{-8}$ A.

We will see shortly that in non-coherent spectrally encoded CDMA systems, the shot noise and the speckle noise set the lower limit for multiple access interference and will limit the capacity of these kinds of systems.

As described before, in the presence of multiple active users, the detectors in the balanced receiver detect the unbalance at the matched transmitter in the presence of all the other interfering users whose transmitted powers are cancelled at the balanced

detector. Although the average signal due to the interferers are cancelled, the large optical signal at each detector give rise to significant shot noise, which does not cancel.

Suppose K users are active, $K-1$ of which are unmatched interfering users. Assume the codes are ideal. Since unmatched channel power splits equally at the photodetectors of the balanced receiver, if a 0 is detected, the upper and lower detectors will detect power,

$$P_U = P_U^0 = P_{rec} + \frac{K-1}{2} P_{rec} \quad (3.16)$$

$$\text{and } P_L = P_L^0 = \frac{K-1}{2} P_{rec} \quad (3.17)$$

respectively.

Similarly, if a 1 is transmitted:

$$P_U = P_U^1 = \frac{K-1}{2} P_{rec} \quad (3.18)$$

$$\text{and } P_L = P_L^1 = P_{rec} + \frac{K-1}{2} P_{rec} \quad (3.19)$$

The output photocurrent for a transmitted 0 is:

$$\begin{aligned} I_{sig} &= I_U - I_L \\ &= \mathfrak{R}P_U - \mathfrak{R}P_L \\ &= \begin{cases} +\mathfrak{R}P_{rec} & \text{for a 0 bit} \\ -\mathfrak{R}P_{rec} & \text{for a 1 bit} \end{cases} \end{aligned} \quad (3.20)$$

In either case, the shot noise in the output is given by [43]:

$$\begin{aligned} \langle I_{sh}^2 \rangle &= \langle I_{sh-U}^2 \rangle + \langle I_{sh-L}^2 \rangle \\ &= 2qI_U B_d + 2qI_L B_d \\ &= 2q\mathfrak{R}P_{rec} K B_d \end{aligned} \quad (3.21)$$

We can see that multiple users degrade the performance of the system by increasing the shot-noise proportionately. For a received power of -20dB ($10\mu\text{W}$) per active user at a receiver bit rate of 1Gbps , using $\mathfrak{R}=0.8\text{A/W}$ for a typical InGaAs PIN photodiode working at $1.5\mu\text{m}$ wavelength range, the shot noise is $\sqrt{\langle I_{sh}^2 \rangle}=5.06\times 10^{-8}\text{A}$ for one user.

Shot noise is due to the particle nature of light [39]. However, in an environment where all the users share the same bandwidth and transmit simultaneously, the incoherent summation of signal powers of the same wavelengths will give rise to excessive fluctuations in the detected power due to the wave nature of light which undergoes constructive and destructive interference [40-42]. The same mechanism also gives rise to the spatial intensity variations in coherent images called “speckle”. For this reason, we call the intensity fluctuation due to the interference from other users **speckle noise**. In fact, the spontaneous emission noise that we saw in the eye-diagram in Fig. 3.12 is also due to the same mechanism. The spontaneous emission from multiple atoms can be regarded an ensemble of non-coherent oscillators. They interfere with each other and give rise to intensity fluctuations in space and time. Speckle fluctuations on the balanced detector are fluctuations in space, but they become time dependent fluctuations as the signals are modulated.

The speckle noise model for a detector detecting a photocurrent I is [40]:

$$\langle I_{sp}^2 \rangle = I^2 \frac{2B_{elec}}{mM\mathbf{n}_{opt}} \quad (3.22)$$

where B_{elec} is the electrical bandwidth of the photodetector and \mathbf{n}_{opt} is the optical bandwidth used. M is the number of modes in a fiber if multi-mode fiber is used and $m=1$ for polarized light and $m=2$ for unpolarized light. The speckle noise is usually cancelled in a double balanced detector as common mode fluctuation [43-44]. However, in the non-coherent spectrally encoded CDMA system, the two photodetectors detect signals coming from different, non-overlapping, complementary spectral components. Instead of having common mode rejection, the speckle noises at the two photodetectors are uncorrelated and add in the balanced detector output. In addition, if B_{opt} is the total optical bandwidth encoded, only one half of the total spectrum will fall on each photodetector, $\nu_{opt} = B_{opt}/2$, because of spectral filtering. $\Re P_U$ and $\Re P_L$ give the photocurrent. Therefore, the output speckle noise is given by:

$$\begin{aligned}
\langle I_{sp}^2 \rangle &= (\Re P_U)^2 \frac{2B_d}{mMB_{opt}/2} + (\Re P_L)^2 \frac{2B_d}{mMB_{opt}/2} \\
&= \Re^2 (P_U^2 + P_L^2) \frac{4B_d}{mMB_{opt}} \\
&= \Re^2 P_{rec}^2 \left[\left(\frac{K-1}{2} \right)^2 + \left(1 + \frac{K-1}{2} \right)^2 \right] \frac{4B_d}{mMB_{opt}} \\
&= \Re^2 P_{rec}^2 (K^2 + 1) \frac{2B_d}{mMB_{opt}}
\end{aligned} \tag{3.23}$$

In our experimental system, since single mode fiber components are used, and the waveguide devices are polarization dependent, $M = m = 1$. There are two important observations from Equation (3.23). First, speckle noise power is proportional to the signal power $I_{sig}^2 = \Re^2 P_{rec}^2$. When the system is speckle noise limited, increasing the signal power would not improve the signal to noise ratio. Second, the speckle noise

grows as K^2 and is the most important noise mechanism when the number of simultaneous users is high. Equation (3.23) also indicates that using more optical frequencies, and multi-mode components, can offset speckle noise. The wider the optical bandwidth used and the more spatial modes in an optical fiber, the more speckle averaging takes place, and the smaller the noise. In our setup, most of the optical power is concentrated in a 10nm wavelength range around the 1530nm center wavelength. Even in the absence of spatially interfering users, speckle noise is still present due to the random nature of the spontaneous emission source. Taking $M = m = 1$, $B_{opt} = 10\text{nm} = 1.28\text{THz}$, other parameters being the same as before, we obtain $\sqrt{\langle I_{sp}^2 \rangle} = 4.5 \times 10^{-7}\text{A}$ for $K=1$. It can be seen that when K is bigger than one, the speckle noise is the most important noise in a non-coherent spectral-intensity encoded CDMA system.

Assuming a large number of active users so that the distribution of shot noise and speckle noise can be approximated as Gaussian, the three noise components arising from different mechanisms are independent and the total noise is their sum:

$$\langle I_n^2 \rangle = \langle I_{th}^2 \rangle + \langle I_{sh}^2 \rangle + \langle I_{sp}^2 \rangle \quad (3.24)$$

The bit error rate in a bipolar signaling scheme is [46-45]:

$$BER = \frac{1}{2} \left[1 - \text{erf} \left(\sqrt{\frac{E_b}{N_0}} \right) \right] \quad (3.25)$$

and
$$\frac{E_b}{N_0} = \frac{I_{sig}^2}{\langle I_n^2 \rangle} \quad (3.26)$$

Figure 3.13 shows the BER plotted against the number of co-channel users at various received power levels. One gigabit per second data rate is assumed for each user

and the optical bandwidth used is assumed to be 5THz (40nm in wavelength). Figure 3.13(a) is plotted for single mode fiber and Fig. 3.13(b) is plotted for a graded index multi-mode fiber with 62.5 μ m core diameter². 324 modes are used in the simulation for this type of fiber (see Appendix C). Owing to the lack of mode averaging for speckle noise in the single mode system, the system is speckle noise limited and increasing the received optical power does not improve the BER in Fig. 3.13(a) (all the curves overlap). Because of mode averaging and relatively small received power, Fig. 3.13(b) falls between the shot noise limited and speckle noise limited scenarios. It is seen from Fig. 3.13(b) that for a -20dbm (10 μ W) received power per user, 34 concurrent users are allowed for a BER less than 10⁻¹⁵ and 51 are allowed for a BER less than 10⁻⁹.

To estimate the throughput, we assume for simplicity, that transmission is lossless except for the splitting loss at the star coupler. Signal propagation loss and connector loss can be easily accounted for by scaling up the transmitter power proportionally. For a network with K subscribers, the received power per user will be P_t/K . In the worst case scenario, all K subscribers are transmitting at the same time. If the system is shot noise limited (e.g. when a large optical bandwidth and multi-mode fiber with many modes are used), the throughput is given by (see Appendix D):

$$(KB_d)_{sh} = \frac{RP_t}{2qK \cdot SNR} \quad (3.27)$$

² This is the most commonly installed fiber in buildings.

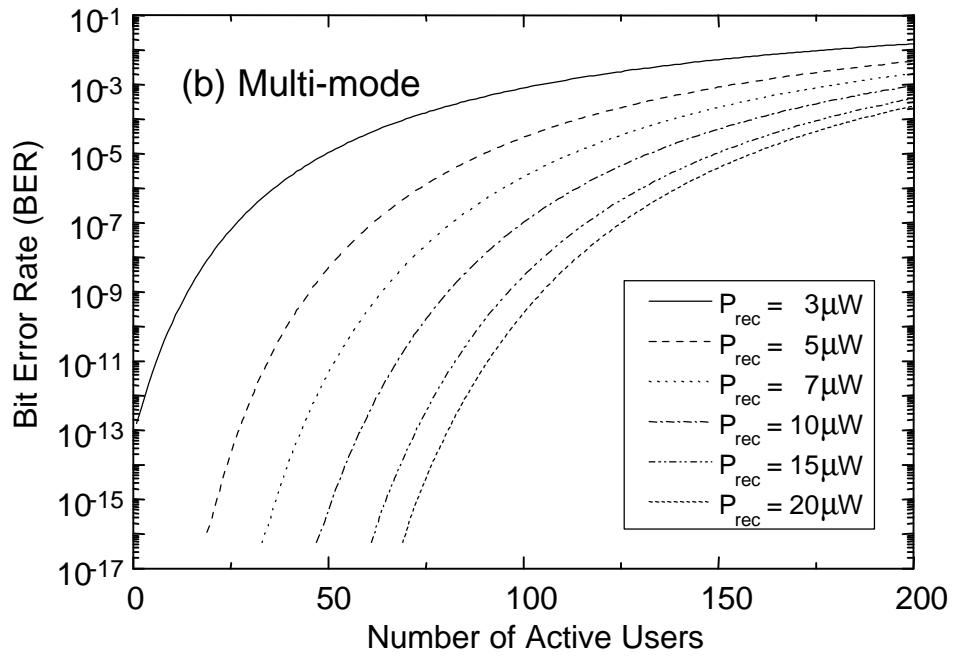
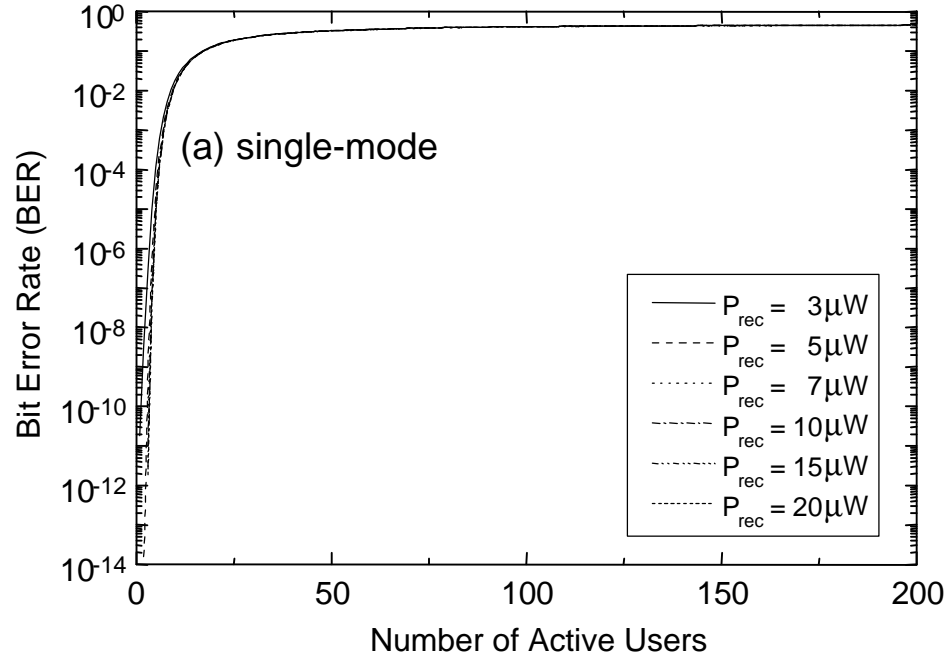


Figure 3.13 Bit Error Rate (BER) vs. number of active users for (a) single-mode system and (b) multi-mode system.

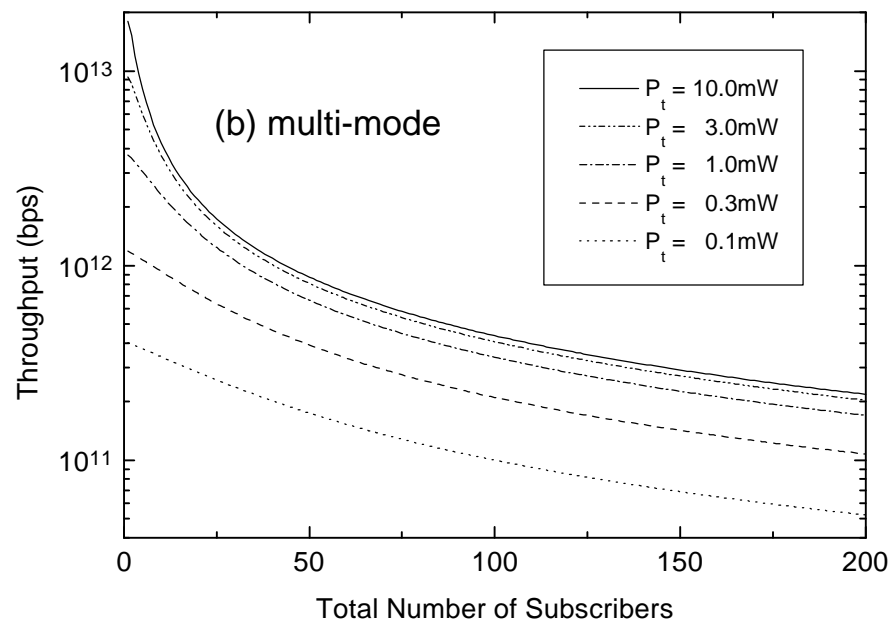
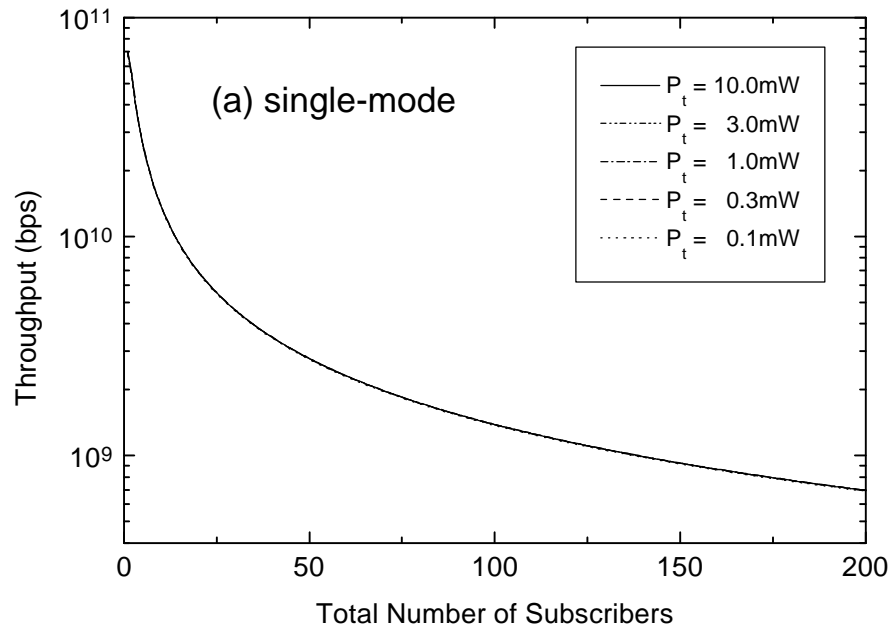


Figure 3.14 Throughput vs. number of subscribers for (a) single-mode and (b) multi-mode systems.

For a large number of users transmitting at moderate power, the system will be speckle noise limited and the throughput is given by (again see Appendix D):

$$(KB_d)_{sp} = \frac{B_{opt}M}{2K \cdot SNR} \quad (3.28)$$

In both cases, the throughput decreases as more users are added to the system. However, when the system is speckle noise limited, the throughput is independent of the transmitted power as expected. Fig. 3.14(a) and Fig. 3.14(b) plot the throughput against K , the number of subscribers, for single mode and multi-mode cases. All the subscribers are assumed active at the same time and the BER is fixed at 10^{-9} . Again, all the curves in Fig. 3.14(a) overlap, showing no improvement for increased transmitter power for a single mode system. Fig. 3.14(b) shows the system operated between the shot noise limited and speckle noise limited scenarios when multi-mode fibers are used. It is seen from Fig. 3.14(b) that when the transmitter power and the number of subscribers are increased, the system approaches the speckle noise limit and further increase of the transmitted power does not give much improvement to the throughput.

3.5 Discussion and Conclusion

Dispersion is a limitation to CDMA systems which all use broadband sources. In CDMA systems employing ultra-short pulses, successful decoding relies upon the reconstruction of the ultra-short pulses, which occupy only a small fraction of a bit period. Especially for coherent schemes [26], dispersion has to be carefully controlled to maintain the optical phase coherence among different spectral components.

Fancy ultra-short pulse sources are unnecessary in the non-coherent spectral intensity encoded system. The encoder and decoder function as spectral intensity filters. The bit energy occupies the full bit period. The proposed system is therefore less vulnerable to dispersion problems.

In fact simple analysis shows, that for the same total aggregate bit rate throughput U , the dispersion limited signal propagation distance for TDM, WDM and our CDM systems are:

$$L = L_T = \frac{f_0^2}{U^2 \mathbf{h}c} \quad \text{TDM} \quad (3.29)$$

$$L = L_W = \frac{K^2 f_0^2}{U^2 \mathbf{h}c} \quad \text{WDM} \quad (3.30)$$

$$L = L_C = \frac{Kf_0^2}{U^2 \mathbf{h}c} \quad \text{CDM} \quad (3.31)$$

where \mathbf{h} is the fiber dispersion coefficient in ps/nm/km and f_0 is the center frequency. In our CDMA system, for example, if a 40nm optical bandwidth is used for encoding and the channel speed is 1Gbps, the dispersion limited transmission distance is about 1km, which is adequate for typical LAN applications.

The transmitter modulates at the data rate and the receiver uses direct detection, which is a mature technology in optical links. However, in systems using ultra-short pulses [26-27], clumsy non-linear optical threshold detection schemes such as second harmonic generations are required for demodulation.

It can be shown that the non-coherent spectral intensity encoded CDMA system performs better than spectrally sliced WDM systems [47] when a broadband spontaneous emission source is used for multiple access and the number of users simultaneously accessing the network is small. For a system that supports K users, the total spectrum is divided into K slices in both CDM and WDM systems. A Spectral intensity encoded CDMA system makes use of the whole available spectrum and is therefore more power efficient and has better tolerance to shot noise. Furthermore, as we have seen, spontaneous emission source output is associated with coherent noise or speckle noise [40-42] which limits the performance. When a system is speckle noise limited, the signal to noise ratio (SNR) does not depend on the received power but the ratio of the optical bandwidth to the data bandwidth. Because a wider spectrum is used in spectrally encoded CDMA, it helps to improve the speckle noise in a spontaneous emission source.

Access by multiple users in a CDMA network will introduce interference by cumulative shot noise and increased speckle noise. The latter is more important and increases the noise to signal ratio in a CDMA network as the square of the number of active users (Equation 3.23). However, since each user in a spectrally sliced WDM system only detects the wavelength of interest, they do not suffer from cumulative shot noise and increased speckle noise. Therefore, as the number of CDMA users increases, the advantage over spectrally sliced WDM will be quickly lost. Figure 3.15 shows the trend for noise to signal ratio of CDMA and spectrally sliced WDM system versus number of active users in the network. An analysis shows that CDMA performs better than spectrally sliced WDM when the number of active users is less than 14 for a network

using 40nm optical bandwidth, 1GHz data bandwidth, 10mW transmitter power and a network of size $K=100$. For the CDMA system we described previously, about 12 simultaneous active users can be supported at 1Gpbs speed per channel in a 40nm optical band for 10^{-9} bit error rate (BER) in the speckle noise limit. For a spectrally sliced WDM system under speckle noise limit, to obtain the similar performance as the CDMA system, about 69 simultaneous users can be supported, a more than five fold increase in capacity.

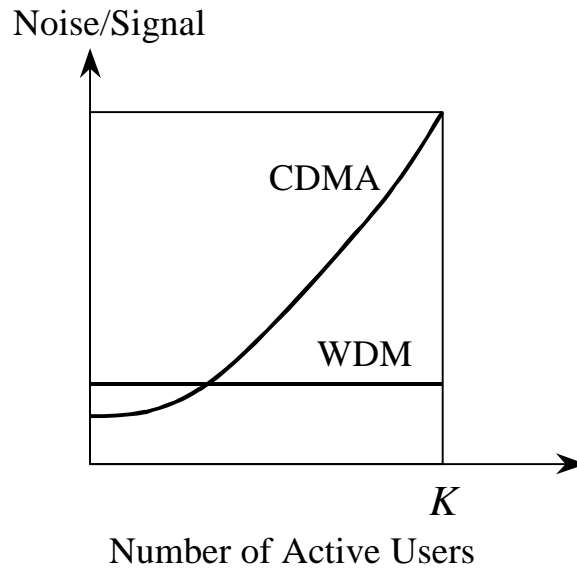


Figure 3.15 Noise to signal ratio versus number of active users for spectral intensity encoded CDMA system and spectrally sliced WDM systems. K is the total number of spectral slices, which corresponds to the total number of allowable users in the system.

In a LAN environment with limited span, most of the loss comes from the splitting loss in the star coupler and component insertion loss, which can be improved by better integration of optical components and by using optical amplifiers. By conservative estimate, given a 10dBm transmitter power, -20 dBm receiver sensitivity, and 15dB

insertion loss in the encoder and decoder, a network with 100 users should be achievable by placing 20dB optical amplifiers after the star coupler. However, this also necessitates a large number of optical amplifiers and renders the system not cost-effective.

In conclusion, we have demonstrated the idea of non-coherent spectral intensity encoded Optical CDMA system using both multi-wavelength source and continuous broadband spontaneous emission source. A novel balanced transmitter has been invented for demonstrating the idea of complementary encoding. We have performed the experiments using both Hadamard codes and a novel cascaded Mach-Zehnder encoder. In both cases, a pseudo-random bit sequence has been successfully transmitted and received. We have also shown adequate unmatched channel rejection in both experiments.

It is proven both in theory and in experiment that full orthogonality can be achieved using non-coherent spectral intensity encoded optical CDMA systems. Unfortunately, the system performance (throughput) is severely limited by speckle interference noise from co-channel users.

Chapter 4 Multi-wavelength Spectral Phase Encoded Optical CDMA Network

Although bipolar signaling achieves full orthogonality, and has the simplicity of being non-coherent, the capacity of the non-coherent spectral intensity encoded system described in the previous chapter is severely limited by speckle noise. In order to avoid speckle noise, we propose the multi-wavelength spectral phase encoded optical CDMA system described in this chapter. Again, a broadcast and select star network (Fig. 4.1) is assumed as the architecture of our multi-wavelength optical CDMA system. A mode-locked laser is used as the broadband optical source for encoding. The mode-locked pulses from each user are synchronized using a time synchronization signal generated by the receiver so that they all arrive at the star coupler at the same time. Absolute optical phase synchronization is not needed.

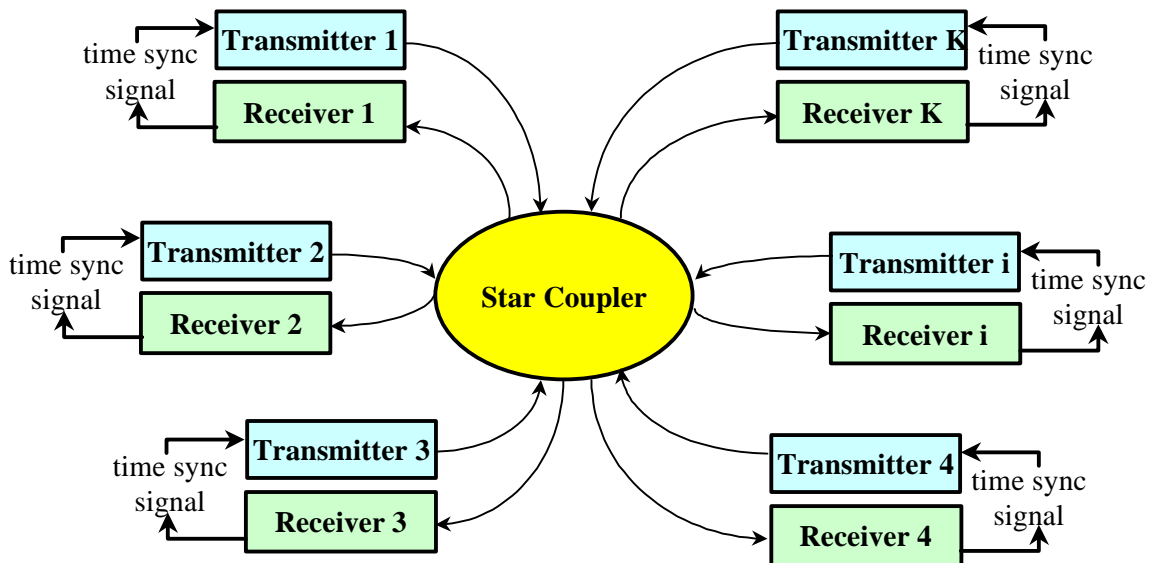


Figure 4.1 Multi-wavelength optical CDMA network.

4.1 Transmitter

The transmitter is shown in Fig. 4.2. A mode-locked laser [48] output is used as the broadband optical source. The output of the mode-locked laser consists of frequency components equally separated in the spectral domain. Because of the phase locking relationship between the spectral components, in the time domain, a mode-locked laser output consists of periodic sharp pulses. If we encode a mode-locked laser output by adding different phase shifts to the various frequency components, the output will come to resemble noise-like periodic bursts. More precisely, the encoded output will look like a multi-mode laser output. This phase encoded mode-locked laser output is our “secret” CDMA carrier. Mathematically, the mode-locked output can be represented by:

$$E(t) = E_0 \exp(i\omega t) \sum_{n=0}^{N-1} \frac{1}{\sqrt{N}} \exp[in(\Delta\omega)t] \quad (4.1)$$

where $\Delta\omega / 2\pi$ is the pulse repetition frequency. The encoded signal from an encoder k is represented by the encoding operation $C_k[E(t)]$ as:

$$C_k[E(t)] = C_k(t) = E_0 \exp(i\omega t) \sum_{n=0}^{N-1} \frac{1}{\sqrt{N}} \exp\{in(\Delta\omega)t + \Phi_{kn}\} \quad (4.2)$$

where Φ_{kn} is the encoded phase on the n th spectral component. The codes are designed to be orthogonal so that two codes C_k and C_h satisfy:

$$C_k \cdot C_h^* = E_0^2 \sum_{n=0}^{N-1} \frac{1}{N} \exp\{i(\Phi_{kn} - \Phi_{hn})\} = E_0^2 \mathbf{d}_{kh} \quad (4.3)$$

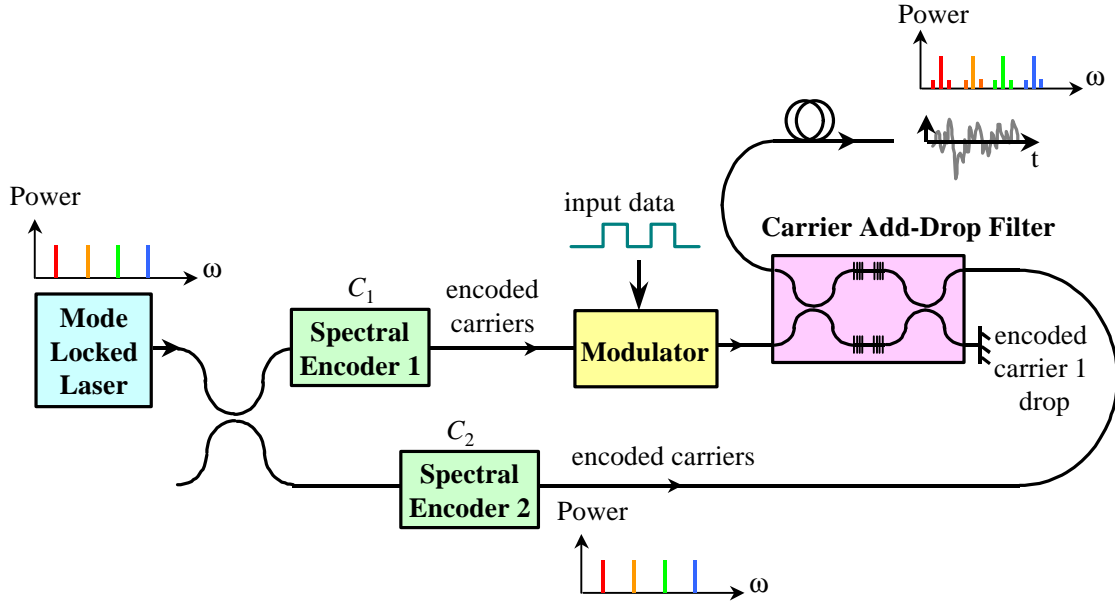


Figure 4.2 Transmitter of multi-wavelength optical CDMA system.

where $d_{kh} = 1$ if $k = h$ and 0 otherwise. From equation (4.3), we observe that the orthogonality is determined by the encoded phase differences between matched frequency components. In the simplest case, if we use 0's and π 's as the encoded phase shifts, the codes correspond to multiplication coefficients of +1 and -1 in amplitude. All the good bipolar codes developed for radio CDMA can be directly applied to our system. One famous family of bipolar orthogonal codes is the Hadamard codes [35], which form rows of a Hadamard square matrix. As another example, two codes are orthogonal when the phase differences between the corresponding spectral components represented by $\exp\{i(\Phi_{kn} - \Phi_{hn})\}$ are uniformly distributed on a unit circle in a complex plane. A new encoder family using cascaded feedback Mach-Zehnder interferometers will be introduced in the latter part of this chapter.

To be more specific, if C_k and C_h are codes from different transmitters, they arrive at the star coupler at different times t_1 and t_2 , then their dot product should be expressed as:

$$C_k(t_1) \bullet C_h^*(t_2) = E_0^2 \exp[i\mathbf{w}(t_1 - t_2)] \sum_{n=0}^{N-1} \frac{1}{N} \exp\{in(\Delta\mathbf{w})(t_1 - t_2) + i(\Phi_{kn} - \Phi_{hn})\} \quad (4.4)$$

which should be compared with Equation (4.3).

In order to maintain orthogonality, we need to synchronize the mode-locked pulses from all the transmitters so that they arrive simultaneously at the star coupler. This is equivalent to say $N(\Delta\mathbf{w})(t_1 - t_2) \approx 0$. So the synchronization requirement is $(t_1 - t_2) \bar{1}/N(\Delta\mathbf{w})$ which is the mode-locked pulse width and the reciprocal of the total CDMA bandwidth. Thus we do not need to synchronize to the absolute optical phase precision between the users. In the following analysis, we assume that all the transmitters are temporally synchronized within the mode-locked pulse width.

Following Fig. 4.2, the mode-locked laser output at the transmitter is separated into two fibers using a 3-dB beam splitter. For the k th user, the first fiber passes through a spectral filter which phase encodes the carrier components as:

$$C_{k,1}(t) = \frac{1}{\sqrt{2}} E_0 \exp(i\mathbf{w}t) \sum_{n=0}^{N-1} \frac{1}{\sqrt{N}} \exp\{i[n(\Delta\mathbf{w})t + \Phi_{kn,1}]\} \quad (4.5)$$

The other fiber's spectral components (for the k th user) are encoded by a different code $C_{k,2}$ in a similar way:

$$C_{k,2}(t) = \frac{1}{\sqrt{2}} E_0 \exp(i\mathbf{w}t) \sum_{n=0}^{N-1} \frac{1}{\sqrt{N}} \exp\{i[n(\Delta\mathbf{w})t + \Phi_{kn,2}]\} \quad (4.6)$$

Continuing in Fig. 4.2, a modulator is placed after the encoded carrier $C_{k,1}$ to impose data modulation. Either phase or intensity modulation could be applied. The modulated output is:

$$X_k(t) = s_k(t)C_{k,1}(t) \quad (4.7)$$

where $s_k(t)$ is the data signal for the k th user. For amplitude shift keying (ASK) $s_k(t)$ takes the values 0 and +1 while for phase shift keying (PSK), $s_k(t)$ is either +1 or -1. Modulation generates information-carrying side bands $s_k(t)C_{k,1}(t)$ around the pure carrier tones $C_{k,1}(t)$. The side bands and the encoded carrier $C_{k,2}(t)$ are combined using a carrier add/drop filter, and then transmitted to the receiver.

The idea of artificially combining a carrier with side bands is emulating amplitude modulation (AM). As explained in Chapter 1, AM has a neat feature that the carrier and the side bands are transmitted together to the receiver. The receiver, usually an envelope detector, demodulates the signal by mixing the side bands with the carrier. The transmitted carrier functions like a transmitter supplied local oscillator (LO), removing the need to have an LO at the receiver. Also, since the carrier and the side bands travel through the same path, they experience the same phase shifts and are always phase synchronized.

For the same reason, we transmit the carrier to the receiver as an externally supplied LO. However, the carrier and side bands are separately encoded so that the receiver will not be able to demodulate the signal by simple envelope detection. First, this enhances the security of the system. Secondly, encoding the carriers suppresses the

interference of carriers from different transmitters by imposing an orthogonal code onto each carrier.

Thus, the transmitted signal for the k th user is:

$$Y_k(t) = s_k(t)C_{k,1}(t) + C_{k,2}(t) \quad (4.8)$$

4.2 Receiver

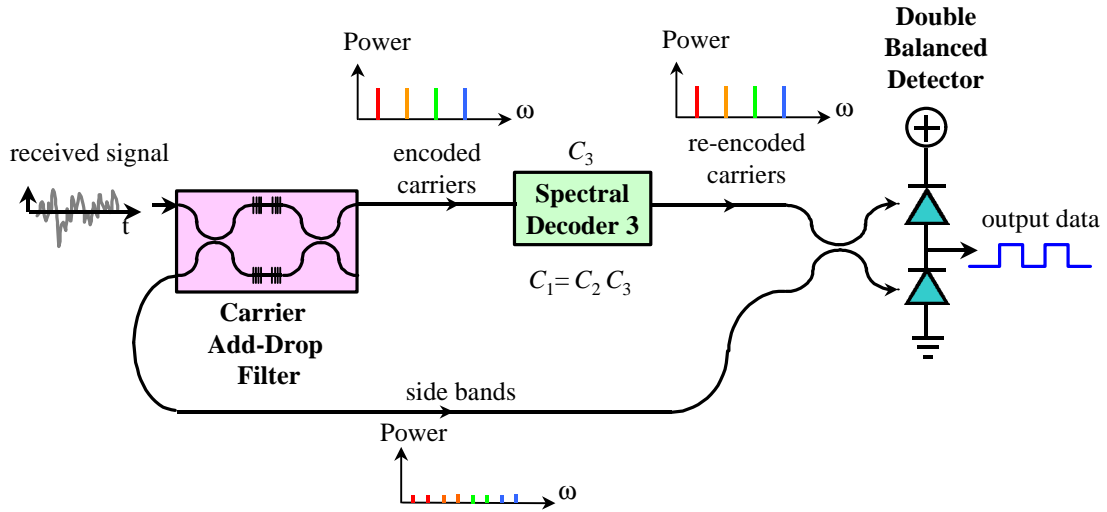


Figure 4.3 Multi-wavelength optical CDMA receiver.

The side bands and the encoded carrier are broadcast to the receivers through a star coupler. Figure 4.3 shows the receiver structure. As shown in Fig. 4.3, the same carrier add-drop filter is used to separate the side bands and the encoded carrier tones. The carrier tones go through another spectral encoder $C_{k,3}$ at the receiver such that $C_{k,1} = C_{k,3}C_{k,2}$, and $C_{k,1}$ is orthogonal to $C_{k,3}C_{j,2}$ for $j \neq k$, where C 's represent the encoded carriers as in Equations (4.5) and (4.6). Thus the receiver reconstructs the original encoded carrier $C_{k,1}$ which is modulated by the transmitted signal. The side bands and

the reconstructed carriers mix at a second 3-dB splitter, which feeds a double balanced detector.

Without loss of generality, let $k=1$ be the desired channel. The input to the second 3-dB splitter consists of the multiplexed side bands $\sum_{k=1}^K s_k(t)C_{k,1}(t)$ and the re-encoded carriers $C_{1,3} \sum_{k=1}^K C_{k,2}(t)$.

The 3-dB splitter output to the balanced detector consists of the sum $R_{U1}(t)$ and difference $R_{L1}(t)$ of the side bands and the encoded carrier of the desired user, i.e. user 1:

$$R_{U1}(t) = \frac{1}{\sqrt{2}} \sum_{k=1}^K s_k(t)C_{k,1}(t) + \frac{1}{\sqrt{2}} C_{1,3} \sum_{k=1}^K C_{k,2}(t) \quad (4.9)$$

$$R_{L1}(t) = \frac{1}{\sqrt{2}} \sum_{k=1}^K s_k(t)C_{k,1}(t) - \frac{1}{\sqrt{2}} C_{1,3} \sum_{k=1}^K C_{k,2}(t) \quad (4.10)$$

The photodetectors used in the balanced receiver are a pair of square law devices followed by a low pass filter (LPF). Therefore, the output from the balanced detector will be:

$$\begin{aligned} Z_1(t) &= \text{LP} \left[\frac{\Re}{2} |R_{U1}(t)|^2 - \frac{\Re}{2} |R_{L1}(t)|^2 \right] \\ &= \text{LP} \left[\frac{\Re}{2} \left(\sum_{k=1}^K s_k(t)C_{k,1}(t) \right) \cdot \left(C_{1,3} \sum_{k=1}^K C_{k,2}(t) \right)^* \right] \end{aligned} \quad (4.11)$$

The square terms of the side bands and re-encoded carrier tones are cancelled at the balanced detector output, eliminating any common mode fluctuations. The remaining term in Equation (4.11) is the low pass filtered cross product between the side bands and the re-encoded carriers. By the code orthogonality requirement, all the dot product terms

are cancelled except for user 1. The operation of $C_{1,3}$ on $C_{1,2}$ regenerates $C_{1,1}$ which is the desired “local oscillator” used to extract the user 1 signal $s_1(t)$. By maintaining mode-locked time synchronization, perfect orthogonality can be achieved.

4.3 Carrier/Side Bands Separation and Combining

By separating the carrier from the side bands, processing them individually and recombining them, not only have we avoided the complexity of a local oscillator at the receiver but we have also achieved full orthogonality and enhanced security. Here, we give two possible examples for carrier and side band separation and recombination.

The first example (Fig. 4.4) for the carrier add/drop consists of a balanced Mach-Zehnder interferometer (MZI) with a pair of identical high finesse Fabry-Perot (FP) filters in both arms. The high finesse FP filter has very sharp frequency transmission at the carrier tone frequencies and very high reflection for frequencies other than the carrier tones. The residual of the encoded carrier tones will pass through the MZI and will be dropped at the carrier drop port on the opposite side of the input signal. The information containing side bands will be reflected to the other port on the same side of the signal. The separately encoded carrier is added to the reflected side bands from the carrier add port of the MZI. A similar MZI arrangement for carrier add/drop filters has been used with fiber gratings as a wavelength division multiple-access (WDM) add/drop multiplexer [49].

Another possible carrier add/drop filter consists of a ring coupler pair is shown in Fig. 4.5. This filter is made up of two weak fiber couplers connected in a ring whose circumference matches the resonant condition for the carrier tones. The carriers will be

coupled out of the carrier drop port because of resonance. The device can be made very compact and has the potential for integrated photonics [50].

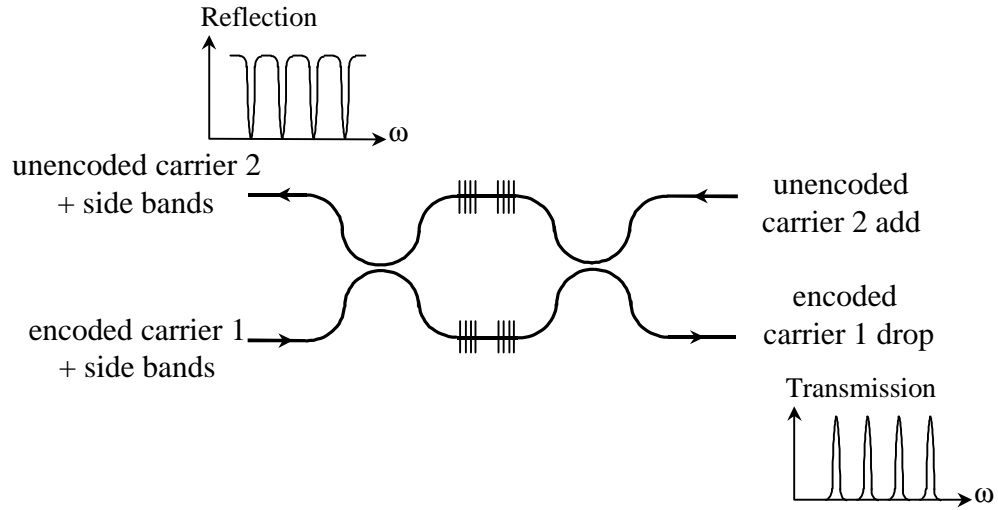


Figure 4.4 A Mach-Zehnder interferometer (MZI) together with Fabry-Perot (FP) filter as carrier add/drop filter.

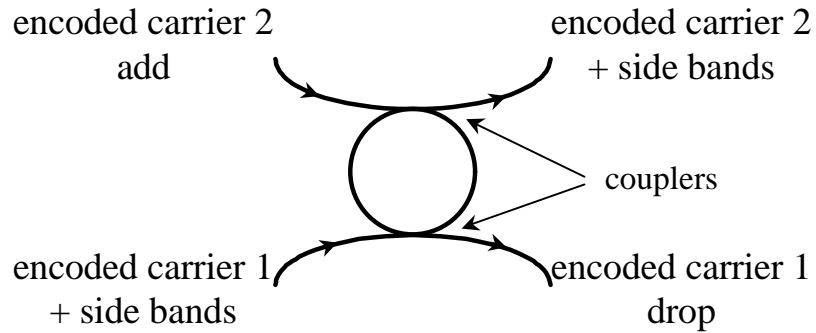


Figure 4.5 A ring resonator as carrier add/drop filter.

4.4 Encoder Design

The phase encoder is another new device required in this system. In this section, we describe the design of an encoder which uses series connected MZI's. The MZIs are

set in a feedback configuration as shown in Fig. 4.6 so that they have only one input and one output. The output phase of the feedback MZI (FBMZI) is determined by three parameters, the feed forward path length difference l_f between the two feed forward paths, the extra phase \mathbf{q} introduced by a phase shifter at the second arm of the MZI and the feedback delay introduced by the feedback path l_b . A general frequency transfer function for an arbitrary FBMZI can be easily derived using feedback network theory. Here, we describe a specific design that will generate orthogonal codes.

We assume N , the total number of frequency components in the mode-locked laser spectrum to be a power of 2, i.e. $N=2^L$, where L is an integer. The feed forward path length difference l_f and the feedback path length l_b can be expressed by the corresponding time delays $t_f=l_f/c$ and $t_b=l_b/c$ where c is the speed of light in the waveguide. For simplicity, we restrict the values of t_f and t_b to integral multiples of a basic time unit $t_0 = 2p/(N\Delta w)$, which is the reciprocal of the total CDMA bandwidth. In addition, let us restrict the phase shift \mathbf{q} to either 0 or p .

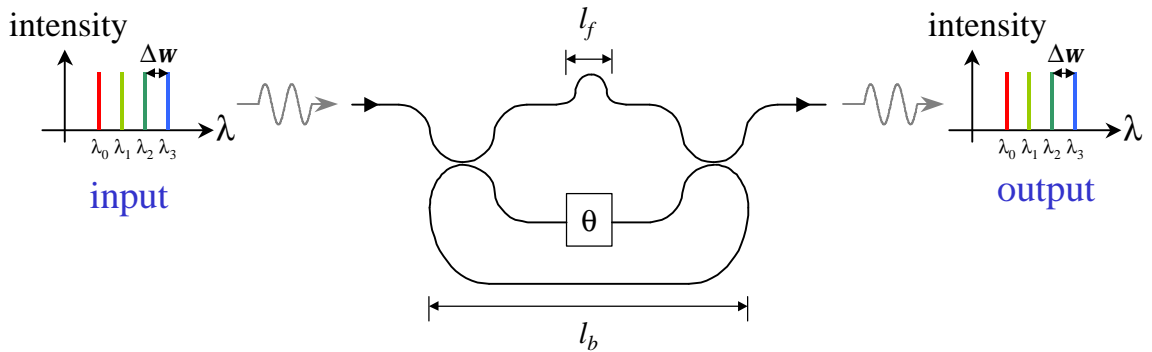


Figure 4.6 The feedback Mach-Zehnder phase encoder.

It can be easily shown [34] that setting the feed forward path difference delay to be $t_f = \frac{1}{2}Nt_0 = \mathbf{p} / \Delta\omega$ corresponds to an MZI whose free spectral range (FSR) is $2\Delta\omega$. We can view the MZI as a 2×2 switch for the frequency components which are separated by $\Delta\omega$. Half of the frequency components (say the even ones) will see the MZI in the through-state and the other half (the odd components) will see the MZI in the cross-state (Fig. 4.7). When a phase shift $\mathbf{q} = \mathbf{p}$ is introduced at the MZI, the roles of the frequency components are changed so that the ones previously in the through-state are now in the cross-state and vice versa.

Components in the cross-state are fed back to the other input port of the MZI and come out of the same output port as those in the through state after a feedback delay t_b which is translated into a phase shift. The 0 and \mathbf{p} phase shifts in the feed forward path represent two binary states of an encoder.

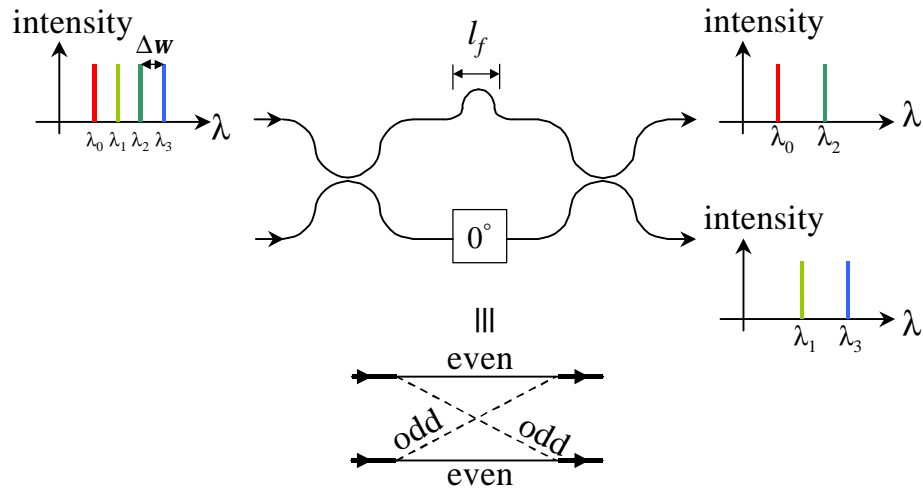


Figure 4.7 By properly setting l_f , the feed forward path length difference, and θ , the MZI functions as a 2×2 switch in either through or cross state for the mode-locked wavelength components.

Let the feedback delay be $t_b = qt_0$, where q is an integer. We now show that series connected FBMZI's as in Fig. 4.7a produce families of orthogonal spectral phase codes. We require the following theorems.

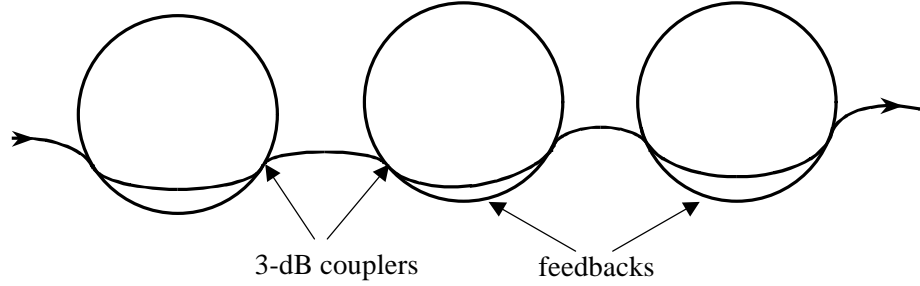


Figure 4.7a Series connected FBMZI's to produce families of orthogonal spectral phase codes.

Theorem 1: If q and N are co-prime (i.e. they have no common factor), the codes generated by the 0 and p states are orthogonal.

Proof: First we notice since $N=2^L$ is a power of 2, if q and N are co-prime, q must be an odd number. We have $n=0, 1, 2, \dots, N-1$ frequency components spaced $\Delta\omega$ apart.

Suppose the even frequencies are in the through state when phase shifter is set to 0, and the odd frequencies are in the cross-state experiencing an extra phase shift $(\omega+n\Delta\omega)t_b$.

When the phase shifter is set to p , the even frequencies are in the cross-state and subject to a phase shift $(\omega+n\Delta\omega)t_b$, while the odd frequencies are in the through state. So the phase difference between the 0 and p states for various components are

$\Phi_n^0 - \Phi_n^p = \pm(\omega+n\Delta\omega)t_b$, where the plus and minus signs are used for the odd and even frequency components. The vector sum of all the phase differences must be 0, to

establish orthogonality. $\Phi_n^0 - \Phi_n^p$ can be re-written as $\pm(\omega t_b + \frac{2pnq}{N})$. Then we can

group all the frequencies into $N/2$ pairs of $(n, n+N/2)$ where $n=0, \dots, N/2-1$. So the phase shifts for each of these pairs will be $\pm(\mathbf{w}t_b + \frac{2\mathbf{p}nq}{N})$ and $\pm(\mathbf{w}t_b + \frac{2\mathbf{p}nq}{N} + q\mathbf{p})$. Since q is an odd multiplier of \mathbf{p} , these two phase shifts represent two points diagonally opposite to each other on the unit complex circle and will be cancelled. Q.E.D.

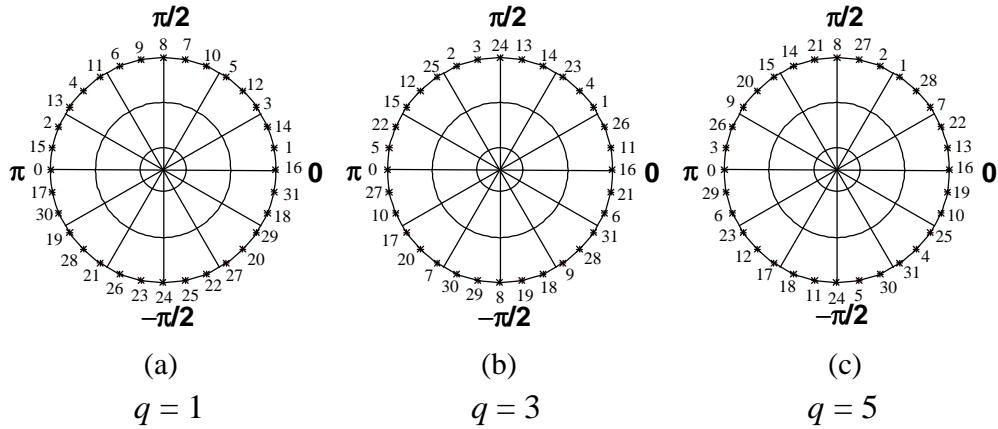


Figure 4.8 Distribution of the phase differences between the 0 and π states for different feedback lengths. There is no common factor between q and N . $N=32$.

In fact, if we ignore the $\mathbf{w}t_b$ term which is common to all the phase terms, the net phase difference for any frequency component n can be written as $\pm 2\mathbf{p}((nq))_N/N$, where $((nq))_N$ represents the product nq modulo N . Since q and N are co-prime, $((nq))_N$ will produce [51] all the values in the set $[0, 1, \dots, N-1]$ with $n=0, 1, \dots, N-1$. This also states that there is no repetition in the encoded phase pattern. The actual sequence produced by the modulo operation is dependent on the value of q which can be considered a cryptographic factor for encoding. Figure. 4.8 shows the encoded phase differences on the unit circle for $q=1, 3$ and 7 . N is chosen as 32 in this calculation.

Theorem 2: If q and N are not co-prime and have as their greatest common divisor (gcd) the integer 2^m , $m < L$, the codes produced by the 0 and \mathbf{p} states are orthogonal within the free spectral range (FSR) of $\frac{N}{2^m} \Delta \omega$.

Proof: q can be written $q=2^m \cdot r$ where r is an odd number. This must be true because $N=2^L$. Using a similar argument as in Theorem 1, the difference phase for the 0 and \mathbf{p} states of the frequency component n is $2\mathbf{p}nq/N = 2\mathbf{p}n(2^m r)/2^L = 2\mathbf{p}nr/2^{L-m}$. We omitted the plus and minus signs for the even and odd frequency components and the common delay phase $\mathbf{w}t_b$. Using the results proved in Theorem 1, the frequency components in the range $n = 0, \dots, 2^{L-m}-1$, will form orthogonal codes. It is also obvious that the encoded phase pattern will repeat for every 2^{L-m} frequency components. Therefore, the code produced by the 0 and \mathbf{p} states are orthogonal within an FSR of $\frac{N}{2^m} \Delta \omega$. For simplicity, we will say the normalized FSR of the encoder is $N/2^m$ in latter. Of course, the orthogonality extends to all the N components. Q.E.D

The value of integer r determines the actual locations of the frequency components on the complex plane. Figure 4.9 on the next page shows the distribution of the phase differences for $r=3$ and 7 , $N=32$, and $m=2$.

Theorems 1 and 2 together state that for all the integers q , the two states formed by the FBMZI encoder are orthogonal to each other. In the next theorem, we will prove that a family of orthogonal codes can be generated by cascading encoders with different free spectral ranges.

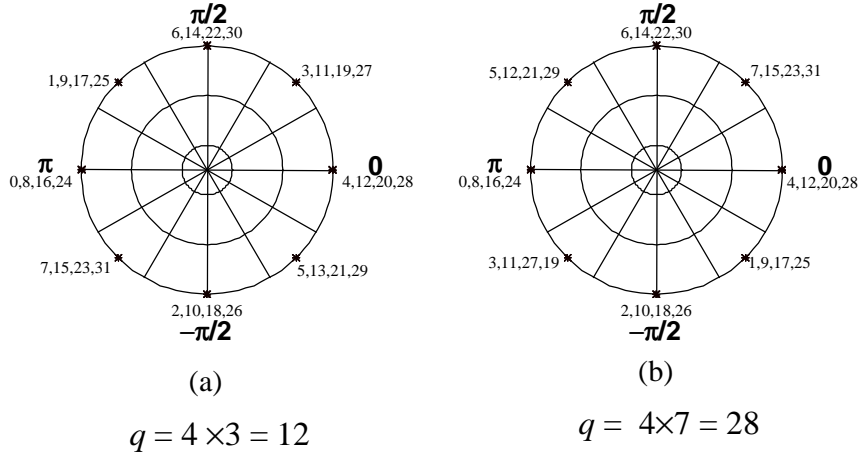


Figure 4.9 Distribution of the encoded phase differences between the 0 and π states for different feedback lengths. q and N are not co-prime and the common factor between them is 4. $N=32$.

Theorem 3: Given two FBMZIs with normalized FSR equal to N and $N/2$ respectively. Each stage has two states 0 and p . The four possible states obtained by combining the two stages generate four mutually orthogonal codes.

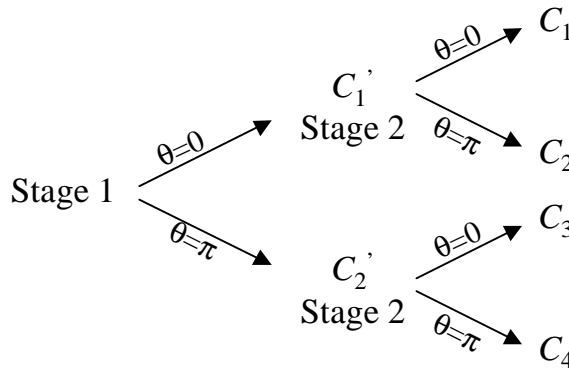


Figure 4.10 Four codes formed by cascading two different FBMZI stages.

Proof: The tree diagram in Fig. 4.10 represents the four possible states. Assume stages 1 and 2 have a normalized FSR of N and $N/2$ respectively. Recall that the orthogonality between two codes depends only upon the relative phase differences between the

matching frequency components, but not the absolute phase. In addition, the encoded phase on each spectral component is accumulated for two stages at the output. We consider the following three cases. Case 1: the two codes generated from the same state of stage 1 and two different states of stage 2 are orthogonal by Theorem 2. Therefore, codes (C_1, C_2) and (C_3, C_4) are orthogonal pair-wise. Case 2: the two codes generated from different states of stage 1 and the same states of stage 2 are orthogonal by Theorem 1. Therefore, (C_1, C_3) and (C_2, C_4) are orthogonal pair-wise. Case 3: the remaining question is the orthogonality between (C_1, C_4) and (C_2, C_3) . The orthogonality between C_1 and C_4 is proved as follows:

By the orthogonality of the two states produced by stage 1 and stage 2, we have:

$$\sum_{n=0}^{N-1} \exp\{i(\Phi_{n,1}^0 - \Phi_{n,1}^p)\} = \sum_{n=0}^{N-1} \exp\{i(\Phi_{n,2}^0 - \Phi_{n,2}^p)\} = 0 \quad (4.12)$$

The superscript in the phase represent the state of the FBMZI and the second subscript represent the stage number in the cascade setting in the above equations. Since stage 2 has a normalized FSR of $N/2$, we have

$$\exp\{i(\Phi_{n,2}^0 - \Phi_{n,2}^p)\} = \exp\left\{i\left(\Phi_{n+\frac{N}{2},2}^0 - \Phi_{n+\frac{N}{2},2}^p\right)\right\} \text{ for } n=0, \dots, N/2-1 \quad (4.13)$$

Also, from the proof of Theorem 1, we know that for stage 1 which has a normalized FSR of N ,

$$\exp\{i(\Phi_{n,1}^0 - \Phi_{n,1}^p)\} = -\exp\left\{i\left(\Phi_{n+\frac{N}{2},1}^0 - \Phi_{n+\frac{N}{2},1}^p\right)\right\} \text{ for } n=0, \dots, N/2-1 \quad (4.14)$$

Since the encoded phase in successive stages accumulates additively, so do the relative phases in the dot product. Therefore:

$$\begin{aligned}
C_1 \bullet C_4^* &= \sum_{n=0}^{N-1} \exp\{i[(\Phi_{n,1}^0 + \Phi_{n,2}^0) - (\Phi_{n,1}^p + \Phi_{n,2}^p)]\} = \sum_{n=0}^{N-1} \exp\{i[(\Phi_{n,1}^0 - \Phi_{n,1}^p) + (\Phi_{n,2}^0 - \Phi_{n,2}^p)]\} \\
&= \sum_{n=0}^{\frac{N}{2}-1} \exp\{i[(\Phi_{n,1}^0 - \Phi_{n,1}^p) + (\Phi_{n,2}^0 - \Phi_{n,2}^p)]\} + \sum_{n=\frac{N}{2}}^{N-1} \exp\{i[(\Phi_{n,1}^0 - \Phi_{n,1}^p) + (\Phi_{n,2}^0 - \Phi_{n,2}^p)]\} \\
&= \sum_{n=0}^{\frac{N}{2}-1} \exp\{i(\Phi_{n,2}^0 - \Phi_{n,2}^p)\} \left(\sum_{n=0}^{\frac{N}{2}-1} \exp\{i(\Phi_{n,1}^0 - \Phi_{n,1}^p)\} + \sum_{n=\frac{N}{2}}^{N-1} \exp\{i(\Phi_{n,1}^0 - \Phi_{n,1}^p)\} \right) \\
&= 0
\end{aligned} \tag{4.15}$$

We have used (4.13) and (4.14) in deriving (4.15). In a similar manner, we can prove the orthogonality between C_2 and C_3 . This completes the proof of Theorem 3. Q.E.D.

Intuitively, cascading one encoder after another can be thought as redistributing the encoded relative phases uniformly on the complex unit circle, hence preserving the orthogonality. The proof of Theorem 3 can be extended by induction to prove that by cascading a series of encoders with L different normalized FSRs (i.e. $2, 2^2, \dots, N=2^L$) one can obtain all 2^L orthogonal codes, which is the complete set expected for an encoding scheme using 2^L spectral components. Different combinations of the 0 or p shifts in the various stages produce the 2^L codes. Thus we have shown how to use L switches to produce 2^L spectral phase codes.

One plausible way of cascading the FBMZIs is to use a waveguide design with “concentric” circles touching each other to form the 3-dB couplers. The waveguides are

nested in cascade as shown in Fig. 4.11. The output waveguide cuts perpendicularly through the loops to eliminate any crosstalk.

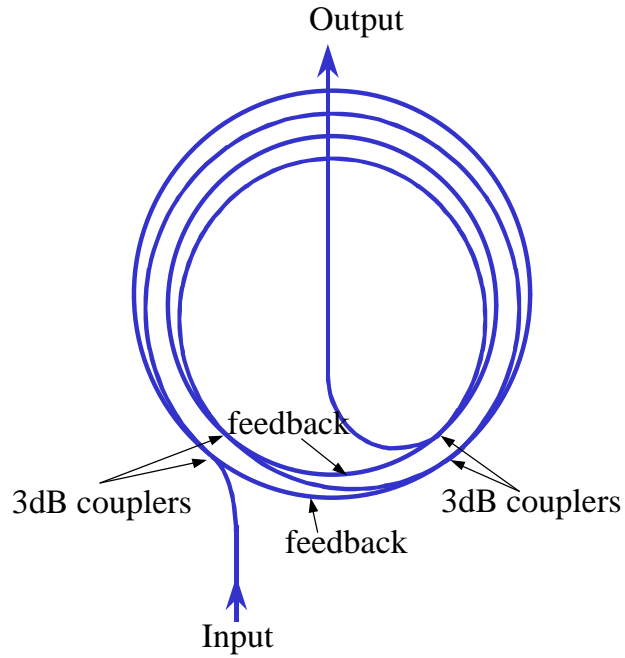


Figure 4.11 Proposed waveguide circuits for cascaded FBMZI to save real estates.

4.5 Performance Evaluation

In this section, we investigate the performance limit of the proposed phase encoded multi-wavelength optical CDMA system. Again, we take user 1 as the intended channel without loss of generality. Assume the carriers $C_{k,1}$ and $C_{k,2}$ have the same amplitude. The value of $s_k(t)$ is 0 or 1 for ASK and -1 or $+1$ for phase shift keying (PSK). Ideally, the carrier decoding by the $C_{k,3}$ does not change the amplitude of $C_{k,2}(t)$, since only phase encoding is used.

From Equations (4.5) and (4.6), we find that for each user the power in both carriers $P[C_{k,1}(t)]$ and $P[C_{k,2}(t)]$ is $E_0^2/4$. Assume 0 and 1 bits are equally probable. The average received power is:

$$P_{rec} = \mathbf{a}P[C_{k,1}(t)] + P[C_{k,2}(t)] = \frac{(\mathbf{a} + 1)E_0^2}{4} \quad (4.16)$$

or
$$E_0 = \sqrt{\frac{4P_{rec}}{\mathbf{a} + 1}} \quad (4.17)$$

where $\mathbf{a} = 1/2$ for ASK and 1 for PSK. Here we have assumed that the received power from all the users are equal. The splitting loss at the star coupler is also ignored.

The useful output signal is given by equation (4.11). Owing to the code orthogonality, only the matched term corresponding to user 1 will survive. So we have:

$$\begin{aligned} Z_1(t) &= \text{LP} \left[\frac{\Re}{2} \left(\sum_{k=1}^K s_k(t - \mathbf{t}_k) C_{k,1}(t) \right) \bullet \left(C_{1,3} \left[\sum_{k=1}^K C_{k,2}(t) \right] \right)^* \right] \\ &= \text{LP} \left[\frac{\Re}{2} (s_1(t - \mathbf{t}_1) C_{1,1}(t)) \bullet (C_{1,3} [C_{1,2}(t)])^* \right] \\ &= \text{LP} \left[\frac{\Re}{2} (s_1(t - \mathbf{t}_1) C_{1,1}(t)) \bullet (C_{1,1}(t))^* \right] \\ &= \frac{\Re E_0^2}{4} s_1(t - \mathbf{t}_1) = \frac{\Re P_{rec}}{\mathbf{a} + 1} s_1(t - \mathbf{t}_1) \end{aligned} \quad (4.18)$$

The average received signal (root mean square) is thus:

$$I_{sig} = \sqrt{Z_1(t)^2} = \frac{\sqrt{\mathbf{a}}}{\mathbf{a} + 1} \Re P_{rec} \quad (4.19)$$

The signals detected by each of the two photodetectors in the balanced receiver are given by $R_{U1}(t)$ and $R_{L1}(t)$ as in equations (4.9) and (4.10). Since the 3dB splitter in

front of the balanced detectors splits the received user power (both side bands and re-encoded carriers) equally, the average optical power seen by each photodetector is:

$$\frac{1}{2}\overline{|R_{U1}|^2} = \frac{1}{2}\overline{|R_{L1}|^2} = \frac{KP_{rec}}{2} \quad (4.20)$$

This detected optical power will contribute shot noise [39] at each photodetector. The shot noise produced is therefore:

$$\langle I_{sh}^2 \rangle_{U1} = \langle I_{sh}^2 \rangle_{L1} = 2qIB_d = q\Re KP_{rec} B_d \quad (4.21)$$

where $I = \frac{1}{2}\Re\overline{|R_{U1}|^2} = \frac{1}{2}\Re\overline{|R_{L1}|^2}$ is the average photocurrent produced at each photodetector. The total shot noise is thus:

$$\langle I_{sh}^2 \rangle = \langle I_{sh}^2 \rangle_{U1} + \langle I_{sh}^2 \rangle_{L1} = 2q\Re KP_{rec} B_d \quad (4.22)$$

Therefore, K multiple users degrade the performance of the system by increasing the shot-noise proportionately.

The thermal noise from the receiver pre-amp is the same as given in equation 3.15 in the previous chapter.

It is worth noticing that because all the signals are split equally between the two photodetectors in the balanced detector and owing to the code orthogonality achieved through synchronization, the common mode fluctuations in the signal and carrier power is cancelled by the balanced detector, except for the shot noise.

The total mean square noise is the sum of thermal and shot noise:

$$\langle I_n^2 \rangle = \langle I_{sh}^2 \rangle + \langle I_{th}^2 \rangle \quad (4.23)$$

The bit error rate (BER) is given by [45-46]:

$$BER = \frac{1}{2} \left[1 - \operatorname{erf} \left(\sqrt{\frac{gE_b}{2N_0}} \right) \right] \quad (4.24)$$

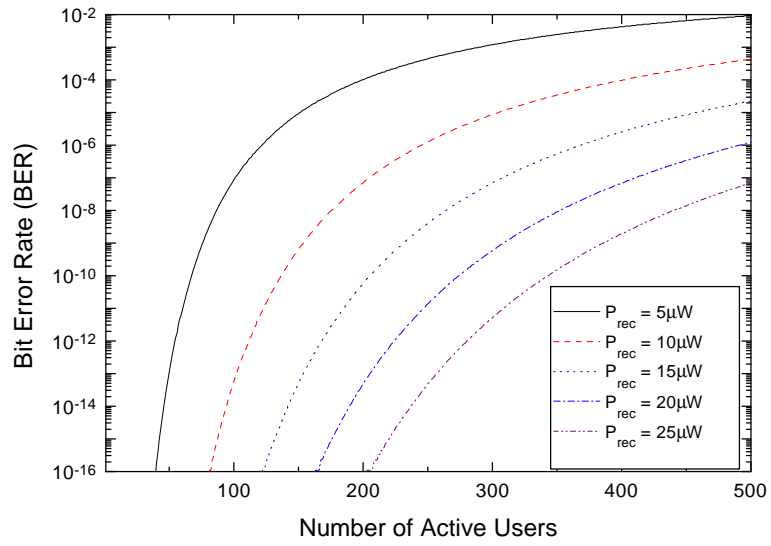
where E_b is the average bit energy, $g=1$ for ASK and $g=2$ for PSK. N_0 is the two-sided noise power spectral density.

$$\frac{E_b}{N_0} = \frac{I_{sig}^2 T_b}{N_0} = \frac{I_{sig}^2}{N_0 B_d} = \frac{I_{sig}^2}{\langle I_n^2 \rangle} \quad (4.25)$$

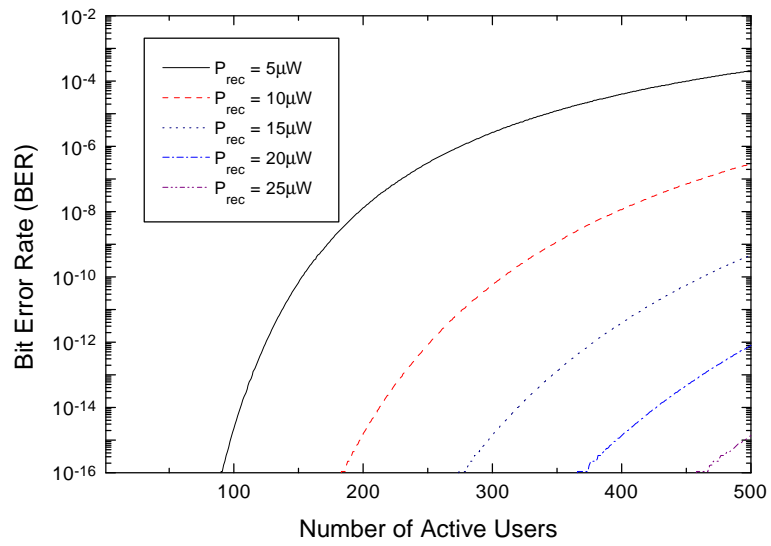
The BER is plotted against the number of co-channel users at various received power levels in Fig. 4.12 for both ASK and PSK. A one gigabit per second data rate is assumed for each user. It is seen from Fig. 4.12 that for -20dBm received power per channel, 87 and 153 concurrent users are allowed for a BER of 10^{-15} and 10^{-9} using ASK while 197 and 346 concurrent users are allowed for the same BER's using PSK. Of course this is the worst case situation. For a system with bursty traffic, the number of concurrent users will likely to be much less than the total number of subscribers, most of the time.

It is seen from the above analysis that the SNR is shot noise limited when the total received optical power $P_{rec}K$ is large and is approximately given by:

$$SNR \approx \frac{I_{sig}^2}{\langle I_{sh}^2 \rangle} = \frac{a \mathfrak{R} P_{rec}}{2q(a+1)^2 KB_d} \quad (4.26)$$



(a) ASK.



(b) PSK.

Figure 4.12 Bit Error Rate (BER) vs. Number of Active Users for (a) ASK and (b) PSK.

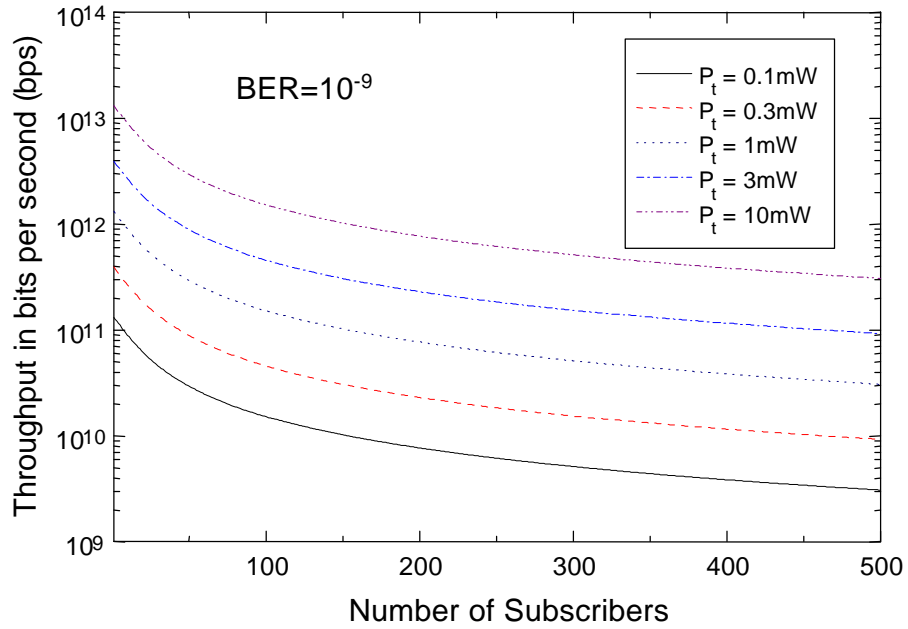
From the transmitter's viewpoint, the signal is broadcast to all the users in the network by a passive optical star coupler. Suppose the network size is the same as the total number of active users (the most pessimistic case). Then the splitting loss is $10\log K$ dB. We define the throughput as the aggregate bit rate that the network can support at a certain bit error rate given a fixed available transmitter power P_t . Neglecting the transmission loss and other non-idealities, the network throughput scales linearly as P_t :

$$SNR \approx \frac{I_{sig}^2}{\langle I_{sh}^2 \rangle} = \frac{a\mathfrak{R}P_t}{2q(a+1)^2 K^2 B_d} \quad (4.27)$$

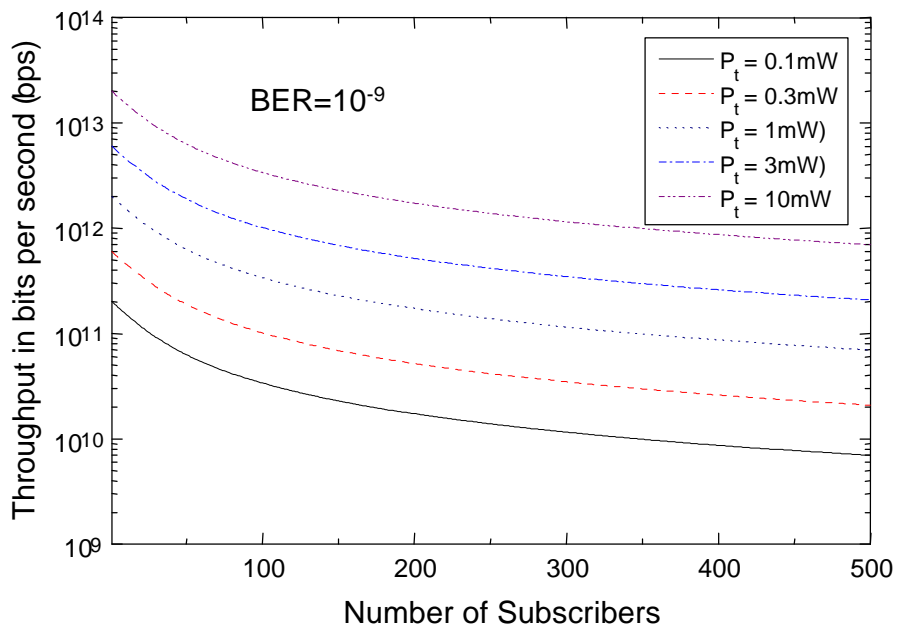
The total throughput is given by:

$$KB_d \approx \frac{a\mathfrak{R}P_t}{2q(a+1)K \cdot SNR} \quad (4.28)$$

For a given available transmitter power, to obtain higher throughput, the total number of users needs to be smaller, which also means that each channel needs to handle a bigger bandwidth. Assuming 10mW available optical power at the transmitter output and 150 concurrent users, the network can support a total capacity of 1THz and 2.3THz for ASK and PSK respectively at 10^{-9} BER. Fig. 4.13 plots the achievable throughput for different values of P_t . We assumed the transmitter power is evenly distributed among all the subscribers who are all active at the same time (again worst case).



(a) ASK



(b) PSK

Figure 4.13 Throughput vs. Number of Subscribers for (a) ASK and (b) PSK.

4.6 Discussion

The codes applied to the pure carrier and the encoded side bands are orthogonal to each other so that simple square law detection will not give any output. This protects the signal from being intercepted by unwanted receivers and enhances system security. One could conceive, as an alternative, to transmit the unencoded carrier that is produced by the mode-locked laser, to act as a “local oscillator”. Since each user broadcasts its signal to all the users in the network, different copies of the unencoded carrier will add with random phase at the receiver and produce speckle. This is due to the difficulty of synchronizing the absolute phase of the optical carrier. The beating of this noisy carrier wave with the side bands will give excess fluctuations in the output signal. Thus, by encoding the pure carriers in each channel with a different code, only the desired receiver, with the properly encoded carrier, will detect the desired side bands.

We have seen that the balanced receiver used in this chapter has the ability to reject the common mode fluctuation in the signal sources and achieve true orthogonality. Eventually, the system will be shot noise limited when the number of users accessing the network is large. When the system is shot noise limited, increasing the signal power improves the BER by increasing the SNR. However, when a system is speckle noise limited as in a non-coherent spectral intensity encoded system, the SNR does not improve by increasing the signal power and the system performance is very capped.

4.7 Conclusion

In this chapter, we have proposed and analyzed a multi-wavelength spectral phase encoded optical CDMA system. This system uses a balanced optical detector as a

balanced mixer and it achieves common mode rejection. By maintaining time synchronization and code orthogonality, speckle noise does not appear in this system. Since we make use of the phase information, a reference “local oscillator” is required. We manage, however, to avoid the complexity of having an optical local oscillator by supplying it from the transmitter, and sending it over the same optical path with the data.

We also proposed a new optical CDMA phase encoder using a feedback Mach-Zehnder interferometer configuration. To generate 2^N different codes, an encoder with only N cascaded stages is required. Such logarithmic scaling property could be very useful for networks having large numbers of users.

While the signals channel interference can be cancelled by using proper orthogonal codes at the balanced receiver, the proposed system is still limited by shot noise, which is associated with the aggregate light being detected. This new proposed optical CDMA system resembles radio CDMA systems most closely. We believe it has the highest throughput of any of the known optical CDMA schemes.

Chapter 5 Demultiplexing TDM, WDM and CDM Signals

5.1 Introduction

In the last chapter, we have seen, as expectedly, that N independent multi-wavelength codes can be generated given N wavelengths. One of the interesting features of the encoder presented in the last chapter is that only $\log_2 N$ switches are required in order to generate any one of the N orthogonal codes. So to demultiplex one channel out of 1000 wavelengths, a demultiplexer complexity of $\log_2 1000=10$ is required. This logarithmic scaling complexity is very favorable in a system with a large number of users.

In this chapter, we will review and compare the demultiplexing complexity of TDM, WDM and CDM systems and we will show that in all three systems, logarithmic demultiplexing complexity is theoretically achievable with proper designs of the demultiplexer.

A broadcast and select architecture is generally assumed in this chapter unless otherwise specified. Each node broadcasts its signal to every other node through a star coupler and the receiver tunes itself to the appropriate node in a way similar to commercial radio broadcasting.

In general, given a set of N transmitters, a receiver can divide the channels into two groups of $N/2$ transmitters first, and select the group of channels, which contains the desired channel. This process can be repeated until the right channel is selected. The process is similar to searching a number from an alphabetically sorted telephone

directory. This principle is called method of bisection and is used in many searching algorithms. The number of steps required in finding any one channel out of N channels is $\log_2 N$.

5.2 Demultiplexing TDM Signals

In a TDM system, data are transmitted in frames. Each frame consists of time slots assigned to different channels as shown in Fig. 5.1. In order to correctly select the time slot for each channel, global time synchronization is required. Each time slot in a TDM system can be a data packet in a packet interleaved TDM system, or it can consist of one bit of information from each channel in a bit interleaved system. Usually, a flag consisting of a particular bit pattern or a high intensity pulse is inserted at the beginning of each frame to delimit the start of a frame and help the receiver to acquire synchronization in case it loses synchronization. High speed optical TDM (OTDM) systems usually use bit interleaving.

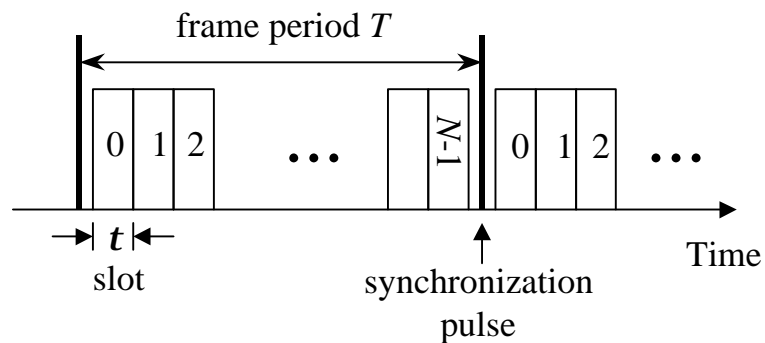


Figure 5.1 A multi-channel TDM signal frame.

In a multi-gigabit OTDM system [52], demultiplexing is achieved by using optical delay lines and fast optical gating to extract the correct time slot. The fast optical

gate opens for a slot duration t for every frame period T . The length of the optical delay lines determines which channel is extracted. The frame synchronization signal also functions as the clock signal in an OTDM system. Suppose each frame consists of N slots of duration t (where $N=2^L$ is a power of 2). To demultiplex channel n ($0 < n < N-1$) from the TDM frame, a delay of $(N-1-m)t$ is required. Therefore, in order to demultiplex any channel, a tunable delay line, which can generate any delay between 0 and $(N-1)t$ is required. This can be achieved by using a tunable delay line matrix consisting of $L=\log_2 N$ switchable sections as shown in Fig. 5.2. At delay stage $0 < m < L$, a delay of either 0 or $2^m t$ is selected using 2×2 optical switches. The states of the 2×2 optical switches and the delay lines whose lengths are in powers of 2 thus represent a binary number system. By properly setting the states of 2×2 optical switches, all the N delays between 0 and $(N-1)t$ can be generated using only $\log_2 N$ delay lines, giving a logarithmic demultiplexing complexity.

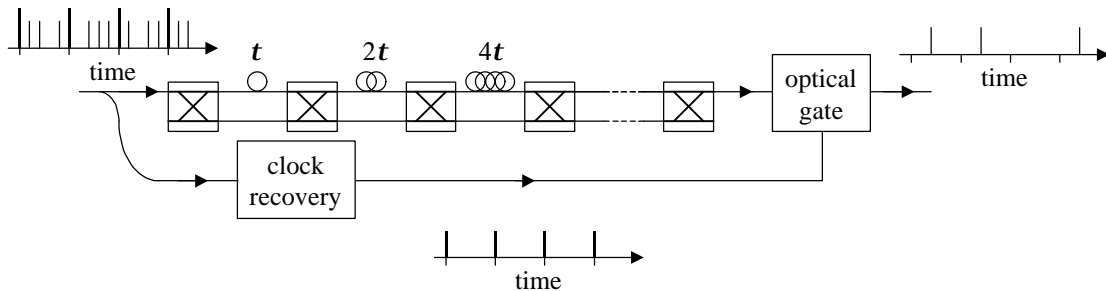


Figure 5.2 Demultiplex TDM channels using $\log_2 N$ cascaded delay lines.

5.3 Demultiplexing WDM Signals

The channels in WDM systems use different wavelengths or frequency slot for transmission. It is also called frequency division multiplexing (FDM) in the radio

domain. Usually the name WDM is used when channels are fairly widely separated in the spectral domain. However, in order to explore the full capacity in an optical fiber, channels are crowded more and more closely together.

WDM channels are demultiplexed using wavelength selective channel filters. There are a few different ways of constructing wavelength selective filters. The classical wavelength selective filter is the Fabry-Perot (FP) filter [34, 43, 53-55], which is a cavity structure consisting of two reflective surfaces. Only the wavelength components satisfying the resonant condition of the cavity will be transmitted from the input of the cavity to the output. Other wavelengths will be reflected.

The simplest WDM demultiplexer will consist of a tunable (FP) filter whose cavity length can be varied to select different wavelength channels. However, there are certain technical challenges FP filters need to overcome. In order to have good selectivity, very high finesse FP filters are required. Finesse is defined as the ratio of the free spectral range to the full-width half maximum (FWHM) of the FP filter. Tunable FP filters are usually mechanical, which consists of movable reflector surfaces, or electro-optic whose effective cavity lengths can be changed by changing the refractive index of the cavity using the electro-optic effect. Mechanically tunable filters have very good tuning range and selectivity, but are usually very slow and not suitable for high speed switching required in network applications. Electro-optic tunable filters have very fast tuning speed but suffer from small tuning range. Nevertheless, the theoretical scaling complexity for a tunable wavelength demultiplexer is one or $O(1)$ using the big O notation adopted in computer science.

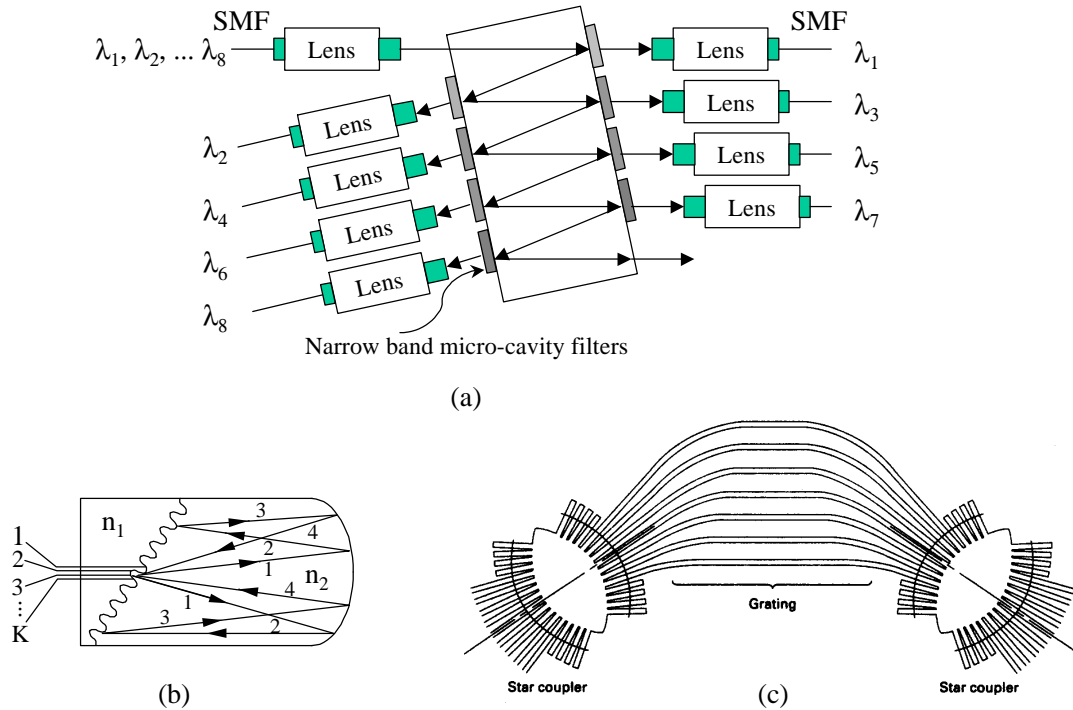


Figure 5.3 WDM demultiplexers using (a) cascaded micro-cavity filters, (b) ruled grating with Stimax configuration and (c) integrated waveguide gratings.

WDM demultiplexing can also be achieved using cascaded thin-film interference filters [Fig. 5.3(a)], a ruled grating in Stimax configuration [Fig. 5.3(b)] [56] or integrated silicon waveguides using a Dragone configuration [Fig. 5.3(c)] [57]. In all these structures, the multiplexed signal is demultiplexed into N individual wavelengths in the spatial domain and the desired wavelength is selected using an array of N switches as shown in Fig. 5.4 [58]. The complexity increases linearly as the number of wavelengths N . Since switches are active components, such a linear scaling is undesirable especially in dense WDM (DWDM) systems where N is large.

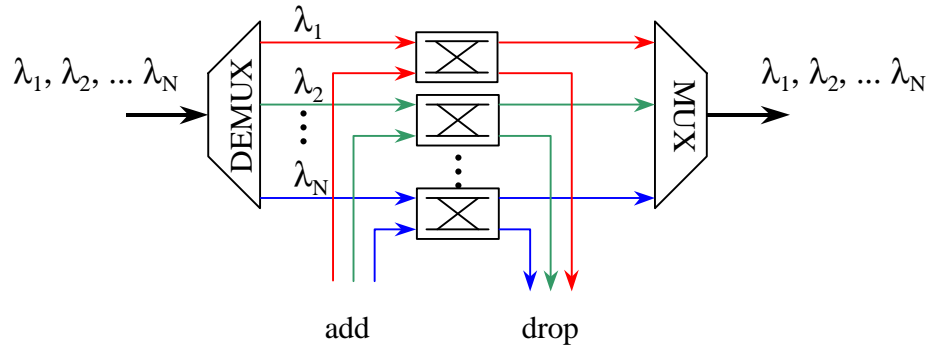


Figure 5.4 Channel selection (add/drop) using the WDM demultiplexers shown in Fig. 5.3 has complexity N .

Optical filters are usually interferometric devices that have periodic frequency response functions. We can make use of the periodic property to achieve the logarithmic demultiplexing complexity in a WDM system. The way to do this is to have a series of periodic rectangular shaped wavelength filters whose free spectral ranges (FSR) form a geometric progression with a multiplication factor of 2. The principle of such a demultiplexer is introduced in Fig. 5.5. Half of the spectral components are filtered out when the input is passed through each successive filter stage. The first stage filter has the smallest FSR. The next stage filter has twice the FSR of the previous stage. So the second stage filters out another half of the spectrum that is left from the output of the first stage filter. Most optical filters have two complementary spectral outputs. By selecting either one of the two complementary output of each filter stage, we can select and discard, at our discretion, either half of the spectral component. Therefore, to demultiplex any wavelength out of N , only $\log_2 N$ filter stages are required. Figure 5.5 shows the filter function of a three-stage cascaded eight-wavelength WDM demultiplexer. The two complementary outputs of each stage are selected using a 2×2

optical switch to the next stage input. These 2×2 switches can be made very fast using electro-optic switches to build a fast tunable optical demultiplexer. Appendix E gives a proposed waveguide structure to realize the rectangular shaped wavelength filters using a one-dimensional photonic crystal [59-60] arrangement.

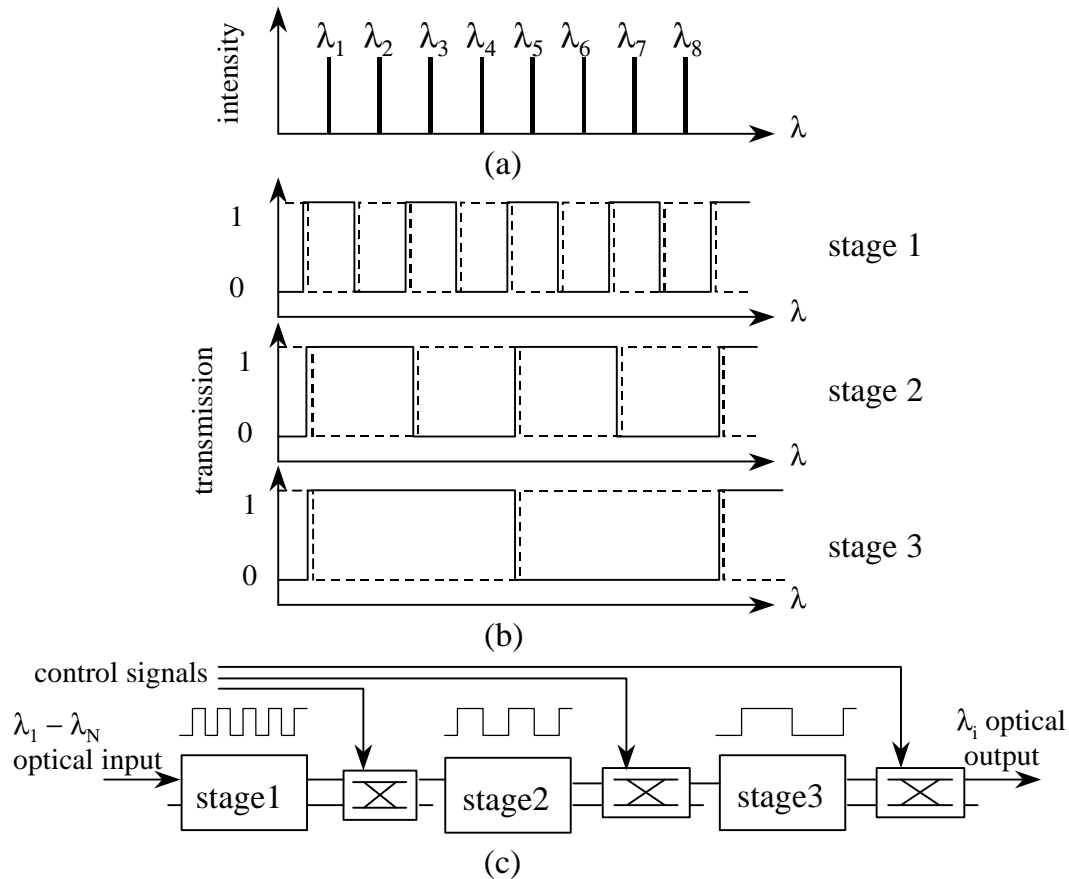


Figure 5.5 WDM channels are demultiplexed with a logarithmic number of switches (a) input multi-wavelength signal, (b) transmission function of each stage, (c) schematic diagram of the demultiplexer.

It should be noted that there are some functional differences between the complexity N WDM demultiplexer in Fig. 5.4 and the logarithmic demultiplexer shown in Fig. 5.5. The design in Fig. 5.4 is basically a wavelength router. It plucks out the

desired wavelength channel(s) and bypasses the unwanted channels. This function is not available in the logarithmic demultiplexer that is assumed to be used in a broadcast and select environment. The logarithmic filter that we propose here simply selects the desired wavelength channel and discards all the unwanted channels. A wavelength router is useful in point to point links and in wide area networks (WAN) [61] for traffic add/drop. It is particularly useful in a WDM ring network where each node only extracts traffic from the particular wavelength of its own interest, without disturbing the traffic for other nodes which uses different wavelengths. However, in a network with a large number of wavelengths, linear scaling would be very costly.

From a practical viewpoint, each add/drop multiplexer adds insertion loss to the signal. Suppose 1dB loss occurs at each add/drop multiplexer, for a ring network with 100 nodes, the worst insertion loss would be 100dB. However, splitting loss in an ideal star coupler with 100 fan out is only $10 \times \log_{10} 100 = 20\text{dB}$. There is still a lot room in terms of power budget for other component insertion losses before the total loss reaches 100dB. Most WAN networks use the ring structure. In a WAN environment, usually, the number of nodes in a ring is moderate and the transmission loss is important in the power budget. The wavelength add/drop multiplexer is therefore a very useful device. However, in an optical LAN environment, the number of nodes could easily be a few hundred. Transmission loss is usually not very important in a LAN, considering the limited span. As we have seen, the cascaded insertion loss from add/drop multiplexers in a ring structure can easily overwhelm the splitting loss in a broadcast and select structure. In this case, a broadcast and select structure may be the best in terms of power budget and

the ease of maintenance. In this case, our proposed logarithmic demultiplexer could be very useful.

5.4 Demultiplexing CDM Channels

As we have seen in the last chapter, for demultiplexing an N -wavelength CDMA channel, a decoder with $\log_2 N$ complexity can be built, requiring only logarithmic demultiplexing complexity, as in TDM and WDM systems.

Here, we would like to give another example of generating CDMA codes with logarithmic demultiplexing complexity, using the rectangular shaped WDM filter as described in Appendix E. The code that we would like to discuss in this section is the Hadamard code, which is discussed in Appendix A.

All N codes (rows) in the $N \times N$ Hadamard matrix [35] \mathbf{H}_n can be generated iteratively in the following way, using an 8-bit code example. Starting with an N -bit vector of all 1s, i.e. (1 1 1 1 1 1 1 1) which is also the first code, a second code is obtained by bit-wise multiplication of the original code by an N -bit mask of alternating 1's and -1's and a period of two bits, i.e. (1 -1 1 -1 1 -1 1 -1). This generates the second code (1 -1 1 -1 1 -1 1 -1). Each of the existing codes (1 1 1 1 1 1 1 1) and (1 -1 1 -1 1 -1 1 -1) is then bit-wise multiplied by another mask similar to the previous one but with twice the period, i.e. (1 1 -1 -1 1 1 -1 -1). This generates two more codes (1 1 -1 -1 1 1 -1 -1) and (1 -1 -1 1 1 -1 -1 1). The process is continued and the period of each new mask is twice that of the previous mask until the mask period becomes N , i.e. (1 1 1 1 -1 -1 -1 -1). Each new mask doubles the number of codes obtained by bit-wise multiplying itself with all the previously generated codes to form new codes. It can be

easily shown by induction that with this process, all the N codes (rows) in an $N \times N$ Hadamard matrix \mathbf{H}_n described in (1) can be generated with $n = \log_2 N$ steps.

The N elements in an N -bit Hadamard Code can be represented using N wavelengths I_1, I_2, \dots, I_N which can be generated by a multi-wavelength laser diode module [36] or a mode-locked laser source [48]. In Chapter 3, we used an arrangement similar to the WDM add/drop filter in Fig. 5.4 to generate Hadamard codes in the 4-wavelength experiment. The encoder and decoder have pretty complicated structures. Here, we give an implementation example of multi-wavelength Hadamard codes using a two-port complementary intensity transfer function of an N -wavelength spectrum. As in Chapter 3, if the m th bit ($1 \leq m \leq N$) of the Hadamard code is a 1, then I_m is sent to the first output port. If the m th bit is a -1 , then I_m is sent to the complementary (second) output port. The 1s and -1 s in a Hadamard code can be regarded as the bipolar difference signal of each wavelength from the two output ports.

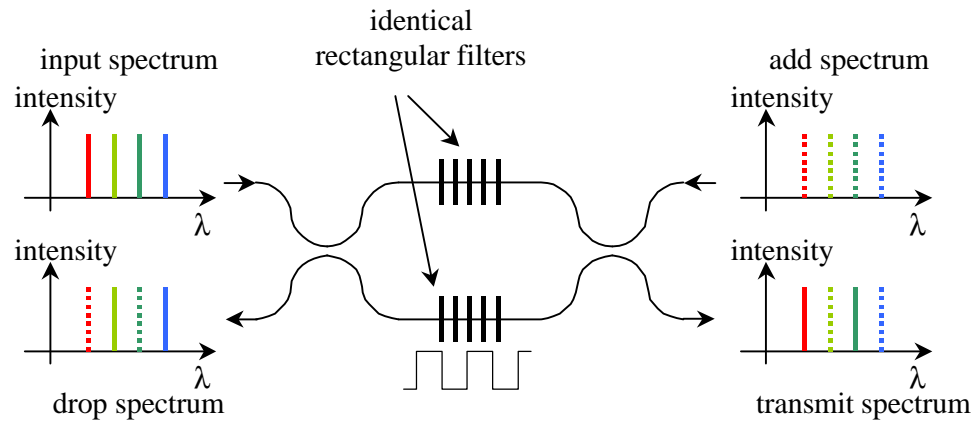


Figure 5.6 A multi-wavelength signal add/drop multiplexer using a Mach-Zehnder interferometer and rectangular shaped wavelength filters (see Appendix E).

The Mach-Zehnder interferometer arrangement shown in Fig. 5.6 (also see Appendix E) has been used with fiber gratings as optical add-drop multiplexer (ADM) for wavelength division multiplexing (WDM) [49]. The transmitted spectrum of the identical filters incorporated in the balanced MZI is passed to an output port of the MZI on the opposite side of the input signal. The reflected signal is dropped at the output port on the same side as the input signal. Different signals at the same wavelengths as the dropped signal can be added to the transmitted signal from the second port opposite to the input port because of filter symmetry. A mask in the last paragraph is represented by an MZI-ADM with the appropriate FSR. ADM's with progressively bigger FSR are cascaded as in Fig. 5.7. The period of each following stage is twice that of the current stage. Each stage is set as masked (state 1) or non-masked (state 0) by a number of switches as shown in Fig. 5.7. By properly setting the state combinations of all the n stages, all $N = 2^n$ Hadamard codes can be produced at the output of the last stage. The codes can be programmed by programming the switches in the encoder.

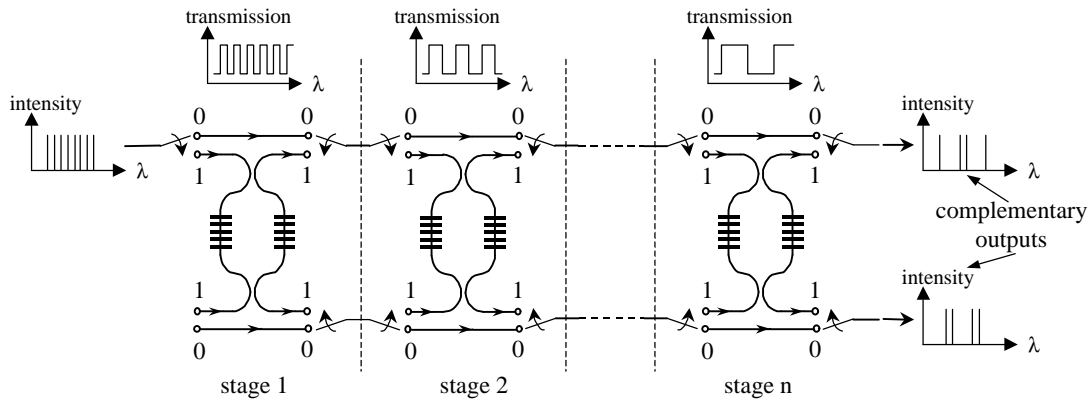


Figure 5.7 Generating multi-wavelength complementary intensity encoded Hadamard codes using multi-wavelength add/drop demultiplexers.

A second representation of Hadamard codes makes use of the phase relationships among different codes. 1's and -1's can be represented by 0 and π phase shifts. A structure to realize the phase representation is shown in Fig. 5.8. The input N -wavelength signal is arranged in a way such that as it bounces back and forth between the series of mirrors, it passes through a series of filters with progressively increasing FSR. Half of the frequency components will pass through each filter before being combined with the reflected signal from that filter. A phase shifter, which can impose a 0 or π phase shift to the signal that goes back and forth through a filter, is placed on the opposite side of that filter. Zero phase shift corresponds to the case of no mask and π phase shift corresponds to a phase shift. By properly setting the phase shifts at various stages, it can be easily shown that all the N Hadamard codes can be represented by the extra phase shifts (modulo 2π) introduced at various wavelengths. The codes produced can be directly applied to coherent phase encoded optical CDMA systems [26, 62].

Thus, we have proposed two optical approaches to generate Hadamard codes in both the intensity and phase representations. The proposed approaches make use of multi-wavelength arrangement to achieve parallel signal processing. The complexity of both schemes grows as $\log_2 N$ for an N bit Hadamard code generation. These approaches could be applied to optical code division multiple access system.

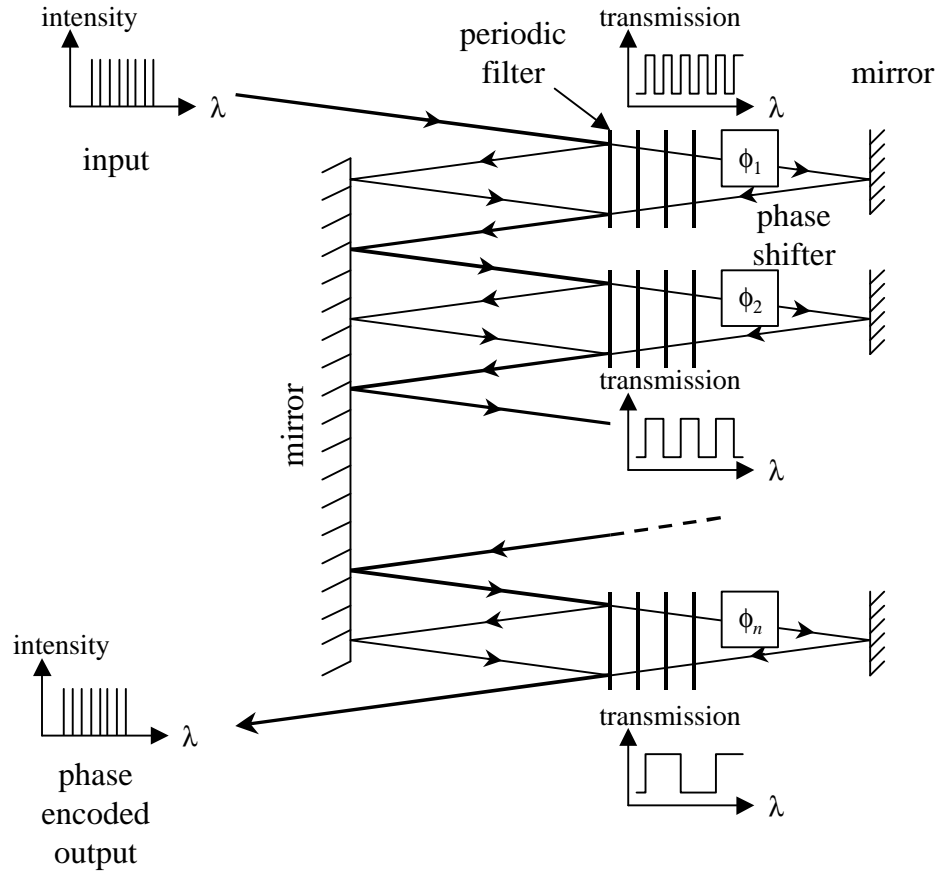


Figure 5.8 Generating multi-wavelength phase encoded Hadamard codes.

5.5 Conclusion

In this chapter, we have discussed the general scaling complexity for demultiplexing signals in TDM, WDM and CDM systems. It is interesting that in all three multiplex access systems, logarithmic demultiplexing complexity can be achieved theoretically. For the WDM system, the simplest demultiplexer is a tunable wavelength filter, which has a complexity of 1 and independent of the number of wavelengths. However, there are still technical challenges that limit its use. We also compared wavelength add/dropped WDM systems, which use wavelength routers, with broadcast

and select WDM systems. A novel WDM demultiplexer with logarithmic complexity has been proposed. The rectangular shaped wavelength filter required in this structure is described in Appendix E.

We describe two additional encoder structures with logarithmic complexity that can be used to generate the Hadamard codes for CDMA systems. The encoders proposed here require the new periodic rectangular filter of Appendix E.

Chapter 6 Conclusion

In this project, we first reviewed the previous work on fiber optic CDMA systems. There used to be a notion that the abundance of bandwidth available in optical fiber would never be fully utilized because of the electronic bottleneck. It was therefore, conceived that if part of the processing, such as channel multiplexing can be done in the optical domain by taking the advantage of the “redundant” bandwidth in optical fibers, then one could improve the throughput of a network. Based on this assumption, Hui [13] and Prucnal [14] proposed the delay line network encoded optical CDMA systems to asynchronously multiplex signals optically.

One of the considerations in designing optical CDMA systems is coding. Direct detection of the optical signal intensity has been established as the most practical in optical communications. Intensity encoding has been used in the delay line encoded systems. Since intensity is a positive signal, it is difficult to maintain orthogonality in those systems. It turns out that the penalty due to non-orthogonality is very large. Even though tremendous efforts have been invested in designing the codes, the bandwidth efficiency and the BER of delay line encoded CDMA systems are still very poor.

The growth of the Internet usage and the proliferation of numerous new network applications in the past five years has revolutionized the field of optical communications. Every Hertz available in optical fibers is now valuable for carrying network traffic and

terabit network demonstrations have been successful. The prevailing trend for optical communication is dense WDM technology.

Nonetheless, numerous proposals [13-33] for optical CDMA systems have attempted to apply the spread spectrum technique in optical fiber. Unfortunately, they all suffer from difficulties which prevent them from being successful. In order for optical CDMA systems to achieve high throughput and high bandwidth efficiency, it is important to maintain code orthogonality. This demands coherent detection, which detects the electric field, or differential intensity detection to obtain negative quantities.

In this project, we studied spectrally encoded optical CDMA systems. Both spectral intensity encoded and spectral phase encoded optical CDMA systems have been studied. Unlike time domain encoded CDMA systems, encoding is carried out in the frequency domain in these systems. We managed to achieve full orthogonality in both the systems we have studied. Balanced detectors, which compute the difference between two positive quantities, are used to obtain the required negative quantities to achieve full orthogonality.

Despite the fact that the spectral intensity encoded system is fully non-coherent, it is able to achieve full orthogonality. However, due to phase variation and bandwidth sharing, this type of systems suffers from beating noise, or the speckle noise as we call it. Since speckle noise is proportional to the signal power, increasing the signal power will not improve the signal to noise ratio when the system is speckle noise dominated, as happens in many optical CDMA systems. The result of speckle noise is a severe limitation in the total achievable throughput. The balanced receiver used in the spectral

intensity encoded system is only balanced in an average sense integrated over the two complementary spectra. There is no common mode cancellation, leaving it susceptible to speckle.

In order to avoid the speckle noise, we devised a spectral phase encoded optical CDMA system using mode locked laser sources. To achieve orthogonality, time synchronization is required. Balanced detection and orthogonality eliminates speckle noise. In order to avoid having an optical local oscillator, the carrier is transmitted together with the side bands to the receiver, as an externally supplied local oscillator. Synchronization of the optical phases is unnecessary. The only synchronization requirement is to the precision of the mode-locked pulse widths, as required in optical TDMA systems. The balanced receiver in this set-up functions as a balanced mixer. The two photodetectors are balanced wavelength-by-wavelength, and common mode rejection is achieved across the full spectrum. Although this system is able to avoid speckle noise, it is limited by cumulative shot noise which is unavoidable in any optical CDMA system, due to the fact the receiver has to detect the optical signal power from all the users. Since shot noise is proportional to only the square root of the signal power, the performance can be improved by increasing the signal power.

In Chapter 5, we showed that in a broadcast and select network, logarithmic demultiplexing is theoretically possible for all three multiple access schemes, TDM, WDM and CDM. However, in a WDM system, using a tunable wavelength filter, one can achieve a scaling complexity of one. In reality, a tunable wavelength filter with the required finesse and high tuning speed cannot be made. Most of the existing WDM

systems today use wavelength routers, which have linear scaling complexity with respect to the number of wavelengths.

So from the scaling complexity point of view, all three multiple access systems are theoretically similar. Whether one system will become popular depends on the manufacturing difficulty and the cost associated with its demultiplexing components. We proposed some possible CDMA encoder and decoder structures with logarithmic scaling complexity in Chapters 4 and 5. In Appendix E, a rectangular shaped wavelength filter will also be presented. Most of these ideas have yet to be built and tested. Nevertheless, they present a theoretical foundation for the possibilities of logarithmic demultiplexing.

In view of transmission in optical fiber, TDM signals are the most limited by dispersion, since each TDM signal pulse occupies a very narrow time slot in the time domain and a large bandwidth in the frequency domain. Therefore, TDM networks are very limited in physical extent. For the same total throughput, WDM signals are least affected by dispersion because each WDM pulse occupies the full TDM frame duration but only a narrow band in the frequency domain. The channels in a CDM system occupy both a wide band as TDM signals and long pulse duration as WDM signals. It turns out that the dispersion limited propagation distance of CDM systems is the geometric mean of that of TDM and WDM [63].

We have also seen in the previous chapters that all CDMA systems are eventually limited by cumulative shot noise. This is due to the fact that a receiver in a CDMA system detects the power from all other channels. Provided there is a way to spatially separate the signals belonging to different codes and to receive the desired channel only,

then it would be possible to avoid cumulative shot noise. This would require a code add/drop multiplexer. Since we started this project three years ago, we have been looking for a code add/drop multiplexer for CDMA systems. But we do not have such a design and we do not think there exists such a passive code demultiplexer. Code orthogonality requires time synchronization, which cannot be detected by a passive filtering device. On the contrary, in WDM systems, each channel can be filtered from the other channels. Therefore, cumulative shot noise does not happen in WDM systems. Similar arguments favor TDM systems over CDMA systems.

Another consequence of the lack of add/drop multiplexers in CDMA systems is that the physical network architecture is limited to broadcast and select. As a result of the second law of thermodynamics, it is impossible to combine signals of the same frequency from two sources into one fiber without suffering loss, since it requires the concentration of energy. On the contrary, it is natural to add/drop WDM channels and examples have been given in Chapter 5. Thus CDMA systems suffer unduly from shot noise, and are disadvantaged by the unavailability of code add/drop multiplexing.

Comparing optical CDMA with radio CDMA, while electrical field detection is widely used in radio communication systems, intensity detection is more practical in optical communication systems. Shot noise is important in optical communication because of the short wavelength, but it is negligible at radio frequencies. Each photon in the signal stream is converted into individual electron-hole pairs through the photoelectric effect. The granularity of photons is reflected as shot noise in the signal

output. In radio communications, however, the wavelength is much longer and the particle nature of electromagnetic (EM) waves is not important.

Security is an advantage associated with CDMA systems. In fact, spread spectrum communication systems were originally invented for military use. Because of coding, CDMA signals are inherently more difficult to demodulate. The encoding at the physical layer maybe useful for systems which need security but cannot afford the encryption delays, such as voice and motion picture transmission. Of course, various levels of security can be built into a system. A combination of physical layer encoding such as CDMA combining with other security techniques can render a system extremely secure to heckers and eavesdroppers. This maybe the biggest advantage of optical CDMA systems and should be a major direction for future optical CDMA research.

To obtain ultimate network throughput, WDM technology has been firmly established as a natural way of multiplexing channels on optical fibers to obtain high throughput and achieve low dispersion. CDMA will not compete with WDM for the ultimate capacity in this author's opinion. If one can find a very low cost implementation of the CDMA encoders and decoders, there might be a chance that this technology could be useful as an option for fiber in the loop (FITL) or low cost optical LAN setups.

Appendix A Hadamard Codes

Hadamard codes have many uses in digital signal processing [35] and code-division-multiple-access (CDMA) communication systems [28-29,62]. An N -element Hadamard code is a row from an $N \times N$ orthogonal Hadamard matrix, which has $(1, -1)$ valued binary entries. The $N \times N$ Hadamard matrix \mathbf{H}_n where $N = 2^n$ is generated by the

core matrix $\mathbf{H}_1 = \begin{pmatrix} 1 & 1 \\ 1 & -1 \end{pmatrix}$ using the Kronecker product recursion

$$\mathbf{H}_n = \mathbf{H}_{n-1} \otimes \mathbf{H}_1 = \mathbf{H}_1 \otimes \mathbf{H}_{n-1} = \begin{pmatrix} \mathbf{H}_{n-1} & \mathbf{H}_{n-1} \\ \mathbf{H}_{n-1} & -\mathbf{H}_{n-1} \end{pmatrix} \quad (\text{A.1})$$

All N codes (rows) in the $N \times N$ Hadamard matrix \mathbf{H}_n can be generated iteratively in the following way, using an 8-bit code example. Starting with an N -bit vector of all 1's, i.e. $(1\ 1\ 1\ 1\ 1\ 1\ 1\ 1)$ which is also the first code, a second code is obtained by bit-wise multiplication of the original code with an N -bit mask of alternating 1's and -1 's and a period of two bits, i.e. $(1\ -1\ 1\ -1\ 1\ -1\ 1\ -1)$. This generates the second code $(1\ -1\ 1\ -1\ 1\ -1\ 1\ -1)$. Each of the existing codes $(1\ 1\ 1\ 1\ 1\ 1\ 1\ 1)$ and $(1\ -1\ 1\ -1\ 1\ -1\ 1\ -1)$ is then bit-wise multiplied with another mask similar to the previous one but with twice the period, i.e. $(1\ 1\ -1\ -1\ 1\ 1\ -1\ -1)$. This generates two more codes $(1\ 1\ -1\ -1\ 1\ 1\ -1\ -1)$ and $(1\ -1\ -1\ 1\ 1\ -1\ -1\ 1)$. The process is continued and the period of each new mask is twice that of the previous mask until the mask period becomes N , i.e. $(1\ 1\ 1\ 1\ -1\ -1\ -1\ -1)$. Each new mask doubles the number of codes obtained by bit-wise multiplying itself with all the previously generated codes to form new codes. It can be easily shown by

induction that with this process, all the N codes (rows) in an $N \times N$ Hadamard matrix \mathbf{H}_n described in (A.1) can be generated in $n = \log_2 N$ steps.

It is well known that an $(N \times N)$ Hadamard matrix of 1's and -1's has the property that any row differs from any other row in exactly $N/2$ positions. All rows except one contains $N/2$ (-1)'s and $N/2$ (1)'s. As an example, for $N = 4$

$$\mathbf{H}_4 = \begin{pmatrix} 1 & 1 & 1 & 1 \\ 1 & -1 & 1 & -1 \\ 1 & 1 & -1 & -1 \\ 1 & -1 & -1 & 1 \end{pmatrix} \quad (\text{A.2})$$

In Chapter 3, we can regard each of the two complementary filters mask as a unipolar (1, 0) sequence in the wavelength domain. This (1, 0) sequence is obtained from a bipolar (1, -1) sequence by replacing each -1 with 0. So a unipolar Hadamard code $\mathbf{X} = (x_1, x_2, \dots, x_N)$, representing a direct spectrum, is obtained by transforming the bipolar code $\mathbf{Y} = (y_1, y_2, \dots, y_N)$ using the operation $x_i = (1 + y_i)/2$. The complementary spectrum is represented by $\bar{\mathbf{X}} = (\bar{x}_1, \bar{x}_2, \dots, \bar{x}_N)$, where $\bar{x}_i = 1 - x_i = (1 - y_i)/2$.

Let \mathbf{U} be another unipolar Hadamard code obtained from the bipolar code \mathbf{V} , which is orthogonal to \mathbf{Y} . The balanced receiver output from code \mathbf{U} , due to the direct spectrum \mathbf{X} is given by:

$$\begin{aligned}
Z &= \Theta_{XY} - \Theta_{X\bar{Y}} = \sum_{i=1}^N \frac{1+y_i}{2} \frac{1+v_i}{2} - \sum_{i=1}^N \frac{1+y_i}{2} \frac{1-v_i}{2} \\
&= \frac{1}{2} \sum_{i=1}^N v_i + \frac{1}{2} \sum_{i=1}^N y_i v_i = 0
\end{aligned} \tag{A.3}$$

The first term sums up to zero from the fact that half of the entries in a Hadamard code (except for the first row in a Hadamard matrix) are -1 's and the other half 1 's. The second term is zero due to the orthogonality of Hadamard codes.

In fact one can also show that:

$$Z = \Theta_{\bar{X}\bar{Y}} - \Theta_{\bar{X}Y} = 0 \tag{A.4}$$

Equations (A.3) and (A.4) together proves the orthogonality of complementary spectral intensity encoding using Hadamard codes.

In the following paragraphs, we show that orthogonal differential unipolar codes can be obtained from transformation of any orthogonal bipolar codes. Basically, any number can be represented as a combination of real, unipolar components. One can represent a bipolar sequence $(Y) = (y_0, y_1, \dots, y_{N-1})$ by its unipolar version $(Y^u) = (y''_0, y''_1, \dots, y''_{2N-1})$. Note that

$$\begin{aligned}
y''_{2i} &= 1 & y_i &= 1 \\
&= 0 & y_i &= -1 \\
y''_{2i+1} &= 0 & y_i &= 1 \\
&= 1 & y_i &= -1
\end{aligned} \tag{A.5}$$

Therefore, the condition $Z = \Theta_{X^u Y^u}(k) - \Theta_{\bar{X}^u Y^u}(k) = 0$ is equivalent to

$$\begin{aligned}
Z &= 2 \left[\sum_{i=0}^{2N-1} x_i^u y_i^u \right] - \sum_{i=0}^{2N-1} y_i^u \\
&= 2 \left[\sum_{i=0}^{N-1} \frac{(x_i + 1)(y_i + 1)}{2} + \sum_{i=0}^{N-1} \frac{(1-x_i)(1-y_i)}{2} \right] - \sum_{i=0}^{2N-1} y_i^u \\
&= \sum_{i=0}^{N-1} x_i y_i = \Theta_{XY}(0) = 0
\end{aligned} \tag{A.6}$$

which is the usual bipolar cross-correlation function. Therefore, all orthogonal ($\Theta_{XY} = 0$) bipolar (-1, 1) codes can be transformed into a unipolar code suitable for complementary spectral intensity encoded optical CDMA systems. For a unipolar sequence of length of $2N$, only N subscribers however, can be accommodated. That is, twice as many frequency slots need to be used.

Appendix B Procedure for Calibrating the Cascaded Mach-Zehnder Encoder

In order for the transmitter and receiver to behave properly, the cascaded Mach-Zehnder (MZ) encoders used in the experiment described in Chapter 3 need to be as identical as possible. However, due to manufacturing errors, the two devices cannot be identical and they need to be calibrated. The manufacturer guarantees that the accuracy in all the path lengths of the MZ is to within $\pm 0.5\mu\text{m}$ absolute error due to lithography mismatches. Therefore, the absolute error in each device is less than one third of the center wavelength of operation, which is about $1.5\mu\text{m}$. What we need to do is to apply a bias to each stage to align the encoder at the transmitter and the decoder at the receiver. The calibration process involves finding these biasing points and obtaining the thermal power (and hence the voltage) required for a π phase shift at each stage.

Both MZ encoders are pigtailed with polarization maintaining single mode fibers. The output from a narrow line width laser source is launched along the fast-axis of the pigtail. The response function from a single isolated MZI is a sinusoid in the frequency domain. The extinction ratio between the peak and valley of the sinusoid is dependent upon the coupling ratios of the splitters used in an MZI. If the couplers are exactly 3-dB, the peak and valley correspond to full transmission and no transmission. The 3-dB coupling ratio is a good approximation in our case.

Suppose the first stage MZ is biased at a point such that all the power at the wavelength of the laser diode enters either one of the two arms of the second stage MZ. No matter what phase shift is introduced at the second stage MZ, there would then be no change to the output due to the change in the phase shift of the second stage, since only one arm has light and interference is impossible. So we measure the output power of the last stage of the encoder and while changing the bias at both stage 1 and stage 2. For each bias voltage of stage 1, the stage 2 bias is changed continuously and the variation of the output power is measured. We look for the minimum power variation due to stage 2 bias change. This corresponds to stage 1 setting that results in all of the power going into either one of the two arms of the next stage MZI. We call this bias the π point. A second π point is also found by increasing stage one bias. From the difference between the two adjacent π points, we can find out the input power requirement at the first stage thermal phase shifter for a π phase shift.

Once stage 1 is calibrated, it is then biased at the π -point. With the stage 1 bias set at the π -point, we can then obtain the π points of stage 3 in the same manner. By the same token, the π points of the fifth and seventh stages can be found recursively in this way.

To obtain the calibration of the even stages, we set the stage 1 bias to the middle of two π points so that 50% of the input power goes into each arm of the second MZ stage. The bias of the second stage is varied gradually. For each value of the second stage bias, the third stage bias is varied and the output power variation is measured. Again, we look for second stage biases (π points) such that the output power variation is

minimized when the third stage bias is changed. Similarly, we extend the principle to find the π points of all the even stages.

Once the π points are found, all the decoders and encoders at the transmitters and receivers are biased at the π points. The bias ensures that the mismatches due to manufacturing are all corrected for and the encoder and decoder are aligned. Various codes can then be generated by introducing 0 or $\pi/2$ extra phase shifts at various stages.

Appendix C Number of Modes in Multi-mode Fibers

The number of modes in a multi-mode optical fiber can be evaluated using the density of states. It can be proven [64] that the number of guided modes M_g in a graded index fiber is given by:

$$M_g = \left(\frac{\mathbf{a}}{\mathbf{a} + 2} \right) (n_1 k a)^2 \Delta \quad (\text{C.1})$$

where $k=2\pi/\lambda$, a is the core radius, Δ is the relative refractive index contrast of the fiber defined using the core and cladding refractive indices n_1 and n_2 as $\Delta=(n_1^2-n_2^2)/2n_1^2$. For a parabolic refractive index profile, $\mathbf{a}=2$ and for a step index profile $\mathbf{a}=\infty$. The numerical aperture (NA) of a fiber is defined as:

$$NA = (n_1^2 - n_2^2)^{\frac{1}{2}} \quad (\text{C.2})$$

Substituting the parameters for a commercial graded index multi-mode fiber with $a = 62.5\mu\text{m}$, $NA = 0.275$ and $\alpha = 2$, we obtain $M_g = 324$.

Appendix D Throughput Calculation for Non-coherent Complementary Spectrally Encoded CDMA

To obtain a certain BER, the minimum SNR requirement is evaluated from Equation (3.25). We also have:

$$SNR = \frac{I_{sig}^2}{\langle I_{th}^2 \rangle + \langle I_{sh}^2 \rangle + \langle I_{sp}^2 \rangle} \quad (D.1)$$

$$= \frac{\mathfrak{R}^2 P_{rec}^2}{8pkTB_d^2 C + 2q\mathfrak{R}P_{rec}KB_d + \mathfrak{R}^2 P_{rec}^2 (K^2 + 1) \frac{2B_d}{mMB_{opt}}}$$

$$8pkTCB_d^2 + [2q\mathfrak{R}P_{rec}K + \mathfrak{R}^2 P_{rec}^2 (K^2 + 1) \frac{2}{mMB_{opt}}]B_d - \frac{\mathfrak{R}^2 P_{rec}^2}{SNR} = 0 \quad (D.2)$$

The symbols are defined in Chapter 3. The received power P_{rec} is equal to P_t/K in an ideal system. Fig. 3.14a and Fig. 3.14b are obtained by solving (D.2) for B_d and plotting KB_d against K (assuming $m = 1$ for polarized light).

Most of the time, the system is interference limited. So we can ignore thermal noise by dropping the first term in Equation (D.2) and obtain:

$$[2q\mathfrak{R}P_{rec}K + \mathfrak{R}^2 P_{rec}^2 (K^2 + 1) \frac{2}{mMB_{opt}}]B_d = \frac{\mathfrak{R}^2 P_{rec}^2}{SNR} \quad (D.3)$$

The first term on the left-hand side represents the shot noise and the second term represents the speckle noise. If the system is shot noise limited, we have:

$$2q\Re P_{rec} KB_d = \frac{\Re^2 P_{rec}^2}{SNR}$$

$$\text{and } KB_d = \frac{\Re P_{rec}}{2q \cdot SNR} = \frac{\Re P_t}{2qK \cdot SNR} \quad (\text{D.4})$$

If the system is speckle noise limited, we have

$$\Re^2 P_{rec}^2 (K^2 + 1) \frac{2}{mMB_{opt}} B_d = \frac{\Re^2 P_{rec}^2}{SNR}$$

$$\begin{aligned} \text{and } KB_d &= \frac{mMB_{opt}}{2 \cdot SNR} \frac{K}{K^2 + 1} \\ &\approx \frac{mMB_{opt}}{2K \cdot SNR} \end{aligned} \quad (\text{D.5})$$

which is independent of the optical power.

Appendix E A Rectangular Shaped Wavelength Filter for WDM Demultiplexing

Optical fibers have 25THz available bandwidth in each of the three low loss operation windows [34]. In order to fully utilize the available bandwidth in fiber channels, and at the same time overcome the difficulties of ultra-fast electronics and fiber dispersion problems, dense wavelength division multiplexed (DWDM) systems time-shared among a large number of access nodes might be the solution for future high-bandwidth tera-bit multi-media and packet switched optical networks.

The ability to select an arbitrary wavelength in a DWDM network in a fraction of the packet duration is essential in realizing high-speed packet switched networks [65]. As described in Chapter 5, the wavelength router approach requires linear scaling complexity for the number of switches employed. Since switches are active components, such a linear scaling is undesirable in a DWDM system with N wavelengths where N is large.

In Chapter 5, we described the principle of a wavelength demultiplexer using the bisection method to achieve $\log_2 N$ scaling complexity for N wavelengths. A rectangular shaped wavelength filter is required in the demultiplexer described. The same filter has also been assumed in the Hadamard encoders in Chapter 5. In this appendix, we propose a photonic crystal waveguide structure to achieve the rectangular shaped filter function.

We present the simulation results and suggest a few possible settings in which the proposed waveguide can be incorporated for switching purposes.

I. Photonic Crystal Filter Design

A. Simple 1-D Photonic Crystal

To produce repeated pass bands and stop bands in the frequency domain, a one-dimension photonic crystal structure is used [59]. A simple 1-D photonic crystal consists of alternate layers of dielectric materials with refractive indices n_1 and n_2 (Figure E.1). It is well-known that such periodic structures will produce periodic stop bands and pass bands in the frequency domain [59,66]. The number of alternate layers used in the structure determines the transition sharpness of the band edges. The more layers used, the faster is the roll-off at the band edge.

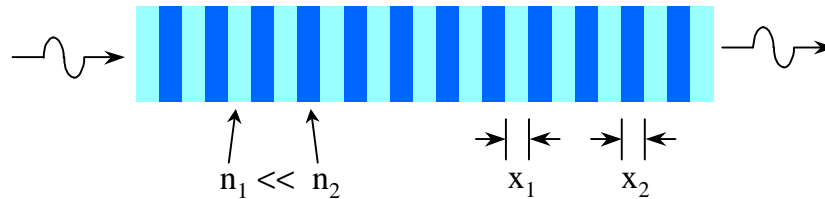


Figure E.1 A simple photonic crystal consists of alternate layers of dielectric materials. To produce equal width pass band and stop band, this system requires a refractive index contrast of 5.83.

The period of the structure ($n_1x_1 + n_2x_2$) determines the repetition frequency Δf of the band structure and is given by $x_i = c/(2n_i\Delta f)$ where c is the speed of light in vacuum. The center frequencies $\omega = 2\pi f = \omega_m$ of the forbidden bands occur at [66]:

$$k_1 x_1 = k_2 x_2 = \frac{(2m+1)}{2} \mathbf{p} \quad m = 0, 1, 2 \dots \quad (\text{E.1})$$

where $k_i = (\mathbf{w}/c)n_i$. The bandgap $\Delta \mathbf{w}_{\text{gap}}$ and the first band center \mathbf{w}_0 is related by [66]:

$$\Delta \mathbf{w}_{\text{gap}} = \mathbf{w}_0 \frac{4}{\mathbf{p}} \sin^{-1} \frac{|n_2 - n_1|}{n_2 + n_1} \quad (\text{E.2})$$

The key to logarithmic scaling is that the stopband and passband have equal bandwidth. This condition is satisfied when $\Delta \mathbf{w}_{\text{gap}} = \mathbf{w}_0$. Substituting into Equation (E.2), we obtain $n_2/n_1 = 5.83$. This actually corresponds to a 50% power reflection at each dielectric interface. However, such a high refractive index contrast is impractical for real physical systems.

B. Photonic Crystals with Effective Bragg Mirrors as Reflectors

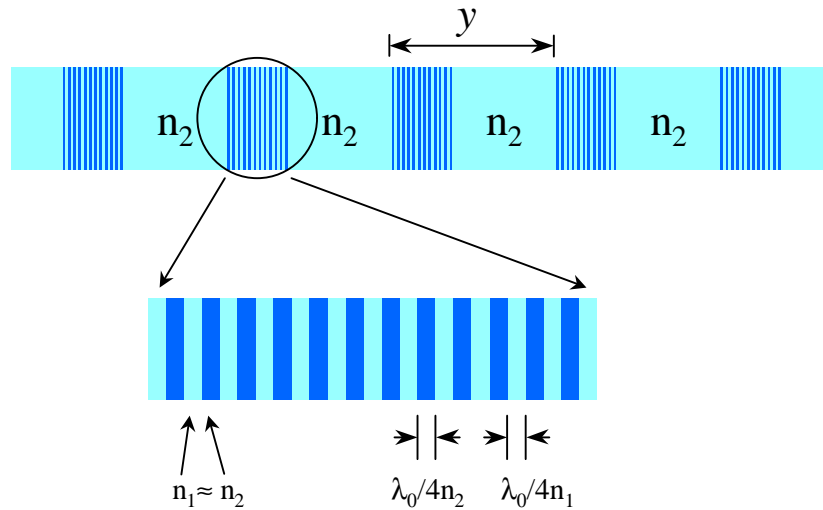


Figure E.2 The top view of a periodic rectangular shaped frequency filter consisting of effective Bragg Mirrors separated apart by distances y determined by the required free spectral range. The difference between the refractive indices n_1 and n_2 is 8.5%.

As we have seen before, equal width transmission band and forbidden band are obtained with periodic 50% power reflectors separated by distances determined by the filter periodicity in the frequency domain.

Since it is difficult to achieve the high reflectivity required with a single reflecting surface, as proved in the last section, we propose to use Bragg mirrors consisting of layers of quarter-wave dielectric materials as the reflectors in our rectangular shaped frequency filter. Figure E.2 shows the top view of such an arrangement. The refractive index and the number of layers in a Bragg mirror are chosen such that each effective mirror has a reflectivity of about 50% in the optical frequency range of interest. The best Erbium doped fiber amplifier (EDFA) in today's technology covers a 80nm bandwidth around the 1.55 μ m communication wavelength [67]. This is approximately a 5% window around the 1.55 μ m center wavelength. In order for the mirror to be effective over such a wavelength window, the number of layers has to be limited to achieve a low Q. On the other hand, it is easier to achieve 50% reflectivity at the center wavelength with lower refractive index contrast when more layers are used.

In our design, we used a refractive index contrast of $(n_2 - n_1)/n_1 = 8.5\%$ and eleven periods of quarter-wavelength layers. The transmission and reflection of such a periodic Bragg mirror are calculated using the transfer matrix method [66] and are plotted in Fig E.3. The input optical signal has a normal incidence on the mirror. The reflectivity is about 50% in the frequency range of interest.

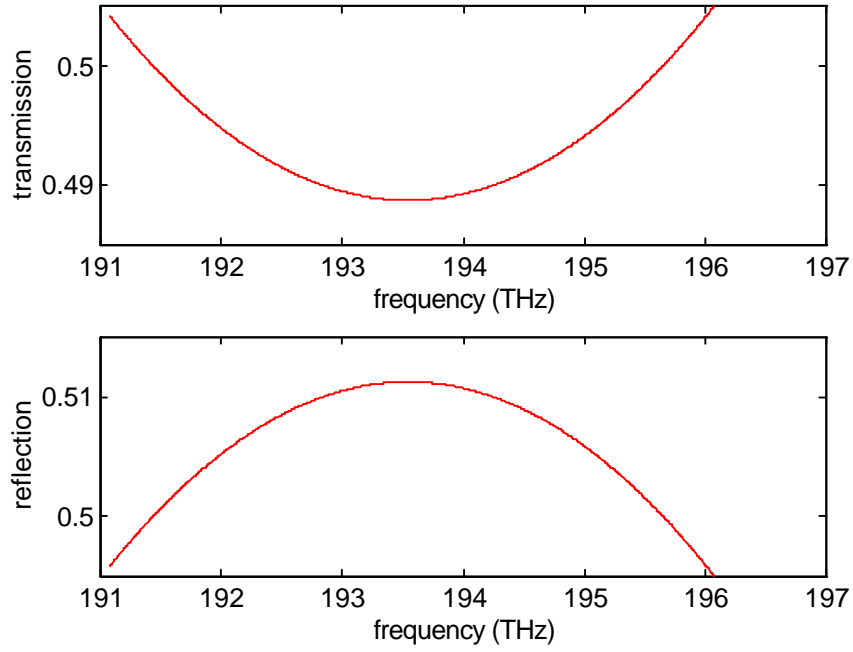


Figure E.3 The simulated transmission and reflection of the effective Bragg mirror used in the Fig. E.2. 11 periods of quarter-wave stacks are used in the simulation and the result obtained corresponds to a 40nm wide region around the 1.55 μm center wavelength.

Arranging these 50% effective mirrors in series as in Fig. E.2 forms our rectangular shaped frequency transfer filter. Again, the number of mirrors used determines the sharpness of the band edge. The separation between the mirrors is given by:

$$y = \frac{c}{2n_2\Delta f} \tag{E.3}$$

where Δf is the desired periodicity in the frequency domain.

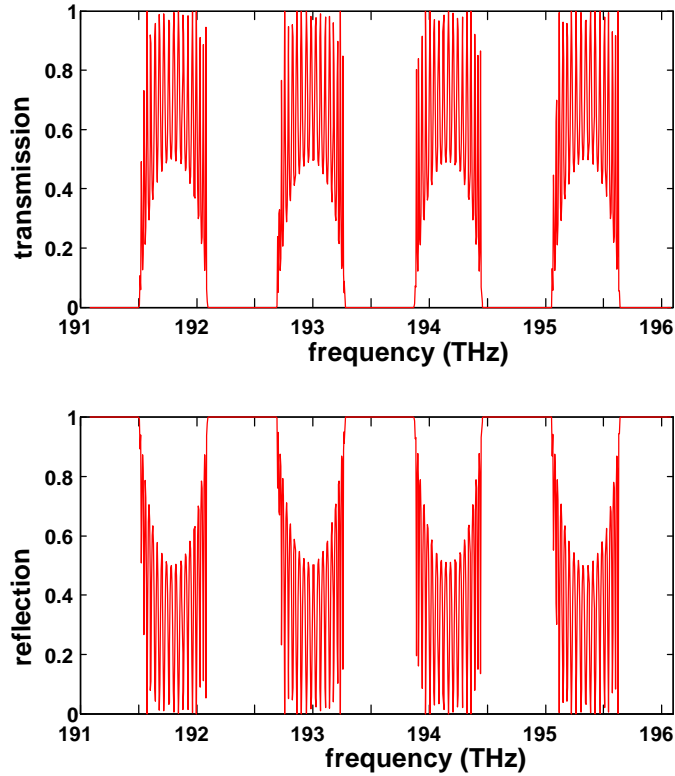


Figure E.4 The simulated transmission and reflection of the filter in Fig. E.2 over a 40nm wide region around the 1.55 μ m center wavelength. 19 effective Bragg mirrors are separated by distances, which will produce four periods in the simulated frequency range. The fringes in the pass bands are due to the reflections at the two end mirrors.

By using 19 mirrors, calculated with the transfer matrix method, we obtained the transmission and reflection spectra shown in Fig. E.4. The filter response is simulated over a 40nm region around the 1.55 μ m center wavelength. Four frequency band periods are included in this simulation. Again, we assumed normal incidence of the input optical signal to the filter. The pass band and stop band have equal bandwidth and the stop band has almost complete attenuation of the input signal. Therefore, we can achieve the same

stop-band width that we would get with a large index contrast, by using a moderate Δn , in discrete groups of many layers.

C. Apodization of Bragg Mirrors

It is seen in the above design that the filter response in the pass band is far from desired. The fringes in the pass band correspond to the reflections at the two end mirrors which have abrupt termination to the surroundings. In order to “smooth” out the pass band, we apodized the mirrors so that the reflectivity gradually decreases as we move from the center mirror towards the two end mirrors. This is done by decreasing the number of periods used in the Bragg mirrors using a Gaussian function rounded to the nearest integer according to the following formula:

$$M_i = \left\lceil M \frac{K+1}{2} \exp \left[- \left(\frac{i - (K+1)/2}{\mathbf{a}} \right)^2 \right] + 0.5 \right\rceil \quad (\text{E.4})$$

where M_i is the number of layers used in the i th mirror and \mathbf{a} determines the width of the Gaussian function. The total number of mirrors K is assumed to be an odd number for simplicity. We used $K = 19$, $M_{(K+1)/2} = 11$ and $\mathbf{a} = 6$ in one of our designs. Using this design, the outermost mirrors will only have one layer. The simulation result is plotted in Fig. E.5. It can be seen that the pass-band ripple is very small.

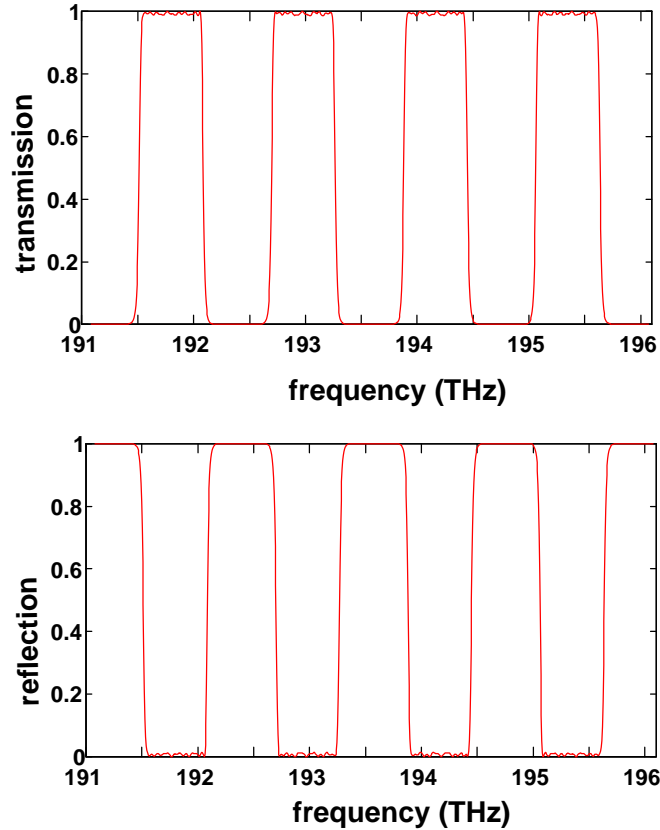


Figure E.5 The simulated transmission and reflection of a Gaussian apodized filter. The pass band ripples are suppressed by the apodization.

D. Physical Implementation of Rectangular Shaped Frequency Filters

Fig E.6 shows the perspective view of a possible physical implementation of the apodized rectangular shaped filter on a ridged waveguide [68-71] made out of common semiconductor materials. The low index of refraction dielectric could be formed, for example, by etching grooves on the ridged waveguide. Each groove is a quarter wavelength ($I_0/4n_1$) thick and the separation between adjacent grooves in a Bragg reflector is also a quarter wavelength ($I_0/4n_2$) where I_0 is the center wavelength of the frequency band covered. Taking Si ($n = n_2 = 3.44$) as the waveguide substrate, each

quarter-wave layer is about $0.11\mu\text{m}$. The distance between two adjacent Bragg reflector is chosen as $y = c/(2n_2\Delta f)$ in the simulation. This distance determines the free spectral range (FSR) of the filter. In our simulated design, the frequency domain period is $\Delta f = 1.25\text{THz}$ ($\sim 10\text{nm}$) which corresponds to a mirror separation of $34.9\mu\text{m}$. Using the data that we have collected, the total length of the filter example in this design is about $654\mu\text{m}$. For the coarse stage, a larger number of mirrors need to be used to get sharper edges. But the separation between the mirrors will decrease quickly as the frequency periodicity increases. Compared to the fiber grating technology, the overall size of the proposed structure is very small and has the potential for integrated photonic implementations.

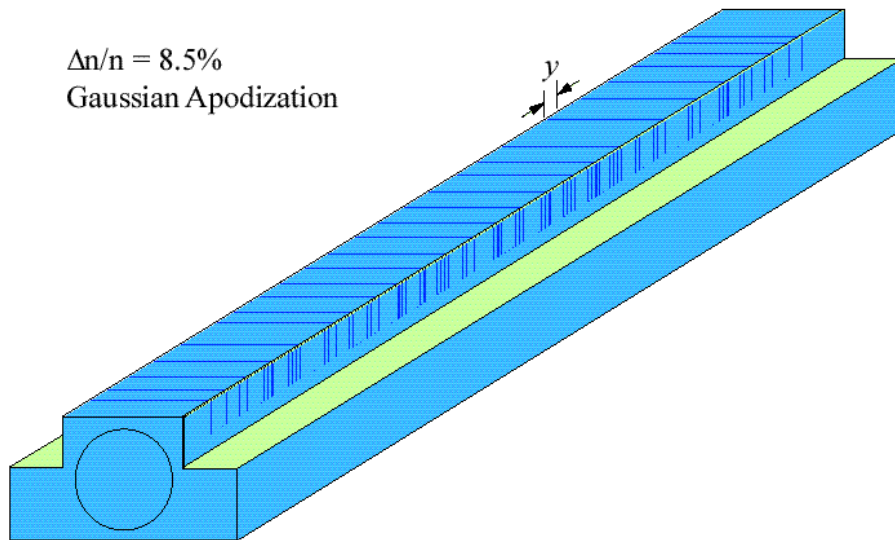


Figure E.6 The perspective view of an apodized periodic rectangular shaped frequency filter in a ridged waveguide structure. The Bragg reflectors with apodized reflectivity are formed by etching grooves in the ridged waveguide. This figure shows the number of layers in each Bragg reflector as prescribed by Equation (E.4) and as used in the numerical simulation.

II. Wavelength Switching Using Logarithmic Filter Chains

In this section, we discuss how to connect the rectangular shaped periodic filters to achieve logarithmic scaling complexities for WDM applications.

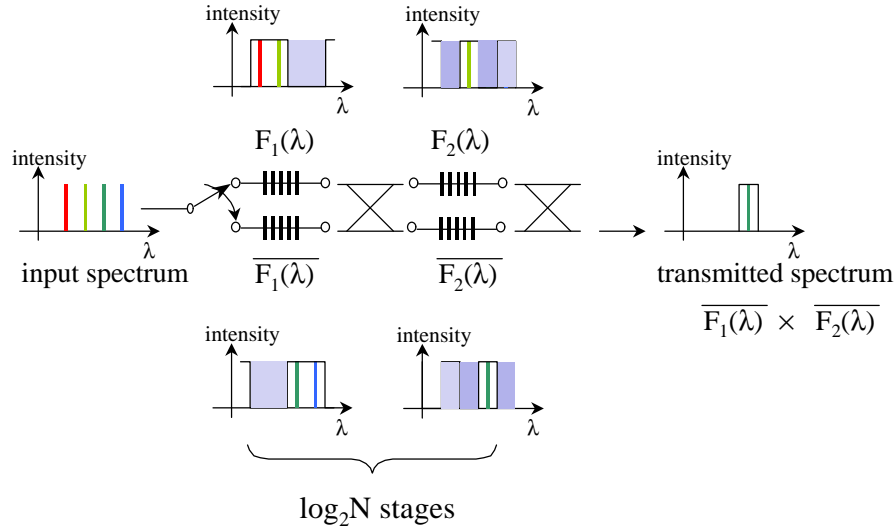


Figure E.7 Wavelength selection using 2×2 optical switches and cascaded complementary periodic rectangular shaped spectral filter pairs.

The first and most straightforward way is to connect pairs of complementary transmission filters with 2×2 switches in series as shown in Fig. E.7. As the frequency period Δf in the filter transfer function is small compared to the center frequency, a small change in the periodicity would cause a slip of a half period in the frequency range of interest without noticeable change in the period. This results in a complementary filter function in the frequency range of interest. Figure E.8 shows an example of two filters whose transfer functions are complementary. Each filter has eight periods over a 40nm wide bandwidth. The mirror separation distances in the two filters are different from

each other by about 1/300 which corresponds to about $0.2\mu\text{m}$ in length if implemented on silicon.

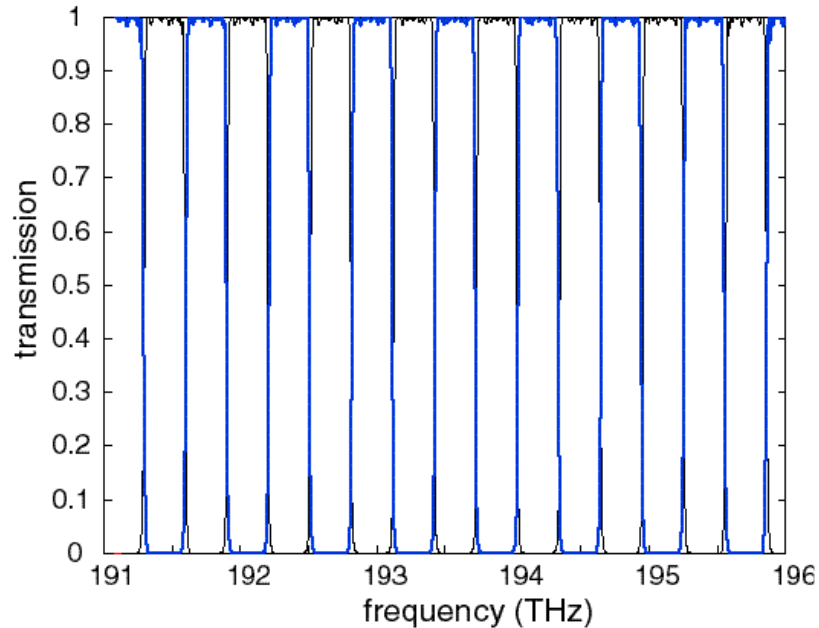


Figure E.8 Simulated result for two filters (thick and thin lines) which are slightly different in periodicity. Over a 40nm wide region around the $1.55\mu\text{m}$ center wavelength, eight periods are included. The two filters look “complementary” to each other.

The second way to obtain the complementary spectral outputs is by using the transmitted and reflected spectrum of the same rectangular shaped filter. The direct spectrum is obtained from the transmitted output. The reflected complementary spectrum can be separated from the input signal by using an optical circulator as shown in Fig. E.9.

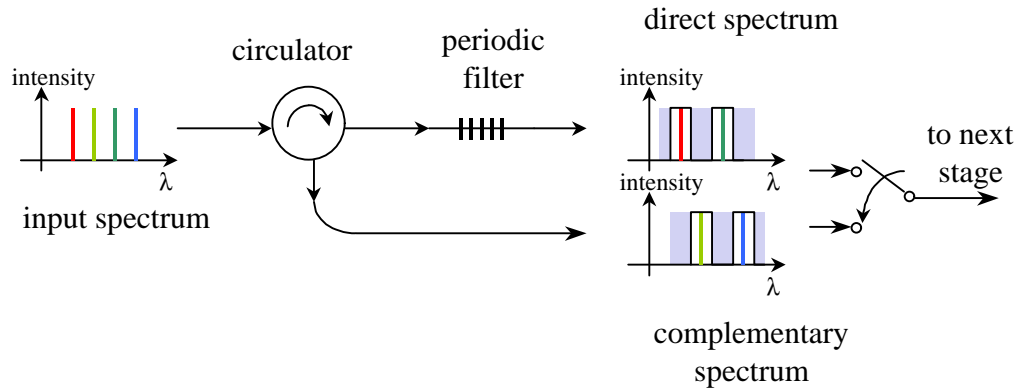


Figure E.9 Obtaining the direct and complementary spectral outputs from the transmitted and reflected filter outputs using an optical circulator.

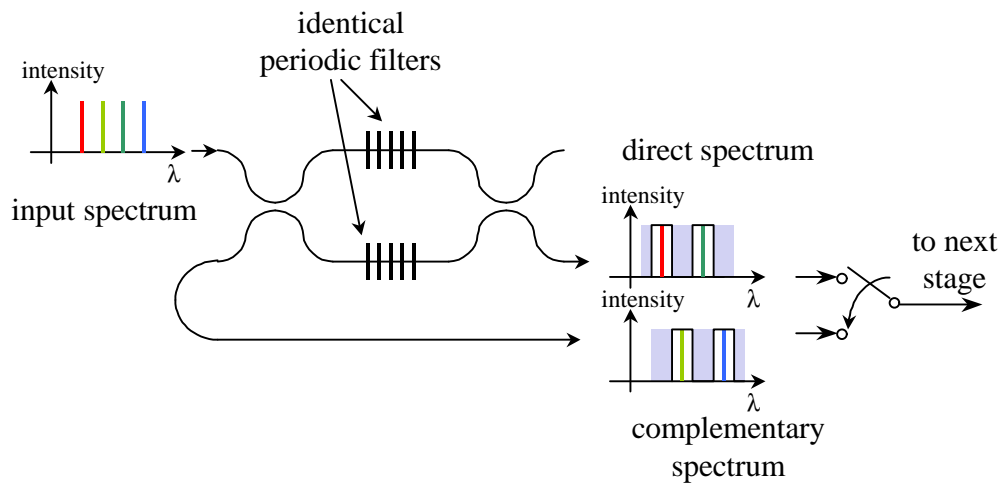


Figure E.10 Obtaining the direct and complementary spectral outputs from a Mach-Zehnder Interferometer (MZI). Identical filters are incorporated in two arms of equal length. The direct and complementary outputs propagate in opposite directions.

The third way to obtain the direct and complementary spectra can be achieved by using a Mach-Zehnder configuration with identical filters incorporated in the two arms (Fig. E.10). The direct and complementary spectra will propagate in opposite directions. This method has been used with fiber gratings for optical WDM add-drop [49].

As pointed out earlier, to pluck out one out of N wavelengths, only $\log_2 N$ stages and $\log_2 N$ switches are required. Electrooptic 2×2 switches with giga-hertz switching speeds are available commercially. A fast WDM demultiplexer with $\log_2 N$ complexity and the capability to filter out any one wavelength at nanosecond speed is therefore possible. Such devices should be good candidates for future dense WDM packet switched optical networks, which will have more flexibility and make better sharing and utilization of the enormous capacity provided by the optical fiber.

Bibliography

1. N.S. Bergano, "WDM Long-Haul Transmission Systems", *OFC'98 Tutorial*, Feb. 22-27, 1998, San Jose, California.
2. D.J.G. Mestdagh, *Fundamentals of Multiaccess Optical Fiber Networks*, Artech House, London, 1995.
3. R.L. Pickholtz, D.L. Schilling and L.B. Milstein, "Theory of Spread Spectrum Communications – A tutorial", *IEEE Trans. on Communications*, Vol. COM-30, No. 5, p855-884, May 1982.
4. R.L. Peterson, R.E. Ziemer and D.E. Borth, *Introduction to Spread Spectrum Communications*, Prentice Hall, New Jersey 1995.
5. G.R. Cooper and R.W. Nettleton, "A Spread Spectrum Technique for High-Capacity Mobile Communications", *IEEE Trans. Vehicular Tech.*, Vol. VT-27, no.4, pp 264-275, Nov. 1978.
6. K.S. Gilhousen, I.M. Jacobs, R. Padovani, A.J. Viterbi, L.A. Weaver and C.E. Wheatley III, "On the Capacity of a Cellular CDMA System", *IEEE Trans. on Vehicular Technology*, Vol. 40, No. 2, pp303-312, May 1991.
7. I. Andonovic, L. Tancevski, M. Shabeer and L. Bazgaloski, "Incoherent All-Optical Code Recognition with Balanced Detection", *J. Lightwave Tech.*, Vol. 12, No. 6, pp1073-1080, June 1994.

8. L. Tancevski, I. Andonovic, M. Tur and J. Budin, "Massive Optical LAN's Using Wavelength Hopping/Time Spreading with Increased Security", *IEEE Photonics Tech. Lett.*, Vol. 8, No. 7, pp935-937, Jul. 1996.
9. L. Tancevski and I. Andonovic, "Hybrid Wavelength Hopping/Time Spreading Schemes for Use in Massive Optical Networks with Increased Security", *J. Lightwave Tech.*, Vol. 14, No. 12, pp2636-2647, Dec. 1996.
10. H.V. Poor and L.A. Rush, "Narrowband Interference Suppression in Spread Spectrum CDMA", *IEEE Personal Communications*, Third Quarter, pp14-27, 1994.
11. D.R. Hughes and D. Hendricks, "Spread-Spectrum Radio", *Scientific American*, pp94-96, Apr. 1998.
12. K. Iversen and D. Hampicke, "Comparison and Classification of All-Optical CDMA Systems for Future Telecommunication Networks", *SPIE Proc. 2614*, 23-36 Oct. 1995, Philadelphia.
13. J.Y. Hui, "Pattern Code Modulation and Optical Decoding – A Novel Code-Division Multiplexing Technique for Multifiber Networks", *IEEE Journal on Selected Areas in Communications*, Vol. SAC-3, No. 6, pp916-927, Nov. 1985.
14. P.R. Prucnal, M.A. Santoro and T.R. Fan, "Spread Spectrum Fiber-Optic Local Area Network Using Optical Processing", *Journal of Lightwave Technology*, Vol. LT-4, No. 5, pp547-554, May 1986.

15. P.R. Prucnal, M.A. Santoro and S.K. Sehgal, "Ultrafast All-Optical Synchronous Multiple Access Fiber Optical Networks", *IEEE Journal on Selected Areas in Communications*, Vol. SAC-4, No. 9, pp1484-1493, Dec. 1986.
16. J.A. Salehi, "Code Division Multiple-Access Techniques in Optical Fiber Networks - Part I: Fundamental Principles", *IEEE Tran. Comm.*, Vol. 37, no. 8, pp824-833, Aug. 1989.
17. F.R.K. Chung, J.A. Salehi, V.K. Wei, "Optical Orthogonal Codes: Design, Analysis and Applications", *IEEE Trans. Info. Theory*, Vol. 35, no. 3, pp595-604, May 1989.
18. J.A. Salehi and C.A. Brackett, "Code Division Multiple Access Techniques in Optical Fiber Networks – Part II: System Performance Analysis", *IEEE Trans. on Communications*, Vol. 37, No. 8, pp 834-842, Aug. 1989.
19. W.C. Kwong, P.A. Perrier, P.R. Prucnal, "Performance Comparison of Asynchronous and Synchronous Code-Division Multiple-Access Techniques for Fiber-Optic Local Area Networks", *IEEE Trans. on Communications*, Vol. 39, No. 11, pp1625-1634, Nov. 1991.
20. A.A. Shaar and P.A. Davies, "Prime Sequences: Quasi-Optimal Sequences for OR Channel Code Division Multiplexing", *Elect. Lett.*, Vol. 19, No. 21, pp888-889, 13 Oct. 1983.
21. E. Park, A.J. Mendez and E.M. Garmire, "Temporal/Spatial Optical CDMA Networks-Design, Demonstration, and Comparison with Temporal Networks", *IEEE Photonics Tech. Lett.*, Vol. 4, No. 10, pp1160-1162, Oct. 1992.

22. R.M. Galiardi, A.J. Mendez, M.R. Dale and E. Park, "Fiber-Optic Digital Video Multiplexing Using Optical CDMA", *J. Lightwave Tech.*, Vol. 11, No. 1, pp20-26, Jan. 1993.
23. D.D. Sampson, R.A. Griffin, and D.A. Jackson, "Photonic CDMA by Coherent Matched Filtering Using Time-Addressed Coding in Optical Ladder Networks", *J. Lightwave Tech.*, Vol. 12, no. 11, pp2001-2010, Nov. 1994.
24. R.A. Griffin, D.D. Sampson and D.A. Jackson, "Optical Phase Coding for Code-Division Multiple Access Networks", *IEEE Photonics Tech. Let.*, Vol. 4, No. 12, pp1401-1404, Dec. 1992.
25. R.A. Griffin, D.D. Sampson and D.A. Jackson, "Coherence Coding for Photonic Cod-Division Multiple Access Networks", *J. of Lightwave Tech.*, Vol. 13, No. 9, pp 1826-1837, Sep. 1995.
26. J.A. Salehi, A.M. Weiner and J.P. Heritage, "Coherent Ultrashort Light Pulse Code-Division Multiple Access Communication Systems", *J. Lightwave Tech.*, Vol. 8, no. 3, pp478-491, Mar. 1990.
27. C.C. Chang, H.P. Sardesai and A.M. Weiner, "Code-Division Multiple-Access Encoding and Decoding of Femtosecond Optical Pulses over a 2.5-km Fiber Link", *IEEE Photonics Tech. Let.*, Vol. 10, No. 1, pp171-173, Jan 1998.
28. Zaccarin and M. Kavehrad, "An Optical CDMA System Based on Spectral Encoding of LED", *IEEE Photonics Technology Letters*, Vol. 4, No. 4, pp479-482, April 1993.

29. M. Kavehrad and D. Zaccarin, "Optical Code-Division-Multiplexed Systems Based on Spectral Encoding of Noncoherent Sources", *Journal of Lightwave Technology*, Vol. 13, No. 3, pp534-545, March 1995.
30. K. Iversen and O Ziemann, "An All-Optical CDMA Communication Network By Spectral Encoding of LED Using Acoustically Tunable Optical Filters", *Proc. 1995 Int. Symposium on Signals, Systems and Electronics (ISSSE'95)*, San Francisco, pp529-532, 1995
31. I. Hinkov, V. Hinkov, K. Iversen and O. Ziemann, "Feasibility of Optical CDMA Using Spectral Encoding by Acoustically Tunable Optical Filters", *Electronics Letters*, Vol. 31, No. 5, pp384-386, March 1995.
32. L. Nguyen, B. Aazhang and J.F. Young, "All-Optical CDMA with Bipolar Codes", *Electronics Letters*, Vol. 31, No. 6, pp469-470, 16th March 1995.
33. L. Nguyen, T. Dennis, B. Aazhang and J.F. Young, "Experimental Demonstration of Bipolar Codes for Optical Spectral Amplitude CDMA Communication", *Journal of Lighwave Tech.*, Vol. 15, No. 9, Sept. 1997, pp1647-1653.
34. P.E. Green, *Fiber Optic Networks*, Prentice Hall, New Jersey, 1993.
35. A.K. Jain, *Fundamentals of Digital Image Processing*, Prentice Hall, 1986.
36. K. Kudo and H. Yamazaki et. al, "Over 75-nm-wide Wavelength Range Detuning-Adjusted DFB-LDs of Different Wavelengths Fabricated on a Wafer", *OFC 97 Post Deadline Paper*, paper PD15, IEEE

37. L. Boivin, M.C. Nuss, W.H. Knox and J.B. Stark, "206-Channel Chirped-Pulse Wavelength-Division Multiplexed Transmitter", *Elect. Lett.*, Vol. 33, No. 10, pp827-829, 8th May, 1997.
38. Z.J. Sun, K.A. McGreer and J.N. Broughton, "Demultiplexer with 120 Channels and 0.29-nm Channel Spacing", *IEEE Photonics Tech. Lett.*, Vol. 10, No. 1, pp90-92, Jan. 1998.
39. R.H. Kingston, *Detection of Optical and Infrared Radiation*, 2/e, Springer-Verlag, Berlin, 1979
40. P.R. Morkel, R.I. Laming and D.N. Payne, "Noise Characteristics of High-Power Doped-Fiber Superluminescent Sources", *Elec. Lett.*, Vol. 26, No. 2, pp96-98, 18th Jan, 1990.
41. P.A. Humblet and M. Azizoglu, "On the Bit Error Rate of Lightwave Systems with Optical Amplifiers", *J. Lightwave Tech.*, Vol. 9, No. 11, pp1576-1582, Nov. 1991.
42. A.J. Keating and D.D. Sampson, "Reduction of Excess Intensity Noise in Spectrum-Sliced Incoherent Light for WDM Applications", *J. Lightwave Tech.*, Vol. 15, No. 1, Jan. 1997, pp53-61.
43. G.P. Agrawal, *Fiber-Optic Communication Systems*, John Wiley & Sons, 1992.
44. K.J. Williams and R.D. Esman, "Optically Amplified Downconverting Link with Shot-Noise-Limited Performance", *IEEE Photonics Tech. Lett.*, Vol. 8, No. 1, Jan. 1996, pp148-150.

45. R.E. Ziemer and W.H. Tranter, *Principle of Communications*, 2/e, Houghton Mifflin Co., 1985.
46. R.E. Ziemer and R.L. Peterson, *Introduction to Digital Communication*, Macmillan, New York, 1992.
47. S.S. Wagner and T.E. Chapuran, "Broadband High-Density WDM Transmission Using Superluminescent Diodes", *Electronics Letters*, Vol. 26, No. 11, pp696-697, 24th May 1990.
48. Y.K. Chen and M.C. Wu, "Monolithic Colliding Pulse Mode-locked Quantum Well Lasers", *IEEE Journal of Quantum Electronics*, Vol 28, pp2176-2185, Oct. 1992.
49. F. Bilodeau, D.C. Johnson, S. Theriault, B. Malo, J. Albert and K.O. Hill, "An All-fiber Dense-Wavelength-Division Multiplexer/Demultiplexer Using Photoimprinted Bragg Gratings", *IEEE Photonics Technology Letters*, Vol .7, No. 4, pp388-390, Apr. 1995.
50. B.E. Little, J.S. Foresi, G. Steinmeyer, E.R. Thoen, S.T. Chu, H.A. Hauss, E.P. Ippen, L.C. Kimerling and W. Greene, "Ultra-Compact Si-SiO₂ Microring Resonator Optical Channel Dropping Filters", *IEEE Photonics Tech. Letters*, Vol. 10, No. 4, April 1998.
51. N. Koblitz, *A Course in Number Theory and Cryptography*, 2nd ed., Springer-Verlag, New York, 1948.

52. S. Seung-Woo; K. Bergman, P.R. Prucnal, "Transparent optical networks with time-division multiplexing", *IEEE Journal on Selected Areas in Communications*, Vol.14, No.5, pp.1039-1051, June 1996.
53. S.R. Mallinson and J.H. Jerman, "Miniature micromachined Fabry-Perot interferometers in silicon", *Electron. Lett.*, Vol. 23, No. 20, , pp1041-1043, Sep. 1987.
54. J. Stone and L.W. Stulz, "Pigtailed high-finesse tunable fiber Fabry-Perot interferometers with large, medium and small free spectral range", *Electon. Lett.*, vol. 23, pp. 781-783, 1987.
55. A.A. Saleh and J. Stone, "Two-stage Fabry-Perot filters as demultiplexers in optical FDMA LANs", *J. of Lightwave Tech.*, Vol. 7, pp. 323-330, Feb. 1989.
56. J.P. Laude and J.M. Lerner, "Wavelength division multiplexing/demultiplexing (WDM) using diffraction gratings", *SPIE-Application, Theory and Fabrication of Periodic Structures*, Vol. 503, pp22-28, 1984.
57. Dragone, "An N×N Optical Multiplexer Using a Planar Arrangement of Two Star Couplers", *IEEE Photonics Tech. Let.*, Vol. 3, No. 9, pp812-815, Sep, 1991
58. R.T. Hofmeister, S.M. Gemelos et. al, "Project LEARN – Light Exchangeable, Add/Drop Ring Network", *OFC 97 post deadline paper*, PD25, IEEE.
59. E. Yablonovitch, "Photonic band-gap structures", *J. Opt. Soc. America B*, Vol. 10, No. 2, pp283-295, Feb. 1993.

60. C.F. Lam, R.B. Vrijien, P. Chang-chien, D. Sievenpiper and E. Yablonovitch, "A Tunable Wavelength Demultiplexer Using Logarithmic Filter Chains", *Journal of Lightwave Technology*, Vol. 16, No. 9, pp1657-1662, Sept. 1998.
61. J.D. Spragins, J.L. Hammond and K. Pawlikowski, *Telecommunications – Protocols and Design*, Addison-Wesley, 1992.
62. C.F. Lam, R.B. Vrijen, M.C. Wu, E. Yablonovitch, D.T.K. Tong, "Multi-wavelength Optical Code Division Multiplexing", *SPIE Proceeding*, Photonics West 1999, San Jose, California.
63. C.F. Lam, *All-Optical Code Division Multiple Access (CDMA) Systems Using Spectral Encoding*, M.Sc. Thesis, UCLA, 1996.
64. J.M. Senior, *Optical Fiber Communications: Principles and Practice*, 2/e, Prentice Hall 1992.
65. P.E. Green, L.A. Coldren et al., "All-Optical Packet-Switched Metropolitan-Area Network Proposal", *J. of Lightwave Tech.*, Vol. 11, No. 5/6, , pp754-763, May/June 1993.
66. P. Yeh, *Optical Waves in Layered Media*, John Wiley & Sons, Ch.5-Ch.6, 1988.
67. A. Mori, Y. Ohishi et. al, "1.5 μ m broadband amplification by Tellurite-based EDFAs", *OFC 97 post deadline paper*, PD1, IEEE.
68. J.S. Foresi, P.R. Villeneuve, J. Ferrera, E.R. Thoen, G. Steinmeyer, S. Fan, J.D. Joannopoulos, L.C. Kimerling, H.I. Smith and E.P. Ippen, "Photonic-Bandgap Microcavities in Optical Waveguides", *Nature*, Vol. 390, pp143-145, 13 Nov. 1997.

69. A. Talneau, C. Ougier and S. Slempek, "Multiwavelength Grating Reflectors for Widely Tunable Laser", *IEEE Photonics Tech. Let.*, Vol. 8, No. 4, pp497-499, April 1996.
70. C. Wei, D. Van Thourhout, I. Moerman, S. Goeman, K. Vandeputte and R. Baets, "An Integrated Optical Add/Drop Multiplexer in InP Based on Elliptic Couplers and Bragg Grating Reflector", *1997 Digest of the IEEE/LEOS Summer Topical Meetings: WDM Components Technology*, paper ThA2, pp28-29.
71. M.C. Oh, M.H. Lee, J.H. Ahn, H.J. Lee and S.G. Han, "Polymeric Wavelength Filters with Polymer Gratings", *Applied Physics Letters*, Vol. 72, No. 13, pp1559-1561, 30 Mar. 1998.